Sub-weekly Scale Interactions between the Sea of Japan and Extratropical Cyclones in Winter

趙, 寧

https://doi.org/10.15017/1866338

Sub-weekly Scale Interactions between the Sea of Japan and Extratropical Cyclones in Winter

NING ZHAO

JUNE 2017

Sub-weekly Scale Interactions between the Sea of Japan and Extratropical Cyclones in Winter

A Dissertation submitted for the degree of

Doctor of Science

by

Ning Zhao

Department of Earth System Science and Technology,

Interdisciplinary Graduate School of Engineering Sciences,

Kyushu University

June 2017

"A journey of a thousand miles begins with a single step."

—— **Laozi**

This thesis is dedicated to

Those I Love

&

Those Who Love Me.

Acknowledgements

I would like to express my gratitude to all the people who contributed to the works described in this thesis.

Foremost, I would thank my parents, my father Tiancheng Zhao and my mother Yuer Tong. They are no more than the ordinary Chinese parents who wish to have a wonderful life staying with their child. Yet, they sacrificed each pieces of their efforts for supporting my study overseas. They are not rich, but they still tried to fulfill many unreasonable requests of mine and support almost every decisions that I made by my own. Without whom, I wouldn't be possible to be here studying, working, laughing, crying, living the every moment of my life.

Every result in this thesis was accomplished under the guidance of my supervisor, Prof. Atsuhiko Isobe. During my three-year study in Kyushu University, he contributed to a rewarding academic experience by giving me intellectual freedom in my study, supporting my attendance at various conferences, engaging me in new ideas, and demanding a high quality of work in all my endeavors. He helped me to find the beauty of science and the interest in researching. I could not have imagined having a better advisor and mentor for my Ph. D. study.

Additionally, I should express sincere thanks to Prof. Naoki Hirose in Re-

search Institute for Applied Mechanics (RIAM) and Prof. Atsuyoshi Manda in Nagasaki University (now at Mie University) for their suggestions before and after my entrance into the Ph. D. course. Also, I would like to show my appreciation to the committee members Prof. Masaru Yamamoto and Prof. Ryuichi Kawamura for their interest in my work and insightful comments.

I would thank all the members of the Ocean Dynamic Group in RIAM, Kyushu University. Special thank would be given to Dr. Shinsuke Iwasaki for his support and help during my study. He and I worked together on many issues including but not limited to this thesis, and without his comments and suggestions my job would have undoubtedly been more difficult. I also benefited from his keen scientific insight and his optimistic outlook on researching works and lives. In the last year of my study, Prof. Shinichiro Kida joined our group. I am deeply grateful to him since I was able to have extra chances for discussions and receiving comments. I want to thank Dr. Kenki Kasamo, Dr. Yasuyuki Miyao, and Mr. Yuichi Iwanaka for their helps in the daily works. Thanks are also given to other graduate students and two secretaries of our group, Mrs. Michiyo Tanaka and Mrs. Miho Irie.

Thanks should be further given to professors who discussed with me about this study including but not limited to Prof. Ren-Chief Lien, Prof. Dongliang Yuan, Prof. Hirohiko Nakamura, Prof. Kaoru Ichikawa, Prof. Tomoharu Senjyu, and Prof. Il-Ju Moon. I would like to express my gratitude to Dr. Bin Wang, Mr. Tianran Liu, and Mrs. Harumi Fujii for their favorable helps

in this three-year lives in Fukuoka, and also to Dr. Xifeng Wang, Dr. Sooyeon Han, Dr. Hidetaka Hirata, Mr. Haoyu Wang and other people who helped me.

I thank all the people in my life, relatives and friends, and others even I don't know the names, for without whom I could not have a wonderful life in these years. Among them, special thank is given to Ms. Xiaozhou Yu, for no reason but only because she does be my best friend for 17 years.

Finally, thank should be given to my girlfriend who almost never appeared in my life.

Abstract

Numerous studies showed the East Asian marginal seas play an important role on the cyclogenesis, while on the other hand, extratropical cyclones can also greatly influence the seas. In this study, we conducted both objective analysis and the sensitivity experiments using a regional numerical model based on the observational and reanalysis datasets and revealed a two-way coupling process that occurs between the Sea of Japan and extratropical cyclones in winter.

The response of the Sea of Japan to winter extratropical cyclones is investigated based on the quantitative analyses of gridded and satellite datasets. Cyclone passages affecting the sea are detected using time series of spatially averaged surface turbulent heat fluxes. As the cyclones develop, there is a strong cold-air outbreak causing twice the normal heat loss over the sea. After removal of sea surface temperature (SST) seasonal trends, we found that cyclone passage (hence, cooling) mainly occurred over 3 days, with maximum SST reduction of -0.4 $^{\circ}$C. The greatest reduction was found along the subpolar front, where frontal sharpness (i.e., SST gradient) increased by 0.1 $^{\circ}$C (100 km)$^{-1}$. Results of a mixed-layer model were consistent with both SST and frontal sharpness, and localized surface cooling along the subpolar front resulted from both horizontal advection and turbulent heat flux at the sea surface. Further analyses show that this localized cooling from horizontal advection is caused by the cross-frontal Ekman flow (vertically averaged

over the mixed layer) and strong northwesterly winds associated with the cold-air outbreak during cyclone passage.

The effects of the cyclone-induced sea surface temperature (SST) anomaly in the Sea of Japan on the following cyclones were investigated based on a regional numerical model. The numerical modeling was conducted with and without the SST anomaly owing to the cooling by a single extratropical cyclone in winter. According to 26 pairs of these sensitivity experiments, we found that cyclones were not always sensitive to the SST anomaly. The low-level trough (hence, strong northwesterly winds) plays an important role on the cyclone sensitivity by controlling the cold air intrusion over the Sea of Japan. A strong (weak) cold air intrusion forms a relatively unstable (stable) and higher (lower) convective layer, which encourages (restrains) the upward penetration of the influences of the SST anomaly. Two specific cyclones (A and B) were analyzed to demonstrate two distinct patterns in cyclone modulation caused by the previously-passing cyclone via SST anomaly: wave-like pattern and path-shifting pattern. The wave-like pattern was formed by the combination of the weakened cyclone and a half-wavelength (hence, short-time) anomalous wave, while the poleward path shifting was caused by the positive potential vorticity anomaly on the northern side of the cyclone center which induced by the enhanced diabatic heating. The wavelet spectra demonstrate that both wave-like and path-shifting patterns were revealed among 20 affected cyclones as well as the two cyclones, although these patterns were likely to appear simultaneously in each

cyclone. Our analyses demonstrated that a cyclone can modulated the following cyclone via the SST reduction over the Sea of Japan, and that the role of the colder Sea of Japan is not only for the weakening source to reduce the cyclone activity, but also for strengthening and/or generating baroclinic waves in surrounding regions.

Contents

List of Figures

Page

List of Tables

Page

Chapter 1

Introduction

1.1 The Sea of Japan

1.1.1 Oceanic Characters

Abutting the East Asian continent, several small seas form a transition zone between the cold and dry East Asian continent and the warm and moist western North Pacific. Thereby, the coupling processes between the atmosphere and oceans are likely to activate over the small marginal seas. Also the influence of the coupling is likely to transfer widely on to the neighboring open oceans because the marginal seas are located "upstream" of intensive westerly winds over the North Pacific. Among these seas, we paid a special attention on the Sea of Japan, a so-called 'mini-ocean', due to the

varieties of oceanological phenomena [e.g., *Choi*, 1996; *Park and Watts*, 2005; *Chu et al.*, 2001].

The Sea of Japan has a steep bottom topography and covers the area more than 10^6 km^2 (Figure 1.1). The Sea of Japan and surrounding regions are connected via four main straits, which are the Tsushima Strait, the Tsugaru Strait, the Soya Strait, and the Tartary Strait. These straits are shallow with a depth of about 100-140 m, except the Tartary Strait less than 20 m. The deepest basin in the Sea of Japan is the Japan Basin (D in Figure 1.1) with the maximum depth over 4000 m, followed by the Yamato Basin (B in Figure 1.1) and Ulleung Basin (A in Figure 1.1). A relatively shallower area is located at the center, which known as the Yamato Rise (C in Figure 1.1).

The ocean general circulation in the upper Sea of Japan is consist of the cyclonic gyre in the northern part, and an eastward flow originated from the Tsushima Strait as Tsushima Warm Current (TWC) in the south [e.g., *Uda*, 1934, 1936; *Kawai*, 2004; *Lee and Niiler*, 2005; *You et al.*, 2010]. The TWC is the most important current in the Sea of Japan, that transports warm saline water formed by a branch of Kuroshio Current and the Taiwan Warm Current [e.g., *Isobe*, 1999]. After entered the Tsushima Strait, the TWC separates into three branches: 1) the near-shore branch that flows along the north coast of Japan [e.g., *Toba et al.*, 1982]; 2) the off-shore branch along the shelf break along the north coast of Japan [*Kawabe*, 1982]; 3) the Eastern Korean Warm Current along the east coast of Korea, followed by eastward flow along the subpolar front [e.g., *Kawabe*, 1982; *Morimoto and Yanagi*, 2001]. Note that a strong seasonality was found in this three-branch pattern [e.g., *Kawabe*, 1982; *Chu et al.*, 2001] and such temporal variation is important on the formation of the intermediate water in the Sea of Japan [*Yoon and Kawamura*, 2002]. On the other hand, the cyclonic gyre is generated by the positive wind stress curl [e.g., *Kim and Yoon*, 1996], including the Liman Cold Current along the Russian coast and the eastward current along the subpolar front [*Kawabe*,

1982]. Many studies on abyssal circulation to date have attempted to clarifying the intermediate and deep waters in the Sea of Japan [e.g., *Senjyu and Sudo*, 1994; *Senjyu et al.*, 2005; *Teague et al.*, 2005], although the abyssal circulation remained unclear owing to the lack of sufficient mooring observations. Recently, a combination among numerical models, profiling float (Argo) and mooring data help reconstruct the abyssal circulations, and elucidate the dynamics within it [e.g., *Choi and Yoon*, 2010; *Park and Kim*, 2013; *Kang et al.*, 2016].

Another interesting phenomenon in the Sea of Japan is the strong temperature gradient at the center of the sea, known as the subpolar front [*Park et al.*, 2007; *Zhao et al.*, 2014]. The main axis of this front is usually determined by the largest SST gradient located near 40 °N, and it is also regarded as the boundary between the warm and saline subtropical water entered from the Tsushima Strait and the cold and less saline subpolar water formed mostly within the Sea of Japan [e.g., *Isoda*, 1994a; *Belkin and Cornillon*, 2003; *Talley et al.*, 2006; *Prants et al.*, 2017]. This front also plays an important role on the subduction and intermediate water formation in the Sea of Japan [*Lee et al.*, 2006]. Furthermore, as those in open oceans, the subpolar front in the Sea of Japan experiences a pronounced seasonal variation such that, in the summer, strong surface heating leads to the vanishing of the surface front (i.e., frontolysis), and that the strong heat advection from the TWC enhances the temperature gradient in winter [*Zhao et al.*, 2014].

1.1.2 Atmospheric Characters

Seasonal variations are not revealed only in the Sea of Japan, but also in the atmosphere aloft. Among the atmospheric features, the East Asian Monsoon is an important component in local weather and climate. In summer, a relatively weak summer monsoon carries the warm and moist air from

the Indian Ocean and Pacific Ocean [*Ding*, 2005] to the eastern Russia, and therefore significantly influences the major seasonal rain belt in the East Asia [e.g., *Yoshikane et al.*, 2001]. As the warm air and weak winds dominate, a weakly stable marine atmospheric boundary layer forms, leading to a weak turbulent heat release in the Sea of Japan [*Dorman et al.*, 2005], although the volume transport from the Tsushima Strait also becomes the largest in a year [*Takikawa and Yoon*, 2005].

During winter, almost completely opposite atmospheric conditions could be found over the Sea of Japan (Figure 1.2). In addition to the situation that the TWC exhibits its minimal volume transport [*Takikawa and Yoon*, 2005; *You et al.*, 2010], the strong winter monsoon bringing cold Asian air from the north causes the extensive heat loss from the sea [*Dorman et al.*, 2004]. *Zhao et al.* [2014] further suggested that the wind-induced Ekman advection helps the formation of the strong subpolar front in the Sea of Japan. In the upper layers, the jet streak (very high wind speed) of the Subtropical Jet located over this region along with the East Asian Trough (EAT, *Song et al.* [2016]). The Siberian High builds up to the rear of the EAT [*Ding and Krishnamurti*, 1987], while the encountered warm air results in a zone with strong baroclinity critical to the cyclogenesis in the East Asia [*Nakamura et al.*, 2002; *Ren et al.*, 2010]. This trough is also highly related to the cold-air outbreak events over the Sea of Japan [*Zhang et al.*, 1997].

1.2 Extratropical Cyclones

Extratropical cyclones, also known as the mid-latitude cyclones or storms, are commonly seen in the mid-latitude, especially during the winter seasons. These synoptic phenomena have a much larger horizontal scale than tropical cyclones, and experience quite different dynamical mechanisms from those

in the tropics.

The evolution of the extratropical cyclones has been studied since the early 20th century. A particular conceptual developing model was introduced by *Bjerknes and Solberg* [1922] within the Bergen School of Meteorology (Norway) which is now known as the 'Norwegian model'. They described a cyclone starting from two oppositely directed flows with different temperatures (e.g., a front). Thereafter, the cyclone is given birth due to boundary bulges towards the colder side, and the cyclone center is located at the top of the ascending warm-air tongue. Also, precipitation is formed due to the ascending warm air. The cyclone deepens as it moves up, forming the distinct warm and cold fronts. Then, the cold front catches up (or, 'wrapping up' as described in *Schultz and Vaughan* [2011]) to the warm front leading to an occluded front, thereby cuts off the cyclone center from the warm sector. Away from the direct warm air supply, the cyclone is isolated within the cold sector, eventually formed a cold-core low and then vanishes later.

The Norwegian model firstly shed a light on the cyclogenesis and provide a possibility to enhance the weather forecasting *Uccellini et al.* [1999]. Nevertheless, on the basis of numerical models which aimed to evaluate the cyclones' life cycle since 1980s, many researchers found that this model may not be the unique answer on the cyclone development [e.g., *Hoskins and West*, 1979; *Keyser et al.*, 1989]. Among them, a new conceptual model for the life cycle of extratropical cyclones was proposed by *Shapiro and Keyser* [1990], namely 'the Shapiro-Keyser model'. This model describes a cyclone starting from a same frontal region as the Norwegian model does. However, in the next phase, the fronts separate (fracture) at the cyclone center and form a 'T-bone' structure. Finally, the warm air is wrapped up at the center constructing a warm seclusion, rather than the 'cut off' process described in the Norwegian model.

In fact, more recent studies suggested that some of cyclones may act as the Shapiro-Keyser model, while others more like the Norwegian model. Some studies further suggested that the model of cyclones may be strongly related to the directions and the strengths of the cold front and warm front [e.g., *Neiman and Shapiro*, 1993; *Schultz et al.*, 1998].

Now, extratropical cyclones have been known as the vital component of both mid-latitude weather systems and the global circulations [e.g., *Chang et al.*, 2002; *Catto et al.*, 2012]. For example, most precipitation extremes are found to occur during the passage of cyclones and the fronts within them [e.g., *Catto and Pfahl*, 2013]. These cyclones play an important role on the global energy balance, transporting energy poleward from the Equator [*Trenberth and Stepaniak*, 2003]. Meanwhile, they also strongly interact with the oceans and seas underneath during their life cycles. Given these facts, the geographical paths of these cyclones, namely the storm tracks [*Chang et al.*, 2002], therefore attract a great attention in both global and regional studies [e.g., *Blackmon et al.*, 1977; *Hoskins and Valdes*, 1990; *Blender et al.*, 1997].

1.3 Connections between Extratropical Cyclones and the Sea of Japan

Extratropical cyclones form recurrently over the East Asian region, because of the collision between cold air from the continent and a warm air masses from the ocean. These synoptic-scale cyclones have a lifespan mainly around 1-7 days. While winter cyclones are strong but short-lived, the summer cyclones are weak with a relatively longer life [*Zhang et al.*, 2012]. Of note, because of the strong air-sea heat and moisture exchanges along the Kuroshio and its extension, namely the anchoring effect [e.g., *Nakamura et al.*, 2004;

Ogawa et al., 2012], the East Asia has also been demonstrated as one of the most active areas for extratropical cyclones by both statistic and numerical studies, especially in winter [*Roebber*, 1984; *Pinto et al.*, 2007; *Shaw et al.*, 2016].

Beside the Kuroshio, SST over the East Asian marginal seas may play a significant role on the cyclone activities in the western North Pacific as well as the cyclones above the seas. This is because these seas are located in a transition zone linking the cool and dry Asian continent and the warm and moist North Pacific, especially in winter. These marginal seas therefore play a role the local atmosphere including the lower-level baroclinity and cyclogenesis [e.g., *Chen et al.*, 2001; *Yamamoto and Hirose*, 2007; *Isobe and Kako*, 2012]. *Xie et al.* [2002] showed the positive correlation between wind and SST in the Yellow and East China Sea and they confirmed the sharp SST gradient increases the cyclone growth rate in this region. *Yamamoto and Hirose* [2007] showed the sharp front in the Sea of Japan could enhance the cyclone activities. More recently, *Isobe and Kako* [2012] further showed a remote effect of a marginal sea on the cyclogenesis over the surrounding regions. On the basis of a regional numerical modeling as a case study, *Yamamoto* [2013] suggested the colder Sea of Japan would weaken the baroclinic wave at the early stage of the cyclogenesis and generate a 'Western Pacific Pattern-like' anomaly in the geopotential height. Furthermore, locating upstream of the storm tracks in the western North Pacific yields the situation that, changes in properties over these marginal seas can spread onto a much larger area via the interactions with eastward-propagating cyclones [e.g., *Hirose et al.*, 2009; *Kelly et al.*, 2010; *Seo et al.*, 2014]; see, for example, the Aleutian Low east of the Japanese Islands [*Overland et al.*, 1999; *Yamamoto and Hirose*, 2011] and North Pacific weather patterns [*Hirose et al.*, 2009].

What do cyclones bring to the seas? Generally, cyclones transfer the momentum to the seas through the surface roughness, and in turn, obtain heat and moisture via sensible and latent heat fluxes from the ocean surface. Numer-

ous studies have showed such processes happened under the tropical cyclones [e.g., *Bao et al.*, 2000; *Dare and McBride*, 2011; *Mei and Pasquero*, 2013], although very few studies have paid attention on that during extratropical cyclones [e.g., *Ren et al.*, 2004] until the first decade of 21st century. In East Asia, *Dorman et al.* [2004] firstly showed a link between the cold-air outbreaks and the passing cyclones based on the observations in the Sea of Japan, and such link was further mentioned by *Isobe and Beardsley* [2007] who suggested that the cyclones could induce a stronger cold-air outbreak and increased surface heat release over the Sea of Japan.

However, it remains unclear to date how the Sea of Japan is affected by the passing cyclones, both mechanically and quantitatively. It has been well clarified that the subpolar front alters extratropical cyclone activity in the Sea of Japan [*Yamamoto and Hirose*, 2007], one may also consider that the subpolar front remains strong after the passage of extratropical cyclones. If frontal sharpness and/or location are temporarily modified by cyclone passages (as is likely because of heat fluxes through the sea surface), a two-way coupling process may occur between the front and cyclones even in the regional scale [e.g., *Iwasaki et al.*, 2014].

For example, considering the surface heat release induced by the passing cyclones over the Sea of Japan, the intensive cooling of the Sea of Japan is likely to occur after the passage. According to *Yamamoto* [2013], the colder Sea of Japan would weaken the cyclones. This suggests the accomplishment of a negative feedback process such that the cyclones weaken the following cyclones via SST decrease in the Sea of Japan. Is this the process the case between the Sea of Japan and extratropical cyclones? In fact, *Yamamoto* [2013] mainly focused on the dynamic process within the area around a specific cyclone, without paying much attention on the large-scale backgrounds, which may have influences during the cyclogenesis, or even before the cyclone generated [e.g., *Yoshiike and Kawamura*, 2009]. Moreover, in a variety of

atmospheric backgrounds (such as upper-level jet or northwesterlies), extratropical cyclones would potentially have a variety structures owing to different dynamical or thermo-dynamical processes undergone [e.g., *Yoshida and Asuma*, 2004, 2008]. Thus, it is necessary to further validate whether or not the weakening effect mentioned above occurs commonly on those cyclones with various backgrounds.

1.4 The Goal of This Study

As described above, the motivation of this study arises from the lack of knowledge in the interactions between the Sea of Japan and extratropical cyclones. Therefore, we focus on figuring out two scientific questions:

1) How does the Sea of Japan response to the winter cyclones?
2) Can the small semi-enclosed Sea of Japan alter the passing cyclones?

In this study, we conducted data analyses using gridded and satellite SST data, and oceanic and atmospheric reanalysis data, in addition to the numerical experiments using a mixed-layer model and a regional atmospheric model. The objective in the present study is to find the answers for the questions addressed above.

This thesis is organized as follows. In Chapter 2, the response of surface temperature over the Sea of Japan to the extratropical cyclones in winter is presented using the mixed layer model. Note that an extended work of Chapter

2 is given in Appendix B for the entire East Asian region. In Chapter 3, the atmospheric response to the Sea of Japan, which was altered by a previously-passing cyclone, is discussed based on the sensitivity experiments using the regional numerical model with and without the SST anomaly caused by cyclones over the Sea of Japan. Finally, the major conclusions of this study are presented in Chapter 4.

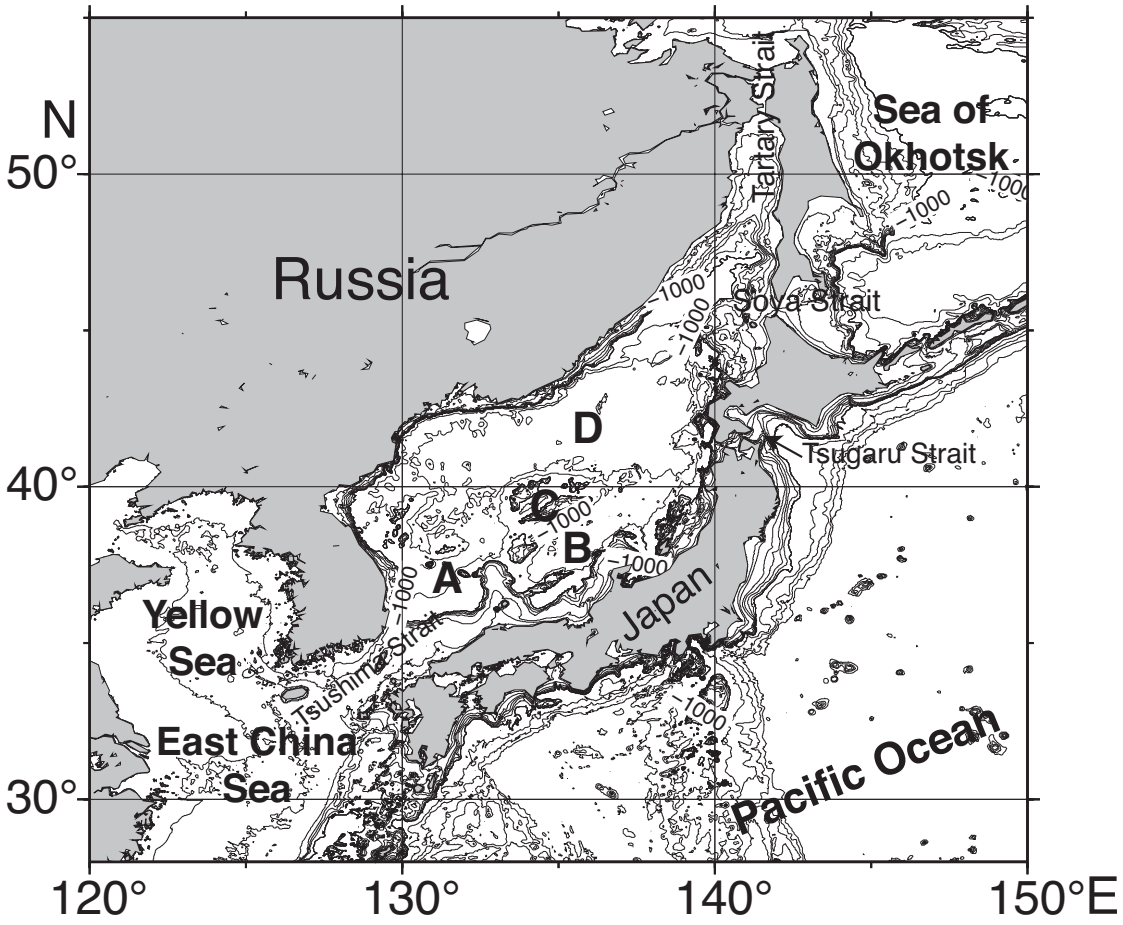

Figure 1.1: The Sea of Japan and surrounding areas where A represents the Ulleung Basin, B the Yamato Basin, C the Yamato Rise, and D the Japan Basin. Bathymetry is represented by contours where the contour intervals are 50 m for depth shallower than 100 m, 200 m for depth shallower than 1000 m, and 1000 m for deeper regions, respectively.

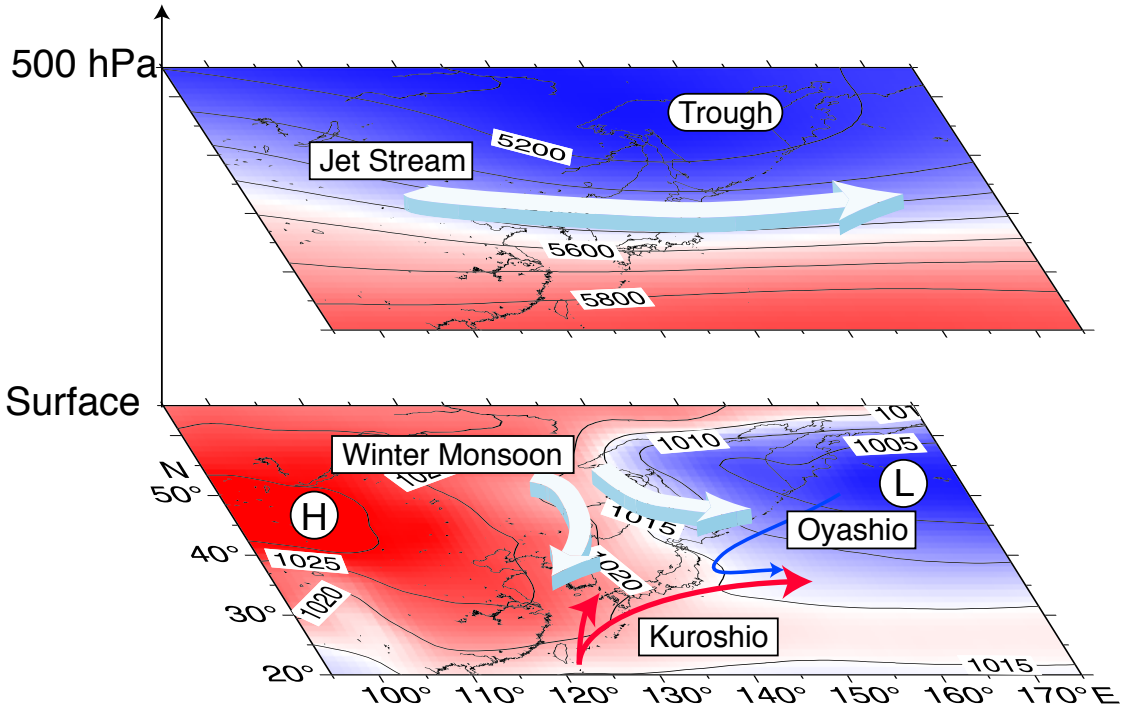

Figure 1.2: General geographical and atmospheric backgrounds of the Sea of Japan. The climatological mean of the sea level pressure and geopotential height at 500 hPa are obtained from the 6-hourly NCEP-DOE Reanalysis 2 dataset and averaged in winters (defined as November to February) of 2003-2011. See detailed introduction of the Winter Monsoon, the Subtropical Jet and the East Asian Trough in the text.

Chapter 2

Intensification of the Subpolar Front in the Sea of Japan During Winter Cyclones

2.1 Introduction

Robust relationships between oceanic fronts and the atmosphere have been demonstrated by many studies (*Small et al.* [2008] and references therein). Atmospheric responses to the sea surface temperature (SST) field have been investigated in the context of the heat supply around oceanic fronts [e.g. *Minobe et al.*, 2008], frontal strength (SST gradient) [e.g. *Nonaka et al.*, 2009; *Sampe et al.*, 2010], and frontal locations [e.g. *Inatsu et al.*, 2003; *Ogawa et al.*, 2012]. Importantly, as pointed out by *Nakamura et al.* [2004], the anchoring

effect of oceanic fronts is central to modulating storm tracks and their associated polar-front jets, which may in turn drive ocean currents [*Trenberth et al.*, 1990] and enhance the front itself.

The sharp subpolar front that separates the sea into a relatively cold and fresh subpolar region and a warm and saline subtropical region [*Isoda*, 1994b; *Belkin and Cornillon*, 2003]. This front enhances low-level baroclinicity (and hence cyclone activity), as suggested by previous studies [e.g. *Yoshiike and Kawamura*, 2009; *Yamamoto*, 2013]. Therefore, it is believed that the subpolar front in the Sea of Japan can be regarded as a "source region" that alters atmospheric processes over the broad East Asian region [*Yamamoto and Hirose*, 2007].

Although the subpolar front clearly alters extratropical cyclone activity in the Sea of Japan as described above, one may consider whether that front remains strong after extratropical cyclones. If frontal sharpness and/or location are temporarily modified by cyclone passages (as is likely because of heat fluxes through the sea surface), a two-way coupling process (i.e., air-sea interaction) may occur between the front and cyclones. In fact, it has been demonstrated that this oceanic front is strongly influenced by cooling from cyclones and their related cold-air outbreaks during winter [e.g. *Dorman et al.*, 2004; *Isobe and Beardsley*, 2007]. However, it remains unclear how the subpolar front is affected by cyclone passage, both qualitatively and quantitatively. Therefore, before considering the two-way coupling processes that may occur between the subpolar front and cyclone activity in the Sea of Japan, we quantitatively evaluate subpolar front variations during extratropical cyclone passages over the sea.

This chapter is organized as follows. Section 2.2 presents data sources and processing. Section 2.3 describes analyses based on gridded datasets, followed by Section 2.4, which introduces mechanisms of surface cooling and

frontal variations over the Sea of Japan during cyclone passage, using a mixed-layer model. Section 2.5 gives the summary. The main content of this chapter is based on our published paper on Journal of Geophysical Research: Oceans [*Zhao et al.*, 2016].

2.2 Materials and Methods

2.2.1 Data Sources

We used four gridded datasets: SST from the National Oceanic and Atmospheric Administration Optimum Interpolation SST analysis Version 2 (OISSTv2) [*Reynolds et al.*, 2007]; SLP from the National Centers for Environmental Prediction - Department of Energy Atmospheric Model Intercomparison Project reanalysis (NCEP-DOE R2) [*Kanamitsu et al.*, 2002]; surface turbulent heat fluxes (sensible and latent heat), shortwave and longwave radiation, and 2-m air temperature from Woods Hole Oceanographic Institution (WHOI) Objectively Analyzed air-sea Fluxes (OAFlux); ocean currents and hydrographic data from the Data assimilation Research of the East Asian Marine System (DREAMS) [*Hirose et al.*, 2013].

Wintertime $1/4^\circ$ daily SST data from the period 2003-2011 were obtained from OISSTv2. Six-hourly mean SLP data during that period with horizontal resolution $2.5^\circ \times 2.5^\circ$ during the same period were acquired from NCEP-DOE R2. To align with other datasets, all SLP data were daily-averaged. OAFlux offers daily 2-m air temperature and sensible and latent heat fluxes on each $1^\circ \times 1^\circ$ grid cell every winter from 2003 to 2011. Among the OAFlux data, the surface shortwave and longwave radiation data used by the mixed layer model analyses (addressed later) were only available through 2009. Thus,

three-dimensional oceanic data ($1/12^\circ \times 1/15^\circ$ temperature, salinity and current velocities), which were also used by the mixed-layer model, were obtained from DREAMS for 2003-2009 only. Surface wind stress was computed using a bulk formula and satellite data from the Quick Scatterometer (QuikSCAT) and Advanced Scatterometer (ASCAT), both downloaded from the website of Remote Sensing Systems (http://www.remss.com). Wind vectors from QuikSCAT and ASCAT were simply averaged for each day during winters from 2003-2009, when at least one of them was available.

2.2.2 Data Processing

We constructed composite maps of SST and SLP based on an analysis of time series of surface turbulent fluxes. Because the passage of extratropical cyclones always results in strong turbulent heat fluxes [e.g., *Zolina and Gulev*, 2003; *Papritz et al.*, 2015], we used that time series to detect cyclones affecting the Sea of Japan. Composite maps depict the modification of the SST field (and hence the subpolar front) by cyclone passage, via surface heat flux.

Procedures for making the composite maps were as follows. Of particular interest is the relatively short-term (several days) fluctuation caused by extratropical cyclones. Therefore, seasonal trends in each winter were removed using a quadratic polynomial, based on the least squares method. Thereafter, the sum of latent and sensible fluxes was averaged over the Sea of Japan (box in Figure 2.2a). To detect extreme flux events during the winters of 2003-2011, we chose periods when the sum of turbulent fluxes in the box was lower than -336 W m^{-2} (downward is positive, Figure 2.2b), corresponding to the 80th percentile of our dataset. The same threshold (80th) was adopted in previous studies [e.g. *Shaman et al.*, 2010; *Ma et al.*, 2015]. Each event was indicated by the "peak day" when the upward heat flux averaged over the box in Figure 2.2a met the aforementioned criterion. This

should also be the local minima in the time series (solid dots in Figure 2.2b). Even if the events occurred consecutively, they would be recognized as a single event when they produced local minima in the daily time series. Subsequently, for all the detected events, we constructed maps of atmospheric and oceanic properties (e.g., SST) averaged daily on "peak days", and days before and after peak days.

To investigate subpolar front locations and strengths, the gradient magnitude (G) is given by:

$$G = \sqrt{(\frac{\partial T}{\partial x})^2 + (\frac{\partial T}{\partial y})^2}, \tag{2.1}$$

where T represents the water temperature, and x and y indicate eastward and northward positions, respectively.

2.2.3 Mixed Layer Model Analyses

The surface mixed-layer model (so-called "slab model") is likely the simplest tool to uncover the temperature modulation in the upper ocean. In the present application, we constructed such a model, in which the mixed-layer depth is defined by that at which seawater density (σ) increases by a certain value $\Delta\sigma$ from the reference depth. The values for both σ and $\Delta\sigma$ were from DREAMS data. The reference depth was set to 10 m, because the mixed layer in the Sea of Japan is always deeper than that depth during winter [*Lim et al.*, 2012]. Horizontal resolution of this model is $1/12^\circ \times 1/15^\circ$ following the DREAMS dataset.

In the mixed-layer model, the time derivative of mixed-layer temperature is expressed by the sum of heat flux, horizontal heat advection, and entrainment terms. We omitted horizontal eddy diffusion because its contribution

is negligibly small in determining frontal structure in the Sea of Japan [*Zhao et al.*, 2014]. Thus, the equation is

$$\frac{\partial T'_{ML}}{\partial t} = \frac{(Q_{net} - Q(-h))'}{c_p \rho h} - \mathbf{U'_{ML}} \cdot \nabla T_{ML} - \frac{w' \Delta T}{h}, \tag{2.2}$$

where T and $\mathbf{U}$ represent temperature and current velocities, respectively, and subscript "ML" refers to the vertically averaged value in the mixed layer. Values with prime symbols represent anomalies from the seasonal trends unrelated to the passage of cyclones, e.g., $T' = T - \overline{T}$, where the overbar represents the seasonal trend (see Appendix A for details of nonlinear anomalous term). Q_{net} denotes net heat fluxes given by OAFlux, h the mixed-layer depth, c_p the specific heat of seawater (3986 J kg^{-1}K^{-1}), and ρ seawater density (constant in the computations at 1025 kg m^{-3}). The penetrative radiative flux at the base of the mixed layer, $Q(-h)$, is given by

$$Q(-h) = Q(0)[Rexp(-h/\gamma_1) + (1-R)exp(-h/\gamma_2)], \tag{2.3}$$

where $Q(0)$ is shortwave radiation at the sea surface (OAFlux). R, γ_1 and γ_2 are 0.58, 0.35 and 23, respectively, which correspond to type I water [*Paulson and Simpson*, 1977].

Entrainment speed anomaly, w', is defined as

$$w' = (\frac{\partial h}{\partial t})' + \mathbf{u'}_{-h} \cdot \nabla h + w'_{-h}, \tag{2.4}$$

where $\mathbf{u'}_{-h}$ is the horizontal velocity anomaly at the base of the mixed layer. The entrainment speed was set to 0 for $w' < 0$ (upward is positive). ΔT is the temperature difference between the mixed layer and layer just below (from DREAMS data). Here, w'_{-h} is the anomaly of Ekman pumping velocity,

computed using wind stress curl as

$$w'_{-h} = curl_z(\frac{\tau'}{\rho f}), \tag{2.5}$$

where τ is the wind stress vector derived from the bulk formula, $\tau = \rho_{air} C_D |\mathbf{U_{10}}| \mathbf{U_{10}}$, and $\mathbf{U_{10}}$ is the 10-m wind vector from QuikSCAT and ASCAT. Air density ρ_{air} is 1.2 kg m^{-3}, and C_D is the drag coefficient calculated following *Large and Pond* [1981].

After calculating the above heat budget equation, temporal variation of mixed-layer temperature ($\Delta T'_{ML}$) can be easily obtained as follows.

$$\begin{aligned} \Delta T'_{ML} &= (\frac{(Q_{net} - Q(-h))'}{c_p \rho h})\Delta t + (-\mathbf{U'_{ML}} \cdot \nabla T_{ML})\Delta t + (-\frac{w' \Delta T}{h})\Delta t, \\ &= \Delta T'_{ML_Q} + \Delta T'_{ML_A} + \Delta T'_{ML_E} \end{aligned} \tag{2.6}$$

where 24 hours was chosen for Δt so that the excursion of anomalous currents ($< O(10)$ cm s^{-1}) was shorter than the grid spacing ($1/12^\circ$ and $1/15^\circ$ for longitude and latitude, respectively) within the time increment. The boundary condition for T_{ML} was from DREAMS data at all straits connected to outside seas.

The computation procedure was as follows. First, T_{ML} (and h and ΔT) on the right-hand side of Equation (2.6) was from DREAMS data on the day prior to peak days, peak days, and one day after peak days. Hence, $\Delta T'_{ML}$s on the peak days, one day after peak days, and two days after peak days were computed separately using Equation (2.6). The computation was done for those 3 days because, as shown later in Section 3, SST variation terminated within 3 days with the passage of extratropical cyclones and surface cooling. These three time computations were conducted around all peak days over the study period; see solid dots in Figure 2.2b for the case of 2004-2005. Temperature increments were all summed over those computations (hence,

we obtained $\Delta T'_{ML}$ two days after minus one day before peak days) and averaged over the study period.

Thereafter, we decomposed the temporal variation of gradient magnitude ($\Delta G'_{ML}$) in the mixed-layer model into contributions of heat flux ($\Delta G'_{ML_Q}$), horizontal heat advection ($\Delta G'_{ML_A}$) and entrainment ($\Delta G'_{ML_E}$), under the assumption of a linear relationship [e.g. *Kazmin and Rienecker*, 1996; *Zhao et al.*, 2014], as

$$\Delta G'_{ML} = \Delta G'_{ML_Q} + \Delta G'_{ML_A} + \Delta G'_{ML_E}. \tag{2.7}$$

The above three components of $\Delta G'_{ML}$ were computed separately using the corresponding three components of $\Delta T'_{ML}$ (right-hand side of Equation (2.6)) over the 3 days. For instance, G'_{ML_Q} on the peak days was computed by substituting the "pseudo" temperature

$$T_{pseudo} = T_{ML} + \Delta T'_{ML_Q} \tag{2.8}$$

into Equation (2.1), where T_{ML} was the temperature field one day prior to peak days in this case. In addition to the peak days, G'_{ML_Q} was computed in the same manner for one day before, one day after, and two days after peak days. Then, three time increments of G'_{ML_Q} (i.e., $\Delta G'_{ML_Q}$) were computed using the above four G'_{ML_Q} estimates. Lastly, these three $\Delta G'_{ML_Q}$ estimates were summed (as $\Delta T'_{ML_Q}$) to quantify the contribution of heat flux to frontal sharpness. Likewise, the contributions of horizontal heat advection ($\Delta G'_{ML_A}$) and entrainment ($\Delta G'_{ML_E}$) to that sharpness were computed.

2.3 Results

Using our threshold, 104 peak days were chosen for periods of strong surface cooling during the winters of 2003-2011. As an example, a time series during winter 2004-2005 is shown in Figure 2.2b, in which solid dots represent the peak days. During these strong flux events, it is likely that there were extratropical cyclones developing near the Sea of Japan, since they have a typical timescale of the extratropical cyclone activity in East Asia [e.g., *Nakamura*, 1992; *Nakamura et al.*, 2002; *Isobe and Beardsley*, 2007]. However, as mentioned by *Dorman et al.* [2004], there might be some events that are not associated with cyclones. For this reason, we visually checked all SLP maps for removal of the non-cyclone days, resulting in 102 days for subsequent analyses.

Composite maps of 1–8-day band-pass filtered SLP around peak days clearly demonstrate strong cooling when extratropical cyclones developed around the Sea of Japan (Figure 2.3). A low-pressure system west of that sea strengthened rapidly from one day before peak days (Figure 2.3a) to peak days (Figure 2.3b). Strong northerly winds (and thus sea surface cooling) are indicated by tightly packed SLP contours over the sea on the peak days. Only 1 day after peak days, the low-pressure system center moved to the south of the Kamchatka Peninsula (at the northeast corner of the map), and the central pressure deepened from -1 to -6 hPa (Figure 2.3a to c). The system moved further northeast and left the Figure 2.domain on two days after peak days (Figure 2.3d). As the low center moved northeastward, the filtered SLP over the Sea of Japan increased (from Figure 2.3b to d), suggesting that both northerly winds and upward heat flux were subdued. It is therefore obvious that these sequential 4 days categorized by heat flux effectively represented a time series of developing extratropical cyclones near the Sea of Japan, as the examples show in Figure 2.1.

The composite maps of turbulent fluxes, air-sea temperature differences, and wind speeds clearly demonstrate how extratropical cyclones modified the Sea of Japan on the peak days (Figure 2.4). The map of wind speed clearly shows a strong cold-air outbreak over the sea, across which the extratropical cyclones passed. Hence, strong surface cooling (< -400 W m^{-2}) covered the entire sea (Figure 2.4a), although upward heat flux in the south was greater than in the north. This inhomogeneity of heat flux is likely attributable to the SST distribution across the Sea of Japan, where the Tsushima Warm Current empties into its southern portion. Nevertheless, the anomaly of turbulent fluxes from the winter average reveals cooling associated with the cold-air outbreak under strong northwesterly wind (see contours of -250 W m^{-2} in Figure 2.4d and wind speed in Figure 2.4c). During the cold-air outbreak, the air-sea temperature difference reached 12 °C (Figure 2.4b), 4 °C greater than the average over the Sea of Japan during winter [*Choi and Zhang*, 2005]. Although the cold air is heated upon moving southeastward over the relatively warm ocean, that air affected the entire Sea of Japan because the anomaly of the difference remained 2 °C even when the cold-air mass reached the Japanese archipelago. In addition to the air-sea temperature difference, the cold air effect across the entire sea is evident in the wind field. A jet-like northwesterly wind (greater than 14 m s^{-1}) was evident near Vladivostok because of an orographic gap (Figure 2.4c) [*Kawamura and Wu*, 1998], from which a wind speed of 6 m s^{-1} higher than the winter average extends southeastward (Figure 2.4f). The combination of the anomalous air-sea temperature difference and wind speed produced the strong cooling that prevailed across the Sea of Japan during the cold-air outbreak associated with extratropical cyclone passage.

After removal of the seasonal trends, temporal variations of meridional SST anomaly (SSTA) profiles across the subpolar front (see lines on the map of G (Equation (2.1)) in Figure 2.5a) show that the timescale required for SST reduction over the Sea of Japan is around 3 days during cyclone passage (Figure 2.5b). First, the temperature decreased about 0.1–0.2 °C on the peak days,

decreasing by another 0.1–0.2 °C during subsequent peak days. Thereafter, SSTA declined slightly from one day (red curve in Figure 2.5b) to two days (dash-dot curve) after the peak days. The reduced temperature remained cool even on 4-days after the peak days. Moreover, the frequency of winter cyclones (i.e., intervals between peak days; Figure 2.5c) shows that nearly half (45%; see right ordinate in Figure 2.5c) arrived within 4 days after the prior cyclone passage. These short intervals imply that, as speculated in the introduction, extratropical cyclones over the Sea of Japan may be affected by prior cyclones because of altered SST and/or frontal sharpness [*Graff and LaCasce*, 2012]. However, the present study did not treat this potential two-way coupling, because the objective was to elucidate a "preconditioning" revealed by temperature, i.e., subpolar front modulation by the passage of earlier cyclones.

Of particular interest is how much SST was reduced by a single cyclone (i.e., cooling) during the typical timescale of passage (we selected "3 days" in the present study because of the tallest bar in Figure 2.5c). We thereby estimated the reduction by taking the difference between SSTAs one day before and two days after peak days. As shown in Figure 2.6 (left panel), SST across the entire Sea of Japan cooled by > 0.2 °C on average after the passage of a single cyclone. It is interesting that this SST reduction was not homogenous across the sea but was locally great along the subpolar front, with a maximum of $>$ 0.4 °C. This cooling pattern substantially deviates from the patterns of turbulent heat flux (Figure 2.4) which shows that it is the ocean process (likely within the mixed-layer) that strongly contributes to the cooling pattern and the change in front, not the heat flux itself.

This temperature reduction contributed more than half (51.4 %) of the total cooling (without detrending) during these three days, and it increased to $>$ 60 % around the subpolar front (not shown). Further, the sharpness of the subpolar front intensified (i.e., frontogenesis) by ~ 0.1 °C $(100$ km$)^{-1}$ (3–4 %

of total frontal sharpness) after the passage of a single developing cyclone (right panel of Figure 2.6). The SST reduction and frontogenesis were both relatively small but statistically significant, as suggested by a t-test with 95% confidence level. Moreover, the intensification of frontal sharpness covered not only over the subpolar front but also the southern regions (see the 0 °C $(100\ \mathrm{km})^{-1}$ contour in the right panel of Figure 2.6). This suggests that the subpolar front was likely to shift southward, enhancing its sharpness with the passage of a single extratropical cyclone. Although further examinations will be required, it is speculated that the synoptic location of the subpolar front may be determined by the tug of war between the cyclones trying to push the front southward (and thus intensifying it) and the Tsushima Warm Current or the insolation that acts to restore the front location to where it is supposed to be.

2.4 Discussion

2.4.1 SST Reduction

Before addressing the cause(s) of the aforementioned SST reduction using the mixed-layer model, we must ensure that our conclusions are robust, and will not be largely influenced by the definition of the mixed-layer depth. Figure 2.7 shows that mixed-layer depth (left panels) and mixed-layer averaged temperature and current fields (right panels) were nearly independent of the choice of $\Delta\sigma$. Thus, for simplicity, we only show results of the case with $\Delta\sigma = 0.03$ kg m^{-3} in the following sections.

The result of the mixed-layer model was compared with the aforementioned SST reductions based on OISST data during the cold-air outbreaks associ-

ated with extratropical cyclones (Figure 2.8). As suggested by the temporal variations of meridional profiles (Figure 2.5b), we show the temperature increment over 3 days, i.e., two days after minus one day before peak days, using Equation (2.6). For ease of comparison, model results with DREAMS resolution were smoothed to the same grid size as the OISST dataset ($1/4°$). Figure 2.8a shows that the mixed-layer model did a reasonable job of reproducing a "local" cooling along the frontal zones at 40 °N. Model results show that temperature reduction was less than the $\Delta SSTA$ by 0.1 °C, probably because of vertical integration over the mixed layer, rather than the sea surface observation from satellites.

The contributions of each component (Figure 2.8b) show that the surface cooling along the subpolar front results mainly from the heat flux (greater than -0.2°C). SST reduction derived from the heat flux ($\Delta T'_{ML_Q}$) was widespread over the area from 38 °N to 42 °N, with the maximum at the area center. The horizontal pattern of turbulent flux anomalies (Figure 2.4d) caused by the cold-air outbreak is unlikely to explain the localization along the subpolar front. Thus, $\Delta T'_{ML_Q}$ should be controlled by mixed-layer depth (left panels in Figure 2.7), such that a relatively shallower (deeper) mixed layer causes a larger (smaller) SST reduction because of a difference in heat capacity. By comparing the mixed-layer depth and current map (Figure 2.7), we can see that the shallow mixed layer in the central Sea of Japan is associated with a cyclonic ocean circulation in a geostrophic sense, especially over the northern region.

Nonetheless, heat flux is the dominant contributor to the localized cooling along the subpolar front. Horizontal heat advection ($\Delta T'_{ML_A}$) provides a non-negligible fraction (-0.1 °C) of the temperature reduction along the front and is further discussed in the next section. Unlike the other two components, the entrainment ($\Delta T'_{ML_E}$) only generates substantial SST cooling (more than -0.2 °C) far from the front, and its contribution is negligibly

small over most of the Sea of Japan. The small entrainment contribution may result partly from the deeper mixed-layer in our analyses (∼70 m; see the frontal region in Figure 2.7) than that estimated in other studies such as *Lim et al.* [2012] (30–50 m; see their Figure 9) because of different datasets and criteria. Nonetheless, our analyses are still acceptable because observed temperature differences are consistent with the modeled ones (Figure 2.8a).

2.4.2 Localized Cooling

Aside from the turbulent heat fluxes associated with mixed-layer depth, further examination is required to uncover the cause of localized cooling along the subpolar front from horizontal heat advection. The current anomalies relative to winter trend provided in the DREAMS data (upper panel of Figure 2.9) show that during the passage of extratropical cyclones, there was a nearly uniform southwestward surface current over the Sea of Japan on the peak days. These detrended current anomalies occupy the entire sea, so we must find a driving force with spatial scale larger than the sea and temporal scale shorter than the winter season. Northwesterly wind anomalies associated with synoptic-scale extratropical cyclones (Figure 2.3b and Figure 2.9 lower panel) are consistent with the southwestward current anomalies in the sense of the Ekman flow (defined by $\tau/\rho f h$ in this study). Therefore, it is believed that this strong northwesterly wind, triggered by cyclone passage, engenders southwestward (cross-frontal) Ekman flow, which transports the cold water mass that ultimately causes the local SST reduction along the front.

To confirm the above scenario, we computed Ekman flow using the wind anomalies (Figure 2.10a) to compare with the current anomalies from the DREAMS dataset. Current anomalies included small-scale features, probably because of the superposition of mesoscale (on the order of $\sim$ several

hundreds of kilometers) eddies. Thus, the anomalous currents are slightly weaker than the Ekman flow. Nonetheless, both represent the same large-scale southwestward flows. In addition, strong current anomalies were found in the central Sea of Japan. To examine whether these current fields could cause the localized cooling along the subpolar front, we calculated horizontal heat advection on the peak days using these two current fields in conjunction with the composite SST field from OISST (Figure 2.10b). Figure 2.10c shows that the temperature reduction that results from horizontal heat advection by the current anomalies is reasonably consistent with that by Ekman flow.

For more quantitative assessment of this basin-wide southwestward Ekman flow, we separated it into cross-frontal (v_n, normal to the isotherms) and along-frontal (u_s, along the isotherms) components, using curvilinear natural coordinates as follows.

$$v_n = -sin\varphi u + cos\varphi v, \quad u_s = cos\varphi u + sin\varphi v, \tag{2.9}$$

where u and v are the Ekman flows in the zonal and meridional Cartesian directions, respectively, and φ represents the counterclockwise isotherm direction relative to the x axis.

Figure 2.11a shows that this southwestward Ekman flow was approximately parallel to isotherms north of the subpolar front (42–45°N), while the cross-frontal components dominated in other areas, especially near the front (over 60 % of total flow). To dramatize the importance of the cross-frontal component around the subpolar front, we normalized this component in two ways. After the normalization by current speed, vigorous cross-frontal Ekman flow was revealed north of 40 °N (Figure 2.11b left). Intensification of the cross-frontal Ekman flow at the front is similar to the observed results in *Thomas and Lee* [2005]. However, their intensification was within a narrow band (<

10 km; see their Figure 2.11), one order of magnitude smaller than our area (Figure 2.11b). In our study, such a pattern was mainly caused by the jet-like wind field that formed by the topography along the Russian coast (see wind speed in Figure 2.4c and vectors in the lower panel of Figure 2.9) and partially by the shallow mixed-layer depth (inversely proportional to Ekman flow) around the front (left panels of Figure 2.7). After the normalization by frontal sharpness (G, in Equation (2.1)), heat advection locally reduced the temperature via this cross-frontal Ekman flow at the frontal region (clearly revealed by the right panel of Figure 2.11b).

It is possible that a frontogenetic process associated with ageostrophic secondary circulations and Ekman pumping/suctions occurs locally along the frontal interface, as shown by theoretical and non-hydrostatic numerical models in *Thomas and Lee* [2005] and *Yoshikawa et al.* [2012]. However, their studies are not applicable to the process revealed by the present analysis. Much finer temporal (sub-inertial timescale) and spatial ($<$ 10 km) scales are both required for reproducing such processes and, as such, could not be captured by our mixed-layer model and datasets. Nonetheless, the aforementioned studies suggest that the sharpness of the subpolar front would be enhanced more than we expected if the fine-scale processes are incorporated in a numerical model approach.

2.4.3 Contribution to Frontogenesis

Figure 2.6 (right panel) shows that the gradient magnitude increased by $\sim$ 0.1 °C (100 km)$^{-1}$ along the subpolar front, because of the passage of a single extratropical cyclone. Using Equation (2.7), we calculated the contributions of heat flux ($\Delta G'_{ML_Q}$) and horizontal heat advection ($\Delta G'_{ML_A}$) to the enhancement of frontal sharpness (note that the entrainment is excluded here, because its effect is negligibly small). The sum of these two components is

shown in Figure 2.12a, and each contribution is depicted in Figure 2.12b. The modeled results reproduced frontogenesis well, in both magnitude and locations. Also shown by Figure 2.12a is that the linear assumption of Equation (2.7) is likely to be justified because the sum of the two components is nearly identical to $\Delta G'$. Looking at each contribution (Figure 2.12b), one sees that heat flux has a secondary effect on the frontogenesis, although that flux accounts for about two-thirds of SST reduction (Figure 2.8b). This is because the heat flux has a spatial scale much larger than the width of the subpolar front. However, even with one-third of the contribution to SST reduction (Figure 2.8b), the horizontal heat advection can be regarded as the primary enhancement of frontal sharpness (see similarity to panel a), because of the localized cooling along the front.

2.5 Summary

The mechanisms of SST reduction and frontogenesis in the winter Sea of Japan are revealed in this chapter (Figure 2.13). Overall, our analyses show that the subpolar front in the Sea of Japan intensifies after passage of a developing extratropical cyclone. Therefore, the suggestion is the formation of a two-way coupling process between the SST (hence the sharp subpolar front) and the extratropical cyclones. Many studies have demonstrated that enhanced frontal sharpness intensifies cyclones [e.g. *Yamamoto and Hirose*, 2007] and/or alters their trajectories via an anchoring effect [e.g. *Ogawa et al.*, 2012]. There remains a question as to how such hydrographical changes in the Sea of Japan affect subsequent extratropical cyclones. This is going to be addressed in Chapter 3.

Also, for a further interest in other marginal seas in the East Asian region, we made an extended analysis including the Yellow Sea, the East China Sea,

Kuroshio region, Kuroshio Extension, and the Sea of Okhotsk. See Appendix B for details.

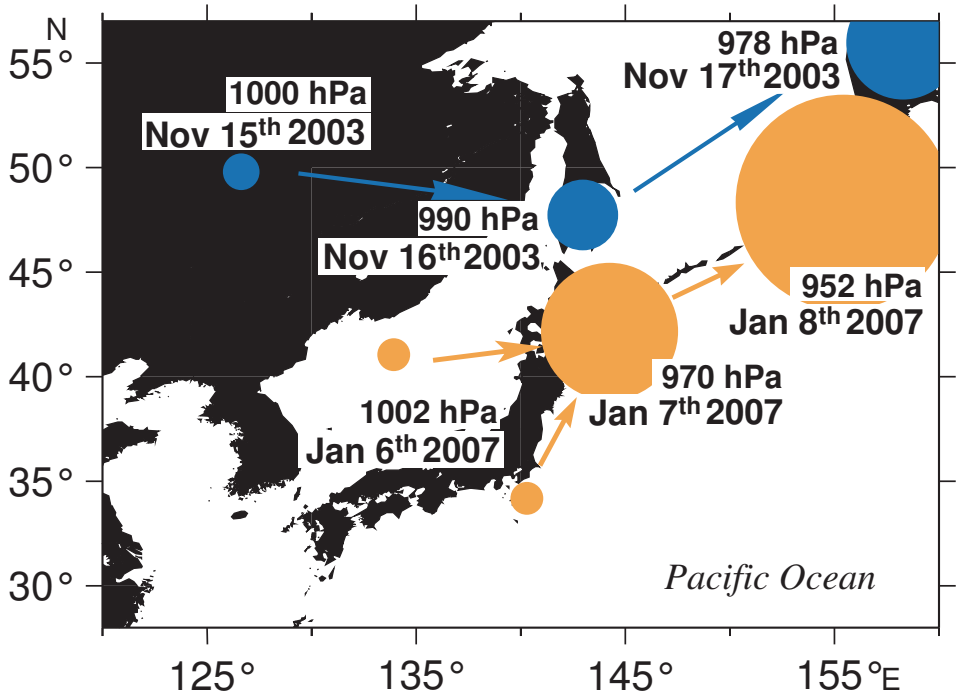

Figure 2.1: Study area and examples of extratropical cyclones in winter. Development of two winter cyclones based on NCEP-DOE reanalysis II dataset is shown by variable circle diameter (D), according to D=2 $\times$ (1010 $-$ central SLP) where the SLP is regarded as a non-dimensional value. Annotations near the circles denote the central SLP and date.

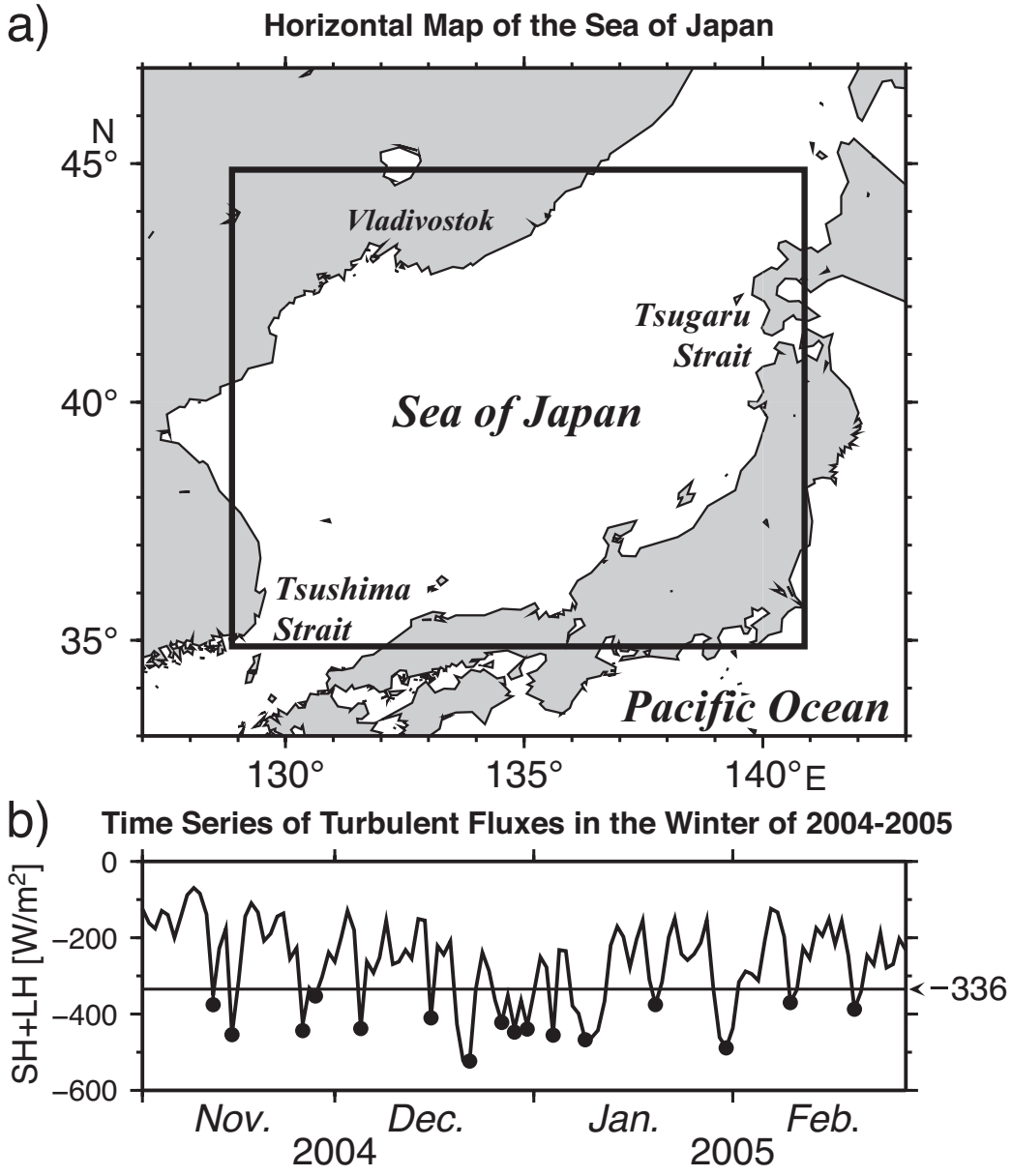

Figure 2.2: Horizontal map of the Sea of Japan, with the box over which was averaged the turbulent heat fluxes (a). Time series of spatially averaged turbulent fluxes in 2004–2005 winter are shown as an example in (b). Solid dots in (b) show peak days (see the text for meaning), and the solid line represents the value of the 80th percentile (-336 W m^{-2}) .

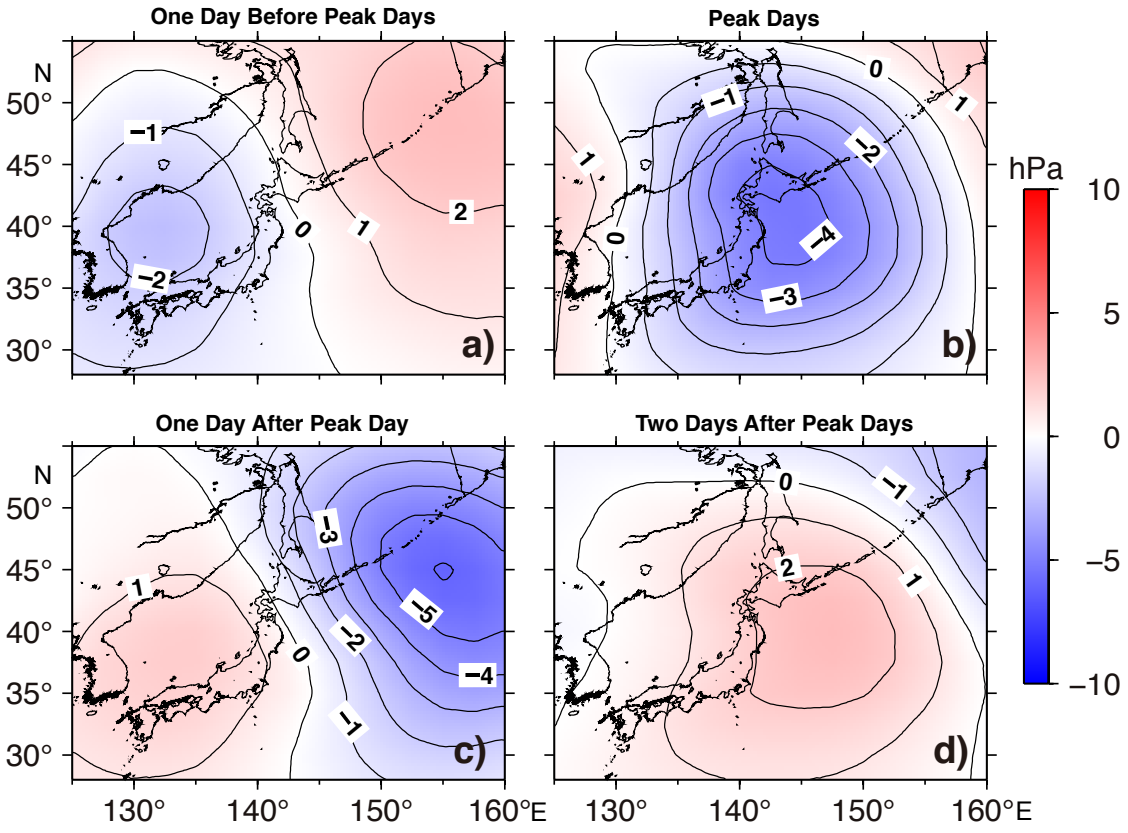

Figure 2.3: Composite maps of 1–8-day band-pass filtered SLP on one day before peak days (a), peak days (b), one day after (c), and two days after (d) peak days. Contour intervals are 1 hPa in all panels.

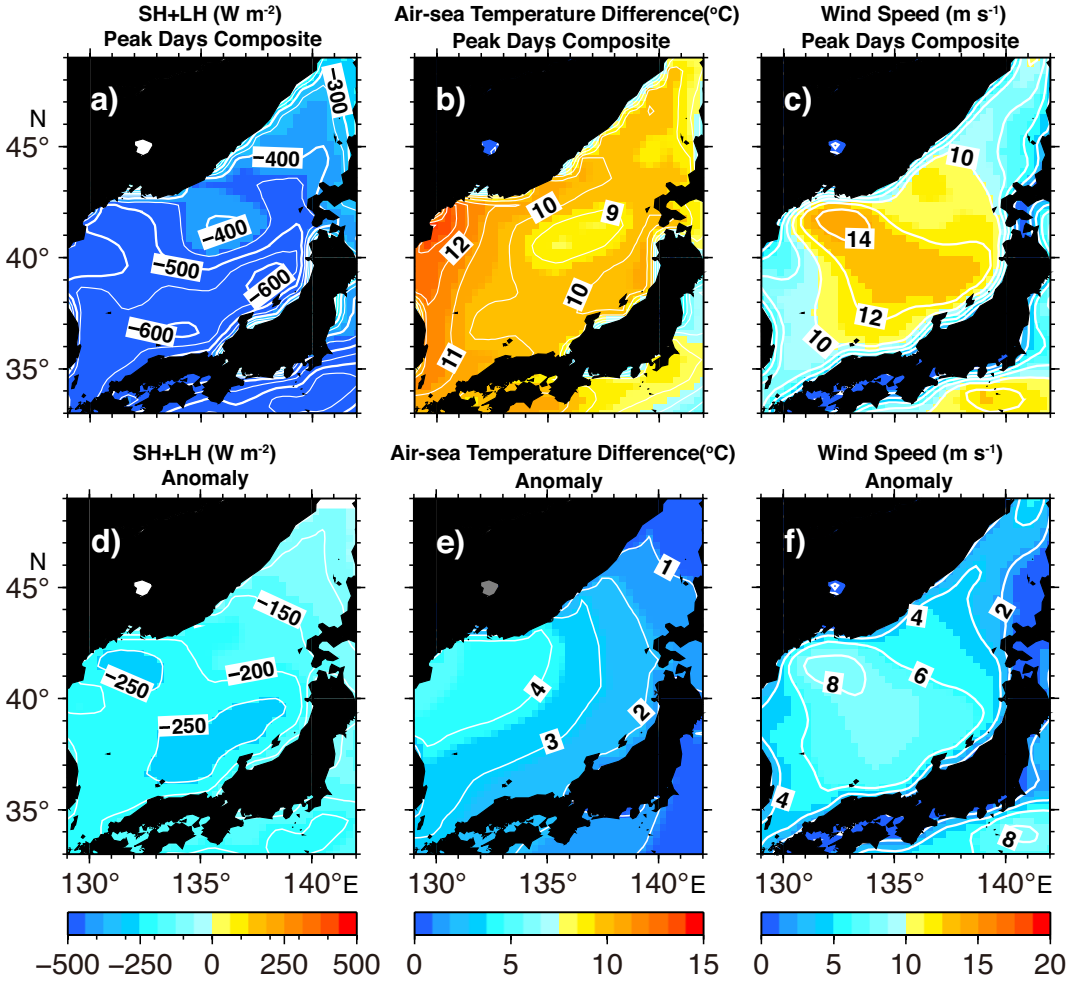

Figure 2.4: Composite maps of turbulent fluxes (a; W m^{-2}), air-sea temperature difference (b; °C), and wind speed (c; m s^{-1}) on peak days. Lower panels also show turbulent heat fluxes (d), air-sea temperature difference (e) and wind magnitude (f), but for anomalies relative to the long-term average in winter. Contour intervals of panels (a, d), (b, e), and (c, f) are 50 W m^{-2}, 1 °C, and 2 m s^{-1}, respectively.

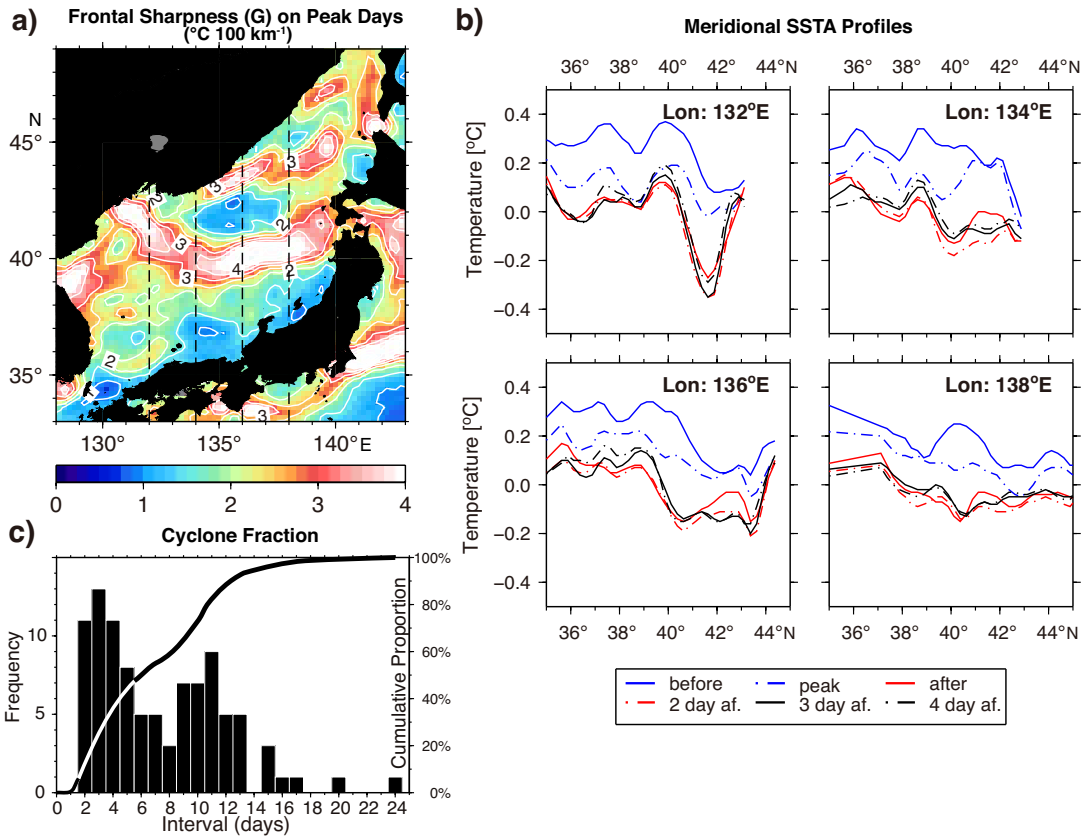

Figure 2.5: Relationship between temperature field and passage of extratropical cyclones. Panel a shows the distribution of gradient magnitude (G) on peak days, by contours (every 1 °C (100 km)$^{-1}$) and color shading. Dashed lines show the locations of four meridional profiles of SSTA, whose data are displayed in panel b. The meridional profiles are composited on six sequential days around the peak days (b), from one day before to 4-days after. Panel c graphs frequency (digits indicate numbers) of the interval (in days) between two consecutive cyclones during 2003–2011. The cumulative proportion is also shown by a bold solid curve.

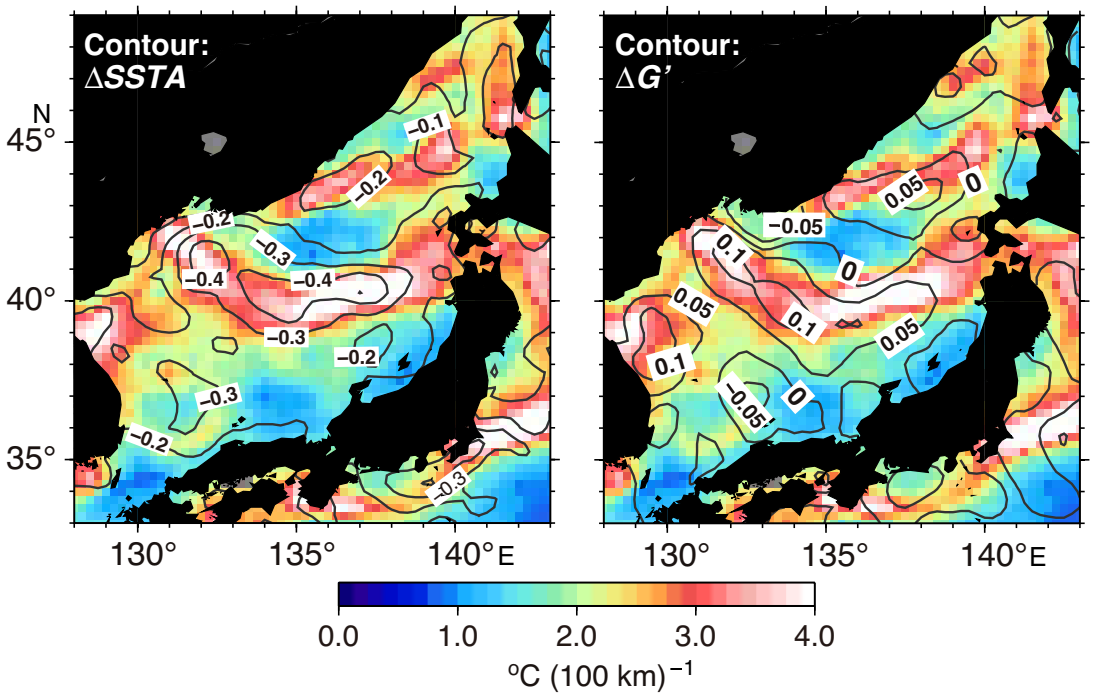

Figure 2.6: Composite maps of temperature differences ($\Delta SSTA$, left panel) and differences of gradient magnitude ($\Delta G'$, right panel) two days after minus one day before peak days, which are superimposed on frontal sharpness during peak days (color shading in both panels). Contour intervals are 0.1 °C and 0.05 °C (100 km)$^{-1}$, respectively.

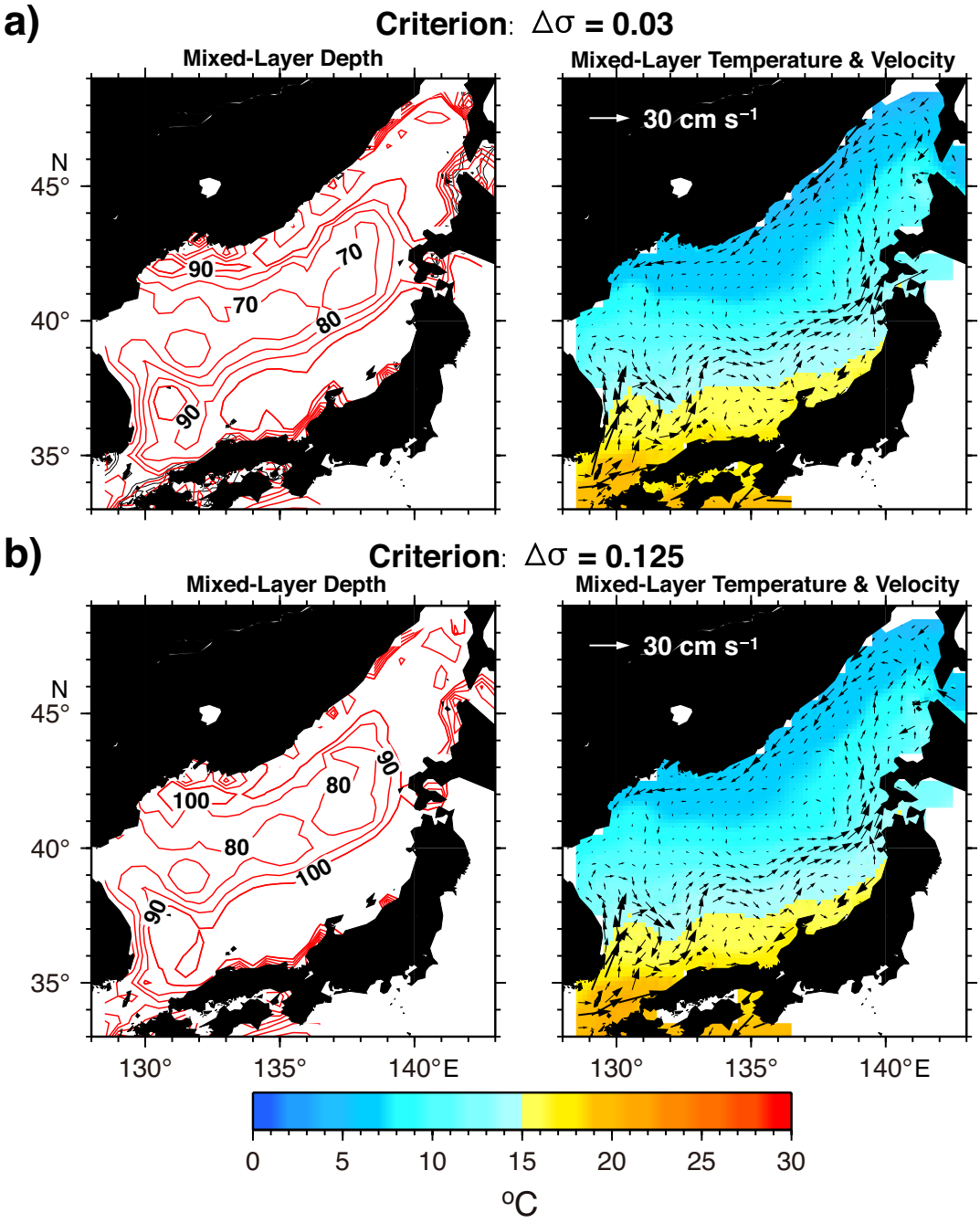

Figure 2.7: Mixed-layer depth (contours in left panels), mixed-layer temperature (color shading in right panels), and horizontal currents averaged over the mixed layer (vectors in right panels), provided by DREAMS data for the Sea of Japan. Panels a and b show the same properties but for different definitions of mixed-layer depth, with $\Delta\sigma = 0.03$ kg m^{-3} (a) and $\Delta\sigma = 0.125$ kg m^{-3} (b), respectively.

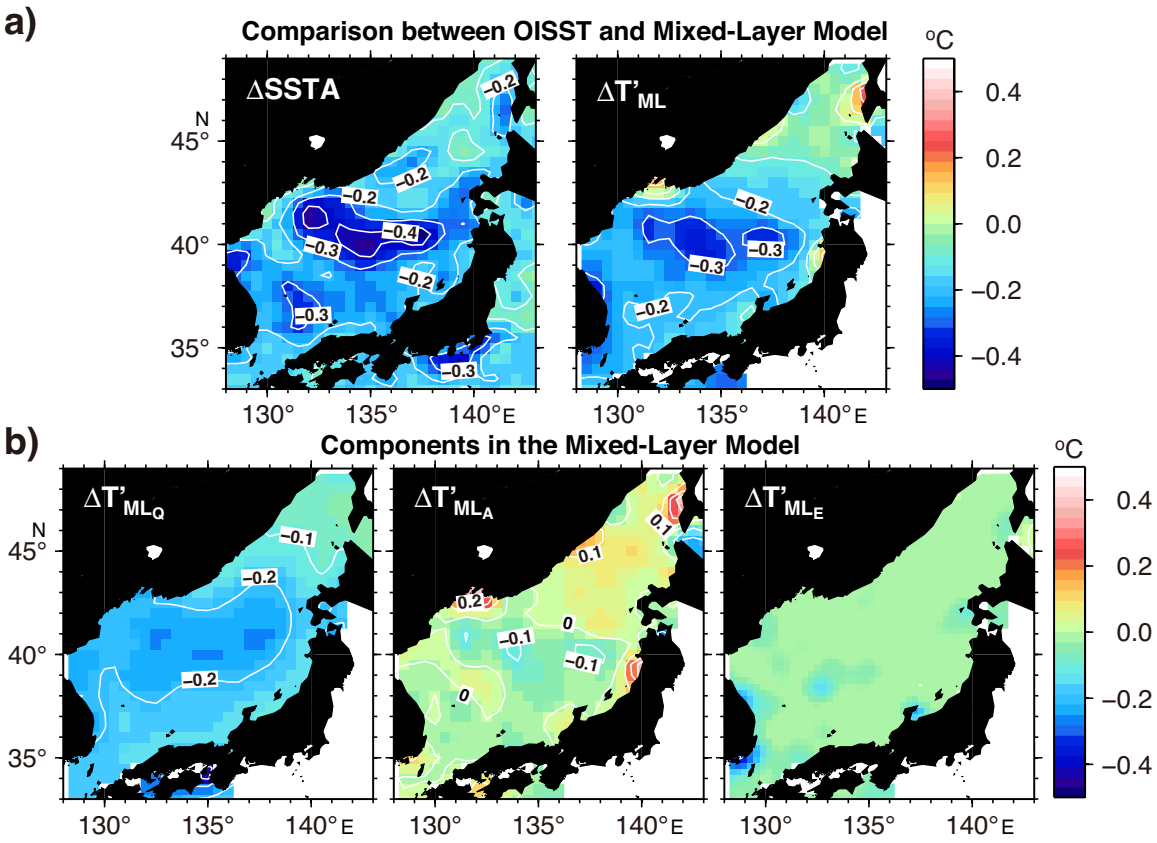

Figure 2.8: Temperature differences estimated as two days after minus one day before peak days (color shading and contours). Panel a shows temperature difference derived from OISST data ($\Delta SSTA$; left) and from mixed-layer model of present study (right). Panel b shows contributions of heat flux ($\Delta T'_{ML_Q}$; left), horizontal heat advection ($\Delta T'_{ML_A}$; middle), and entrainment ($\Delta T'_{ML_E}$; right) to SST reduction in panel (a). For ease of comparison with OISST data, results were smoothed onto coarse grids ($1/4° \times 1/4°$) as used by OISST data. Contour intervals of all panels are 0.1 °C.

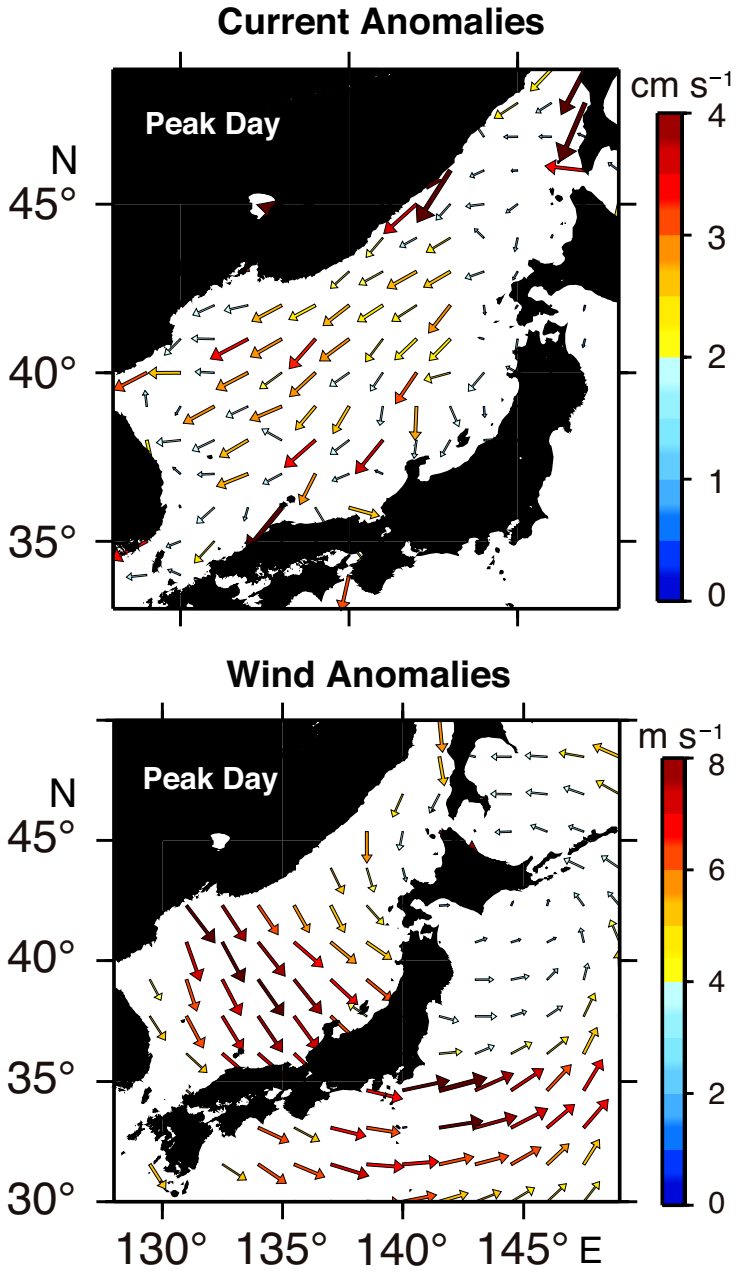

Figure 2.9: Current (upper panel) and wind (lower panel) anomalies on peak days. To avoid overcrowding, current vectors are plotted every sixth grid. Speeds of current and wind are shown by vector colors and length.

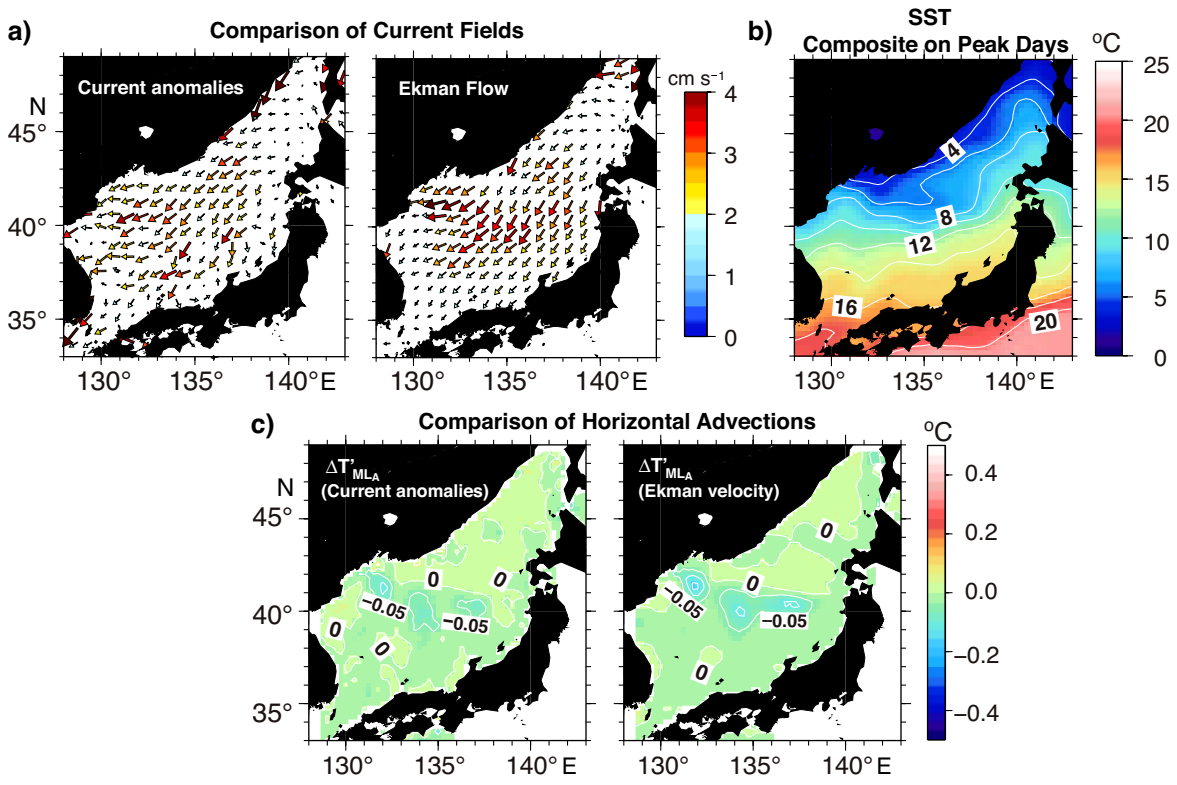

Figure 2.10: Comparison between current anomalies and Ekman flow. Panel a depicts current anomalies obtained from DREAMS (left; same as Figure 2.9 but at higher resolution) and Ekman flow calculated from either QuikSCAT or AS-CAT (right). Wind speed is represented by vector colors and length. Panel b shows SST map composited for the peak days using OISST data. Panel c shows temperature reduction estimated using the values in panels a and b for 24 hours on peak days. Contour intervals are 2 °C and 0.05 °C in (b) and (c), respectively.

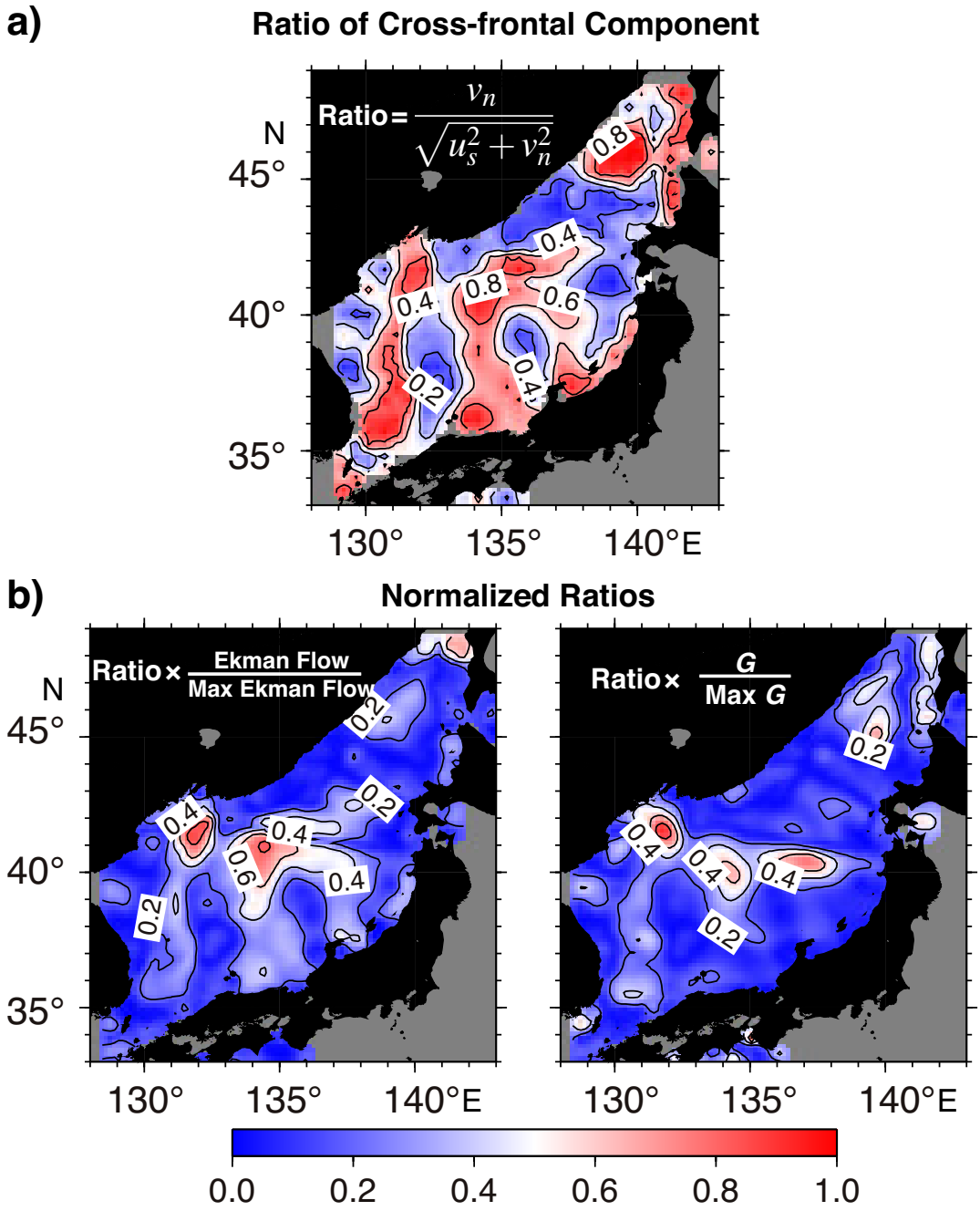

Figure 2.11: Ratio of the cross-frontal component (v_n) to total Ekman flow ($\sqrt{v_n^2+u_s^2}$) (a) and ratios (b) normalized by the maximum Ekman flow (left: (a) $\times(\sqrt{v_n^2+u_s^2}/(\sqrt{v_n^2+u_s^2})_{Max})$) and maximum frontal sharpness (right; (a) $\times(G/(G)_{Max})$). Subscript "Max" denotes the maximum value in the study area. Contour interval is 0.2.

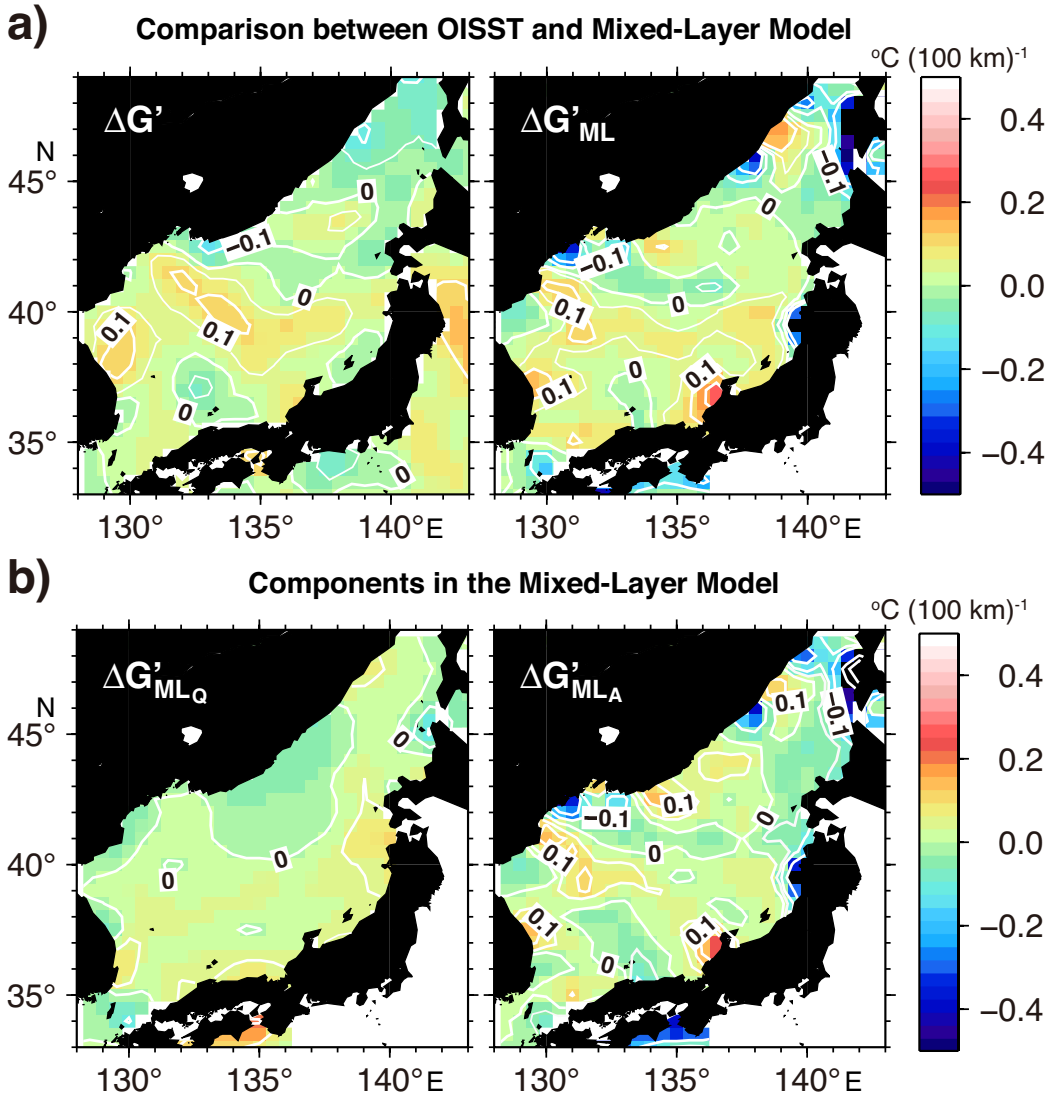

Figure 2.12: Comparison of differences of gradient magnitude ($\Delta G'$). Panel a shows estimated $\Delta G'$ for two days after minus one day before peak days based on OISST data (left; same as the right panel in Figure 2.6). Right panle is the same as the left but for mixed-layer model. Panel b shows contributions of heat flux ($\Delta G'_{ML_Q}$, left) and horizontal heat advection ($\Delta G'_{ML_A}$, right) to $\Delta G'_{ML}$ computed by the mixed-layer model. As in Figure 2.8, results were smoothed onto coarse grids ($1/4° \times 1/4°$). Contour intervals of all panels are 0.05 °C (100 km)$^{-1}$.

Chapter 3

Modulation of Extratropical Cyclones owing to Previously-passing Cyclones via the SST Anomaly over the Sea of Japan in Winter

3.1 Introduction

It is well-known that sea surface temperature (SST) features such as oceanic fronts (i.e., the SST gradient) are critical on cyclone development [e.g., *Small et al.*, 2008; *Kwon et al.*, 2010, and references therein]. Sensitivity studies demonstrated that a strong (weak) SST gradient could lead to an intensified (weakened) cyclone activities and poleward (equatorward) shift of storm tracks [*Brayshaw et al.*, 2008; *Sampe et al.*, 2010] . Moreover, based on both

observed and modeled evidences, some recent studies demonstrated that the mesoscale SST features have a great impact on the air-sea interactions [e.g., *Chelton and Xie*, 2010; *Putrasahan et al.*, 2013; *Masunaga et al.*, 2016] and therefore the cyclogenesis [e.g., *Willison et al.*, 2013; *Ma et al.*, 2017].

Results in Chapter 2 showed that, the Sea of Japan experienced a strong surface cooling, under which SST reduces over -0.5 °C along the subpolar front region, and such SST reduction maintains, at least, during the course of 4 days until the recovering to the SST before the cyclone passage. It suggested that the Sea of Japan may become the link between two consecutive cyclones, acting as an "oceanic bridge", such that an extratropical cyclone passing over the Sea of Japan modulates the following cyclone passing over the sea. This idea is likely to occur because the period for the SST reduction to maintain ($>$ 4 days) is comparable with the sub-weekly scale of the interval of extratropical cyclones. Yet, it is still unknown whether this small (~ -0.25 °C on average) and basin-scale temperature anomaly could make any modification detectable in the synoptic scale atmospheric circulation. If this is the case, it is worthwhile to uncover how will the Sea of Japan affect the following cyclone.

In the this chapter, we focus on figuring out two scientific questions raised above: 1) Does the Sea of Japan become an oceanic bridge to link two consecutive cyclones? 2) Does a colder Sea of Japan weaken all the passing cyclones? Following the approach in *Yamamoto* [2013], we will conduct sensitivity experiments on individual cyclones by a regional numerical model, and attempt to find possible roles of the Sea of Japan on the winter extratropical cyclones.

This chapter is organized as follows. Section 3.2 introduces the data source, the model setup and the algorithms for detecting and estimating cyclones. Section 3.3 describes the results of cyclone responses and the detailed ef-

fects of the Sea of Japan on the cyclone activities, followed by section 3.4, which discuss the relationships between cyclone sensitivity and large-scale background environment, and the roles of the SST reduced Sea of Japan on cyclogenesis.

3.2 Materials and Methods

3.2.1 Data Sources

The atmospheric data used in this paper is the 6-hourly National Centers for Environmental Prediction (NCEP) Final (FNL) Operational Global Analysis data [*NCEP*, 2000]. The FNL dataset has a horizontal resolution of 1 degree in latitude and longitude and 27 vertical layers from surface to 10 hPa, collected from November 2003 through February 2011 following Chapter 2. This dataset is used for both initial and lateral boundary conditions in the numerical model and the pre-processing of cyclone detection. The Optimum Interpolation Sea Surface Temperature (OISST) is used as the lower boundary conditions and its horizontal resolution is 0.25 degree in both latitude and longitude [*Reynolds et al.*, 2007; *Banzon et al.*, 2016].

3.2.2 Tracking Centers and Paths

For consistence with the numerical sensitivity experiments on SST modification described in the next subsection, we used the sea level pressure (SLP) from NCEP-FNL to track the extratropical cyclones near the Sea of Japan (115 °-170 °E, 25°-60 °N) during eight winters, as defined from November

to February, in years of 2003-2011. We adopted a simple method of identification and tracking the cyclones among various methods established to date [e.g., *Hodges*, 1999; *Inatsu*, 2009; *Flaounas et al.*, 2014]. Firstly, the cyclone centers were identified as the local minima where the sea level pressure (SLP) lower by 0.5 hPa than the adjacent eight grids (i.e. within a $3^\circ \times 3^\circ$ box in the FNL dataset), and all centers lower than 1010 hPa were recorded. Thereafter, we seek the center of the same cyclone after 6 hours on a $10^\circ \times 7^\circ$ longitude-latitude box, slightly larger than that in *Flaounas et al.* [2014], of which center was identical to the cyclone center. The tracking of the cyclone center was continued until the cyclone moved beyond the lateral boundary of the searching domain. Note that all cyclones with a life time shorter than 24 hours were removed. Finally, among the identified 136 cyclones, we randomly chose 26 cyclones for the sensitivity experiments so as that the cyclones were not concentrated eccentrically around specific trajectories and years.

3.2.3 Model Configuration

Following *Yamamoto* [2013], the numerical sensitivity experiments were conducted using a regional model based on the Weather Research and Forecast (WRF) Version 3.7.1 [*Skamarock et al.*, 2008]. The model domain is shown in Figure 3.1 and resolutions are listed in Table 3.1.

In the present application, two sets of numerical experiments were conducted to examine whether or not the Sea of Japan acts as an oceanic bridge to link two consecutive extratropical cyclones. First, for comparison, control experiments to reproduce selected 26 cyclones were conducted (BF run), where climatological winter SST averaged from 2003 to 2011 was given as the lower boundary (contours in Figure 3.1) for simplicity. Second, the same experiments except that a negative SST anomaly is given within the Sea

of Japan were conducted (the color shading in Figure 3.1; AF run). This anomaly was obtained in the previous chapter containing the SST decreased owing to the cooling generated by the passage of a single cyclone over the Sea of Japan. The modeled difference between BF and AF runs provided us with an influence of a previously-passing cyclone on the following cyclone via SST in the Sea of Japan. All calculations started four days before the target cyclone generated (or appearance of cyclone centers detected by the algorithm described above), and the model was thereafter during the subsequent nine days. The modeled atmospheric properties were saved every 3 hours over the course of each computation. Since we used the same climatological SST field for all cyclones in BF runs, it is hard to validate our results with the observations and/or reanalysis data. Nevertheless, our results shown later were likely to be reliable because the ensemble simulations provided us with a robust result (see Appendix for details).

3.2.4 Indicators of the Effect on Cyclones

Generally, the development of the extratropical cyclone can be evaluated by the deepening rate of the central SLP. In this study, the 12-hour cyclone deepening rate (CDR, *Yoshida and Asuma*, 2004) was calculated for all cyclones, and the changes of CDRs in two runs were used for showing to what extent the cyclones were modified. The formula of CDR in Bergeron (hPa hr^{-1}) can be written as:

$$CDR = [\frac{p(t-6) - p(t+6)}{12}] \frac{sin60^\circ}{sin\frac{\phi(t-6) - \phi(t+6)}{2}}, \tag{3.1}$$

where p is the SLP at the cyclone center, ϕ the latitude, and t the time. We thereafter introduced two criteria for estimating the modifications based on their differences ($\Delta CDR = CDR_{\mathrm{AF}} - CDR_{\mathrm{BF}}$), where the subscripts denote

AF and BF runs, respectively. The cyclones were categorized into: "affected cyclones" when they meet three conditions, $|\Delta CDR| > 0.1$, $CDR_{\mathrm{BF}} > 0.5$, and the duration period longer than 6 hours enough for removing some occasional events, while the others were referred to as "unaffected cyclones". Note that the results were mostly independent of the lower limit of CDR_{BF}, and $|\Delta CDR| > 0.1$ was chosen for removing the unexpected small disturbances.

On the other hand, unlike the deepening rate only offering the local changes at the center of cyclones, the standard deviation (SD) of the geopotential height could show more details of the cyclone activities [e.g., *König et al.*, 1993; *Chang et al.*, 2002] in a Eulerian view. Although the cyclone activities away from the surface level would be less influenced by the orography, the influences in upper layers (such as trough and jet at 500-hPa height) become more dominant than SST in determining the cyclone path, especially on the early stages of the cyclogenesis. Therefore, we used the SDs of the geopotential height at 850-hPa level during the cyclone's lifespan in extracting both the activities of the target cyclone and the cyclone path. Similar results were found when using the 1-8 day bandpass-filtered geopotential height (not shown).

3.3 Results

3.3.1 Effect on the Cyclogenesis

Among the 26 simulated cyclones, we found 20 cyclones (76.9%) were well affected by the cold Sea of Japan, while the remaining 6 cyclones (23.1%) were nearly unaffected. Figure 3.2 shows the paths of the cyclones. Accord-

ing to the criteria defined in Section 3.2.4, we found the cyclones categorized into the affected groups in both the intensifying ($\Delta CDR > 0.1$) and weakening ($\Delta CDR < -0.1$) periods in AF runs; see colored paths in Figure 3.2a. Of note, it seems likely that there is no apparent rule to determine which period comes first. These results suggest that the Sea of Japan cooled by a single cyclone indeed affects the subsequent cyclone, although the influence(s) is (are) more complicated than we might have imagined as either intensifying or weakening monotonically.

The paths of affected cyclones (Figure 3.2a) were mostly located in the southern domain compared to those of the unaffected cyclones (Figure 3.2b). The locations of maximum deepening rate were concentrated in the western North Pacific in the affected cyclones (stars in Figure 3.2a). By contrast, the unaffected cyclones developed greatly over the Sea of Japan or the Sea of Okhotsk, and their paths were unlikely to be influenced by SST reduction within the relatively small Sea of Japan. According to the previous studies [e.g., *Yoshida and Asuma*, 2004; *Yoshiike and Kawamura*, 2009], these differences in cyclone paths were strongly related to the large-scale background circulations, and thus, the suggestion is a potential connection between the cyclone sensitivity to the SST anomaly and the backgrounds.

3.3.2 Response of Cyclone Activities

Among the 20 affected cyclones, we mainly focus on two specific cyclones because they provide us with examples of two distinct responses revealed in remaining cyclone activities as well (shown later). The time evolution of their central SLPs and their paths are shown in Figure 3.3 along with their CDRs.

The first cyclone (hereafter, Cyclone A) was developed in 2005 with a minimum central SLP of 954.3 hPa (Figure 3.3a) and a maximum CDR over 2.00 Bergeron. It generated (firstly detected by our algorithm) over the Sea of Japan on December 25th, and then moved eastward to the Pacific Ocean until it passed through the eastern boundary of our domain. In the sensitivity experiment, the central SLP anomaly (AF-BF runs) of the Cyclone A oscillated in the course of the path (see the dashed curve in the inset graph of Figure 3.3a). Similar oscillation can also be seen in the time series of CDR (shown by the dark and light gray shadings). However, it seems likely that the cyclone path in the AF run was almost identical to that in BF run.

The second cyclone (hereafter, Cyclone B) was developed over the East China Sea (identified on January 20th, 2006), and passed south of Japan with a minimum central SLP of 946.4 hPa and a maximum CDR of 1.96 Bergeron. It traveled northeastward in most part of its lifetime, but abruptly turned westwards to the Sea of Okhotsk during the final part of its path. Unlike the Cyclone A, Cyclone B was greatly intensified (decreased by $>$10 hPa) in the sensitivity experiment and its path was also shifted poleward except in the area around 50 °N at the abrupt turn; compare solid and dashed curves in Figure 3.3b.

Figure 3.4a represents the activities of the Cyclone A and B based on the SD of 850-hPa geopotential height. The maps of increasing SD consistent with the cyclone development along the SLP-based tracking algorithm see the white dots on the solid curves in the left panels. The right panels in Figure 3.4 showed the modifications in their activities obtained by the sensitivity experiments in terms of the SD difference between AF and BF runs. Of particular interest is that the wave-like pattern revealed in the central SLP anomaly of the Cyclone A (inset graph in Figure 3.3a) is not spatially homogeneous along the path, but takes a form of a superposition of multiple waves as suggested by the alternative appearance of the large and small SDs

along the path (upper right panel). Meanwhile, the positive and negative SD anomalies on both sides of the Cyclone B's path (lower right panel) is consistent with, the path shifting, because the positive anomalies are revealed along the path in the AF run (broken curve in Figure 3.3b).

Although, both path shifting (including poleward and equatorward) and wave-like patterns were, more or less, included in each cyclone in the AF runs. The Cyclone A and B were chosen for discussion hereinafter because of remarkable appearance of these two patterns.

3.4 Discussion

3.4.1 Switch of the Cyclone Sensitivity

According to our results, the large-scale background circulations may play an important role on the cyclone sensitivity on the SST reduction over the Sea of Japan. Figure 5a shows the composite maps of the lower-level potential temperature anomalies (AF-BF runs) of the affected and unaffected cyclone cases during the four days prior to the cyclone generation, along with the geopotential height and wind vectors in BF runs. Considering that the SST anomaly applied in AF runs was approximately -0.25 °C on average, we found the local atmosphere was reasonably cooled by > 0.1 K by the SST anomaly before the affected cyclones generated. On the other hand, the temperature reduction was not so large in the case of unaffected cyclones. Furthermore, during the affected cyclone experiments, a deeper (shallower) lower-level trough located over the Sea of Japan which induced the strong wind blowing over the Sea of Japan (the Sea of Okhotsk); see contours of geopotentisal height (Figure 3.5a) and the magnitude of south-

westward component in the 10-m wind field (Figure 3.5b) in both BF runs. Such difference of the response in the lower-level atmosphere would not be changed even if we make the composite maps during the whole simulation periods (not shown), suggesting that it was controlled by a larger scale phenomenon rather than the cyclone itself.

The strong northwesterly winds before the cyclone generation conveyed colder air mass onto the Sea of Japan. Figure 3.6a shows the composite maps of equivalent potential temperature (θ_e) and lower-level baroclinity defined as the horizontal gradient of θ_e. The duration of the composite was the same (four days) before cyclone generation as Figure 3.5. Compared to the unaffected cyclone cases, the Sea of Japan in the affected-cyclone cases was covered by atmosphere colder by $\sim$ 8 K; see the latitudes of isotherms of 280 K and 304 K by yellow curves in Figure 6a and thick contours in Figure 3.6b.

Owing to the above-mentioned cold air mass in winter, the relatively warmer Sea of Japan heats and unstablizes the atmosphere aloft in the affected cyclone cases, inducing the upwelling and vertical mixing within the marine atmospheric boundary layer. The changes in SST could therefore be transported upward via these processes. Figure 3.6b shows the vertical thermal structures of the atmosphere over the Sea of Japan. In general, the warm Sea of Japan makes the marine atmospheric boundary layer unstable because of the enhancement of winter convection. Thereby, it is likely that the winter convection enhanced especially in the affected cyclone cases well mixes the lower-layer atmosphere more rapidly and reached a higher level than unaffected ones; see the denser red shading in unaffected cases and the dashed line higher in affected cases (Figure 3.6b). Apparently, the influences of the reduced SST therefore penetrated upward more easily in affected cyclone cases than unaffected ones.

Furthermore, the southeastward migration of the cold air-mass intensifies

the lower-level baroclinity south of Japan (above the warm Kuroshio current), while the intensified baroclinity was mostly invisible in the unaffected cases (color shading in Figure 3.6a). Such conditions are favorable for air-sea interactions around oceanic fronts [*Parfitt et al.*, 2016] and the cyclogenesis, leading to the occurrence of storm tracks there (Figure 3.2a). The similar structures could be seen even after the cyclone passed (not shown), suggesting these conditions were related to the low frequency variability in the atmosphere, not to a single cyclone. Explicitly, intensive westerly winds (hence, southeastward migration of the cold air-mass) over the Sea of Japan provide a favorable condition for extratropical cyclones to be "affected". First, the cyclones well developed owing to the lower-level baroclinity enhanced south of Japan. Second, the developed cyclones become sensitive on SST over the Sea of Japan, because the upward penetration of the SST influence is readily to occur.

3.4.2 Cyclone A: the Wave-like Pattern

The wave-like pattern revealed in the SD field of the Cyclone A (Figure 3.4a) might be explained by a linear superposition of the multiple waves with different periods (hence, wavelength). We next demonstrate whether or not the multiple waves actually generated east of Japan (see the SD anomalies revealed only in these area in Figure 3.4a), and explore the periods, wavelength, and phase of these waves.

Figure 3.7a shows a Hovmöller diagram of the geopotential height at 850-hPa level (contour) and its anomaly (AF-BF runs) normalized by the maximal SD (color shading) along the Cyclone A's path (Figure 3a). Although the diagram was depicted to emphasize the Cyclone A, an alternative extratropical cyclone before passing the Cyclone A was also revealed because the Cyclone A moves along the storm track in the western Pacific region

[e.g., *Nakamura et al.*, 2004]. Between these two cyclones generated on December 22th and 25th, 2005 (see the red dots), it seems that the anomalies were weak and incoherent. Thereafter, the magnitude of anomalies became large as the latter cyclone (i.e., Cyclone A) deepens, revealing approximately a half of the wave period in comparison with the baroclinic wave shown by the geopotential-height contour. Moreover, it is found that the anomalous wave moved eastward along with the cyclone. The above result suggests that the anomalous wave (i.e., anomalies in geopotential height) was generated by the SST reduction over the Sea of Japan.

The characteristics of the anomalous waves superimposed on the Cyclone are well demonstrated using a Morlet wavelet analysis (Figure 3.7b; *Torrence and Compo*, 1998) to the time series of geopotential height at the location of the cyclone center (shown by the dashed line in Figure 3.7a). The wavelet spectra at both 850-hPa and 500-hPa levels in BF runs (upper and lower left panels in Figure 3.7b) show that the baroclinic wave, formed by two cyclones passing from December 21th to 30th, had the strongest wave period at 4.5-day (see the black lines for global mean), but with a wider distribution ranged from 2 to 6 days, the typical time scale for synoptic eddies (extratropical cyclones).

Right panels of Figure 3.7b show the differences in wavelet power spectra between the AF and BF runs (AF-BF). A significant spectrum decrease is revealed at 4-6 days' period with the peak at 4.5-day, indicating the weakening of cyclone activities. However, we also found an increasing signal at 3-days' period suggesting that an energy transfer occurs from long to short time variation.

Investigating the phases of anomalous waves mentioned above further uncovers the relationship between these waves and Cyclone A. A band-pass filter (second-order Butterworth filter) was used to separate the anomalies

by different time scales. According to the wavelet analyses, we chose 4 days as the demarcation of long-time (4-6 days) and short-time (2-4 days) in cyclone activities. As shown in Figure 3.8, both the long-time and short-time anomalies propagated along with the cyclones at the same speed, and they were both enhanced especially with the Cyclone A.

The long-time anomalies (Figure 3.8b) had the same wavelength as the cyclone itself (see the dashed line and dotted line in Figure 3.8c). The phase was approximately opposite before December 25th, but was shifted by $\sim \pi/2$ after. This result consists with the negative SD anomalies in the right panel of Figure 3.4a and the reduced wavelet spectra of the 4.5-day period activities. As mentioned in the next subsection, the phase shift with the same propagation speed revealed in the latter half period on the Cyclone A suggests the path of the Cyclone A is slightly changed in AF run compared to BF run. On the other hand, the short-time anomaly (Figure 3.8a) had a wavelength of approximately half of the baroclinic wave (i.e., the cyclone; Figure 8c), which corresponds to the increased 3-day signal in the wavelet power spectra. However, it is revealed that this short-time anomalous waves propagated along with the long-time anomalies after the generation of the Cyclone A, and thus, both waves can be regarded as the modulation of the cyclone owing to the SST reduction over the Sea of Japan.

3.4.3 Cyclone B: Intensifying and Path Shifting

In this subsection, we will give a brief discussion on the intensifying and path shifting effects of the negative SST anomaly in the Sea of Japan. As shown in Figure 3.3b, the Cyclone B was greatly intensified and its central SLP deepened over 10 hPa, while its path was slightly shifted poleward.

The Cyclone B took a southern path passing over the Kuroshio and its extension. This is a typical Pacific Ocean-Ocean type cyclone, defined by Yoshida and Asuma (2004), which is strongly related to the diabatic heating [e.g., *Fu et al.*, 2014; *Hirata et al.*, 2015]. The diabatic heating rate (Q_{d}) can be estimated by:

$$Q_{\mathrm{d}} = \frac{\partial \theta}{\partial t} + \mathbf{U} \cdot \nabla \theta, \tag{3.2}$$

where θ and $\mathbf{U}$ are the potential temperature and the three-dimensional wind vectors, respectively , and other notions are standard. Then, following *Tamarin and Kaspi* [2016], the tendency of the potential vorticity (PV) due to the diabatic heating can therefore be approximately given by

$$\frac{dPV_{\mathrm{diab}}}{dt} = -g(f+\zeta)\frac{\partial}{\partial p}Q_{\mathrm{d}}, \tag{3.3}$$

where g the gravitational acceleration, f is the planetary vorticity, and ζ is the relative vorticity.

Figure 3.9 shows the meridional cross-section of anomalies of the diabatic heating (LHS of Equation 3.2), the PV tendency due to the diabatic heating, and vertical velocity around the center of Cyclone B when it reached the maximum CDR. An enhanced diabatic heating (color shading) can be seen near the cyclone center (labeled by L in the figure) associated with the positive (negative) PV tendency anomaly at the lower levels (higher levels), located at the northern side of the cyclone center, and the increased upward velocity from surface to the 300-hPa level (thick contours). The cyclone therefore deepened due to the enhanced diabatic heating, and further shifted poleward due the generated positive PV anomaly at lower levels. Such processes described above consists with the results in *Tamarin and Kaspi* [2016] which on the basis of an idealized zonally symmetric moist GCM.

Figure 3.10 showed the composite map of the anomalies (AF-BF runs) surface turbulent heat fluxes through the sea surface during the lifespan of the

Cyclone B. Besides the reduced heat flux in the Sea of Japan, the positive anomalies could also be found in surrounding regions. The time evolutions of surface turbulent heat fluxes averaged within five regions (red boxes in Figure 3.10) were shown in Figure 3.11. First, the positive anomaly of heat flux appeared in the Kuroshio region (see arrows in the figures) when the Cyclone B was recognized in the domain. It should be noted that the cyclone had not yet been modified sufficiently at this moment (Figure 3.2b) in comparison with the magnitude of anomalies in the other areas. The positive anomalies thereafter appeared remarkable in the Kuroshio Extension and Oyashio regions due to the intensified cyclone propagating eastward (see the path showed in Figure 3.10). Meanwhile, the vertical integrated vapor fluxes, that crossing the eastern and southern boundaries of the Sea of Japan, remained unchanged (Figure 3.12). It is demonstrated that the reduced heat fluxes in the Sea of Japan (Figure 3.10 and 3.11) didn't influence the moisture supply to the passing cyclone, but remained locally.

According to the above-mentioned results, the negative SST anomaly reduced the local surface heating in the Sea of Japan especially in the period of affected cyclones when intensive northwesterly winds strengthen the linkage between the Sea of Japan and atmosphere above it. Therefore, the Sea of Japan act as a "source" of cold air-mass, allowing the cold air spreading onto the surrounding areas. The Cyclone B was therefore intensified due to the enhanced upward heat and moisture fluxes in those regions. Furthermore, the effect of the Sea of Japan is transported to a much wider area by the modulated propagating cyclone. Thus, besides the local effect on the passing cyclone, the colder Sea of Japan also plays a role on farther regions remotely via the 'atmospheric bridge' as suggested in *Yamamoto* [2013].

3.4.4 Do they occur in other cyclones?

In the above subsections, we have mentioned two specific extratropical cyclones modulated by the SST reduction owing to the previous cyclone over the Sea of Japan in winter. It is therefore natural to raise a question whether other affected cyclones undergo the same modulation processes, that is, path shifting with monotonic intensification (Cyclone B) or weakening *Yamamoto* [2013], and energy transfer to other waves (Cyclone A). Unlike the aforementioned two cyclones, however, it is likely that the above modulation processes occurred simultaneously in each cyclone. Investigating the anomalies of wavelet spectra of geopotential height (AF-BF runs as right panels of Figure 3.7b) has a merit to discuss the modulation processes separately.

Figures 3.13 and 3.14 showed the wavelet spectra anomalies of all 20 affected cyclones at 850-hPa and 500-hPa levels, respectively, based on the results of wavelet analysis of geopotential heights at the locations of the cyclone centers when each cyclone greatly developed (six hours after they reached maximum CDRs because of the 12-hourly deepening rate we used in this study).

Although there is a variety of patterns in the wavelet power spectra, most of the changes were concentrated in two specific periods as mentioned in the subsection 4.2: they are around 4.5-day and 3-day (see the peaks of global means). Both intensified and weakened signals can be seen in the 4.5-day period anomalies (the main period of cyclone), suggesting that the Sea of Japan can play both strengthening and weakening roles (probably with the path shifting shown by *Tamarin and Kaspi* [2016]).

Of note, among the affected cyclones, few of them had reducing or increasing energy simultaneously in both long-time and short-time anomalies or at both 850-hPa and 500-hPa levels (Figure 3.13 and 3.14). These results suggest

the occurrence of the energy transfer (i.e., wave-to-wave interactions) between waves with different frequencies and levels during the cyclogenesis. Unsteadiness and nonlinearity are likely to be critical for the occurrence of such interactions, and thus, an idealized numerical experiment may help to uncover dynamical processes for the wave-like pattern to appear, although this approach is beyond the scope of present study and shall be the next step of this work.

3.5 Summary

In this chapter, we investigated the atmospheric response of extratropical cyclones to the SST anomaly in the Sea of Japan which induced by the previously-passing cyclones. We conducted a set of sensitivity experiments based on a regional numerical model (WRF). Results showed that the Sea of Japan could become a link between two consecutive cyclones passing near the Sea of Japan under some favorable conditions, acting as an "oceanic bridge". Our analyses demonstrated that a cyclone can modulated the following cyclone via the SST reduction over the Sea of Japan, and that the role of the colder Sea of Japan is not only for the weakening source to reduce the cyclone activity, but also for strengthening and/or generating baroclinic waves in surrounding regions.

Table 3.1: Settings of Two Runs Performed by WRFV3

Run	BF	AF
Domain	Mother Domain: 230×132 (30 km) Nest Domain: 181×217 (10 km)	
Vertical Resolution	35 sigma layers	
Period	9 days for each cyclone with prior 4 days for spinning up	
Lower Boundary	Winter Climatological SST (contour in Figure 3.1)	with extra ΔSST (color shading in Figure 3.1)

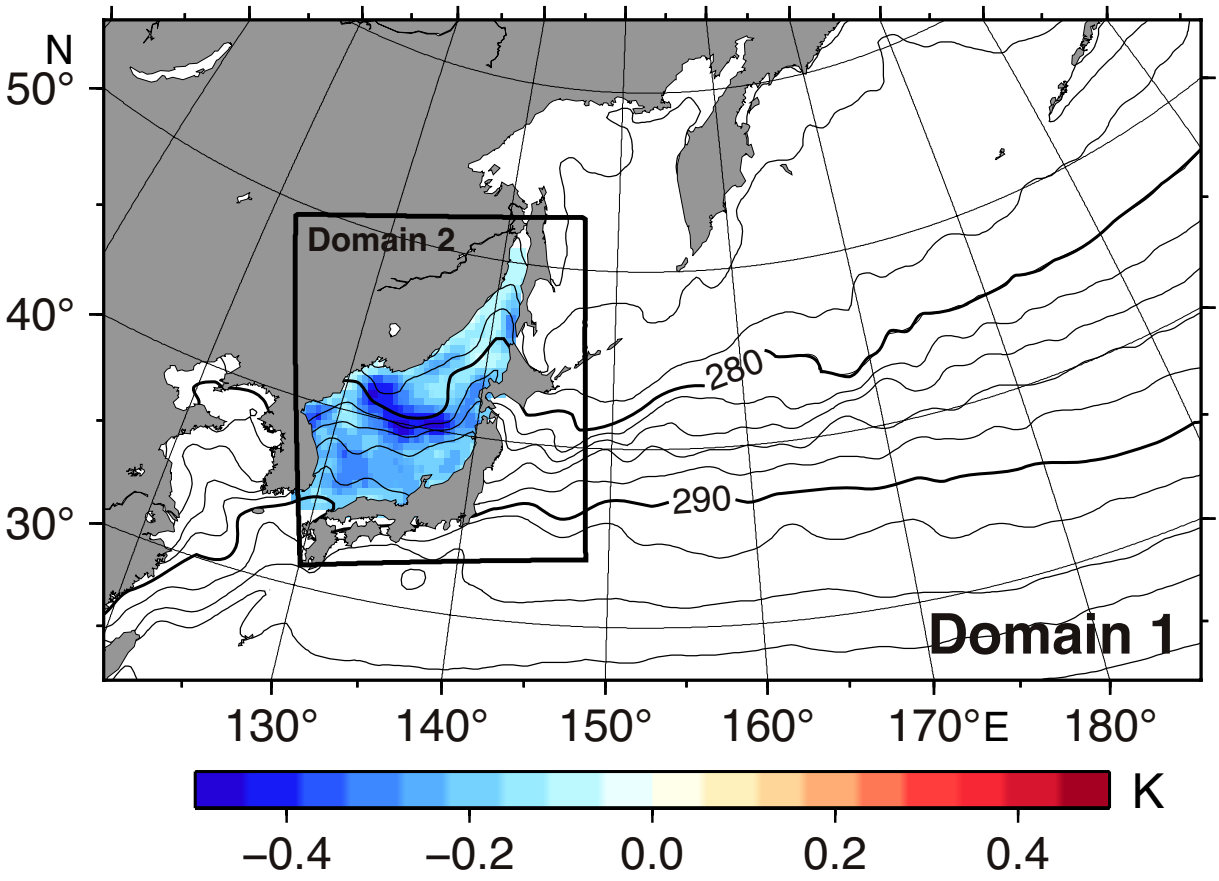

Figure 3.1: WRF model domains overlapped by climatological mean SST during the winters (NDJF) of 2003-2011. Color shading shows the SST anomaly used in the AF runs.

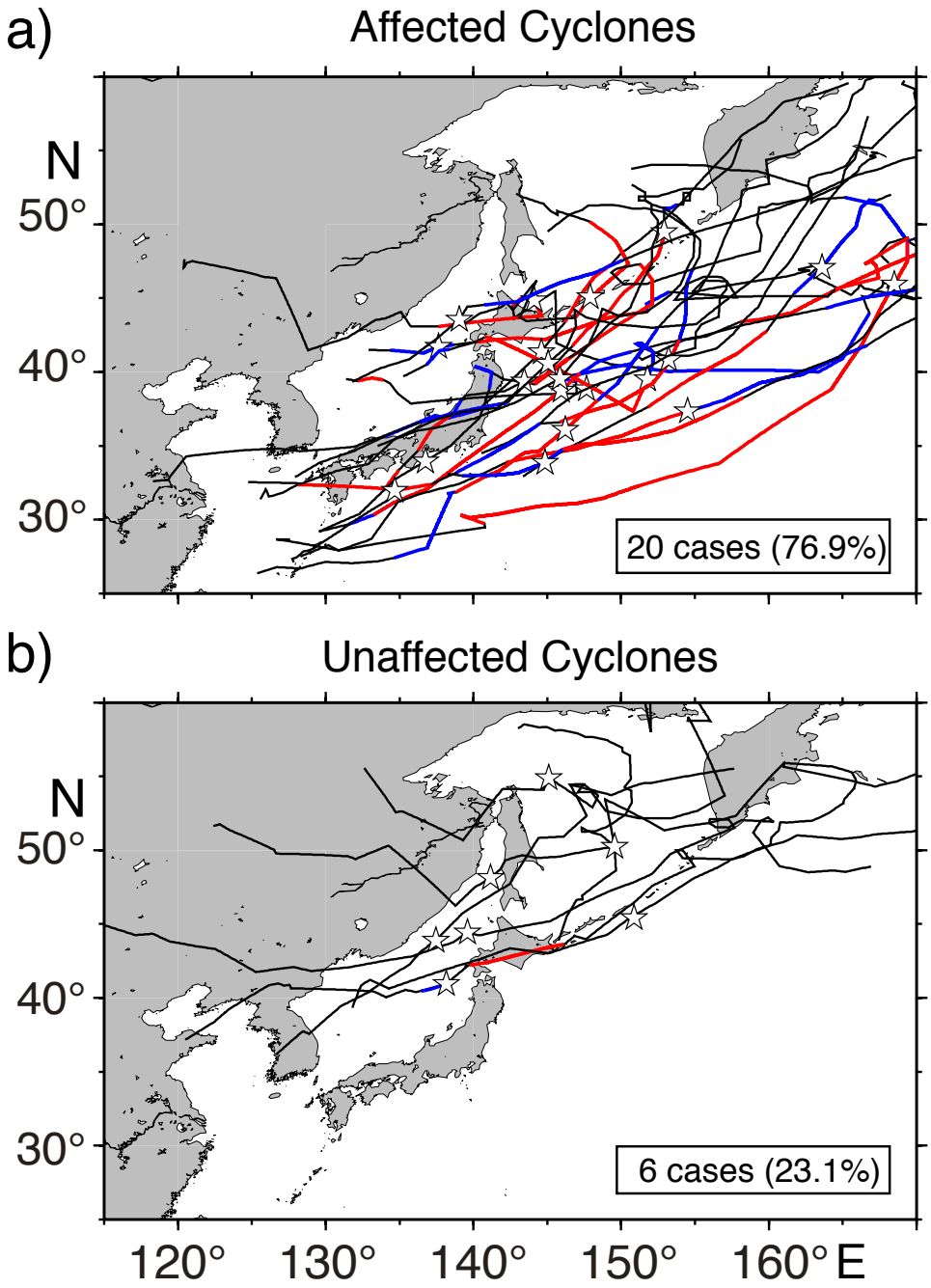

Figure 3.2: Paths of simulated cyclones: a) 20 affected cyclones and b) 6 unaffected cyclones. Red curves show the intensifying periods (> 0.1 Bergeron), while blue curves show the weakening periods (< -0.1 Bergeron). Stars indicates the locations of maximal CDR of each cyclone. See text for details.

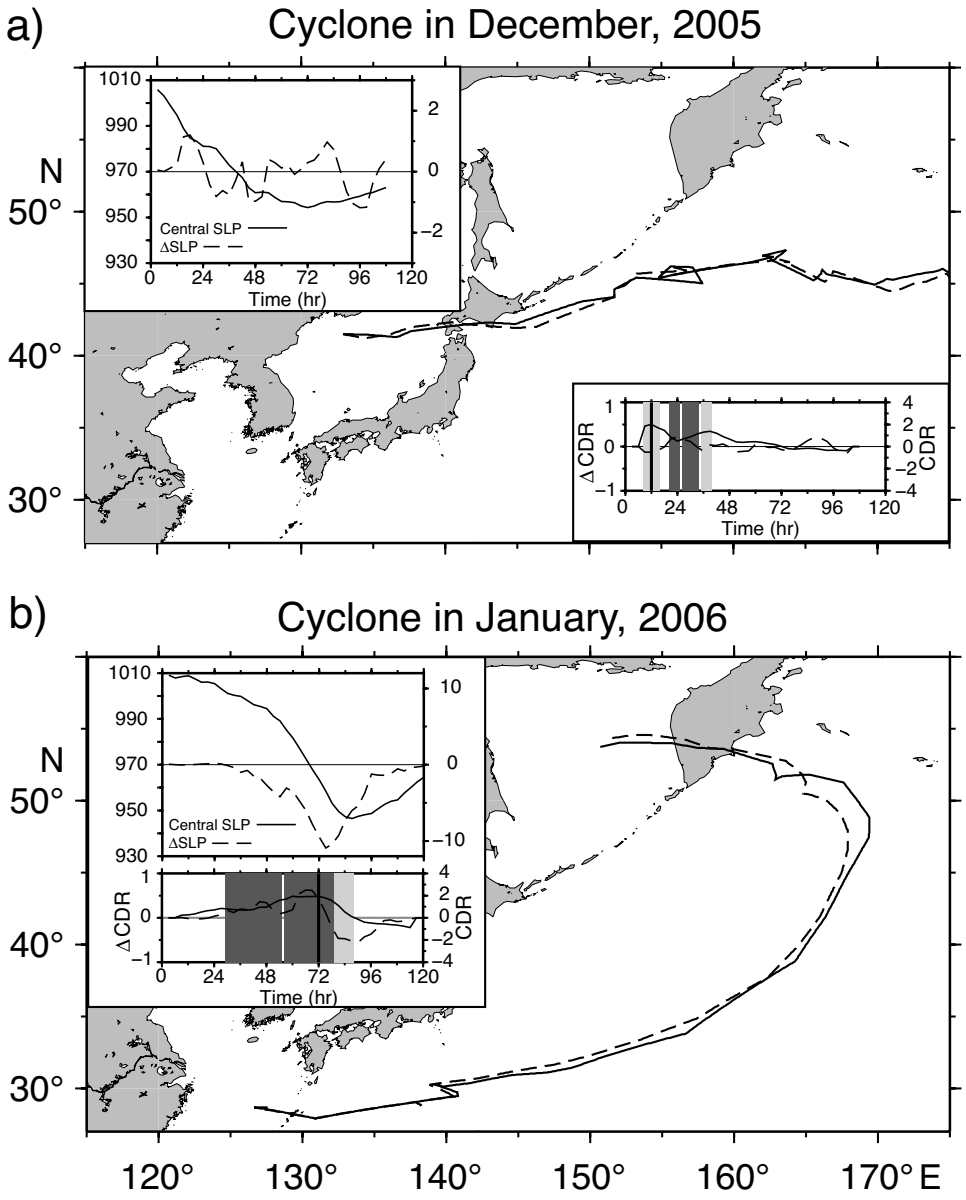

Figure 3.3: Paths of Cyclones A and B in BF (black curves) and AF runs (dashed curves), respectively. The inset panels show the time evolutions of the central SLP and CDR in BF runs (black curves) and their differences between the AF and BF runs (AF-BF, dashed curves). The intensifying (weakening) period is represented by the dark (light) grey shading.

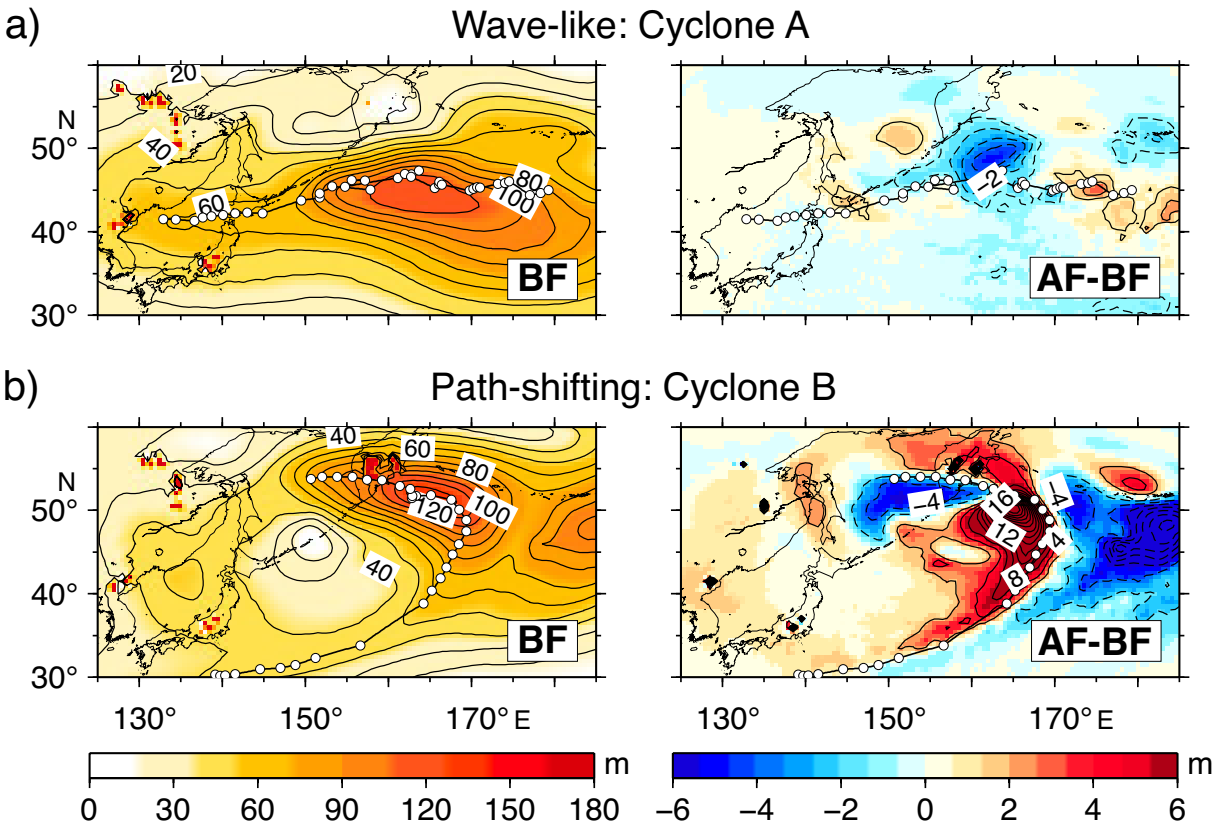

Figure 3.4: Cyclone activities of Cyclone A (a) and B (b) which represented by the standard deviation of geopotential height at 850-hPa level in BF runs (left panels) and their differences between the sensitivity experiments (AF-BF, right panels). Contour intervals are 10 m in left panels, and 1 m in right panels, except the right part of panel b which is 2 m for avoiding overcrowding. Cyclone paths determined by the minimal SLP are shown by black curves and white dots every 3 hours.

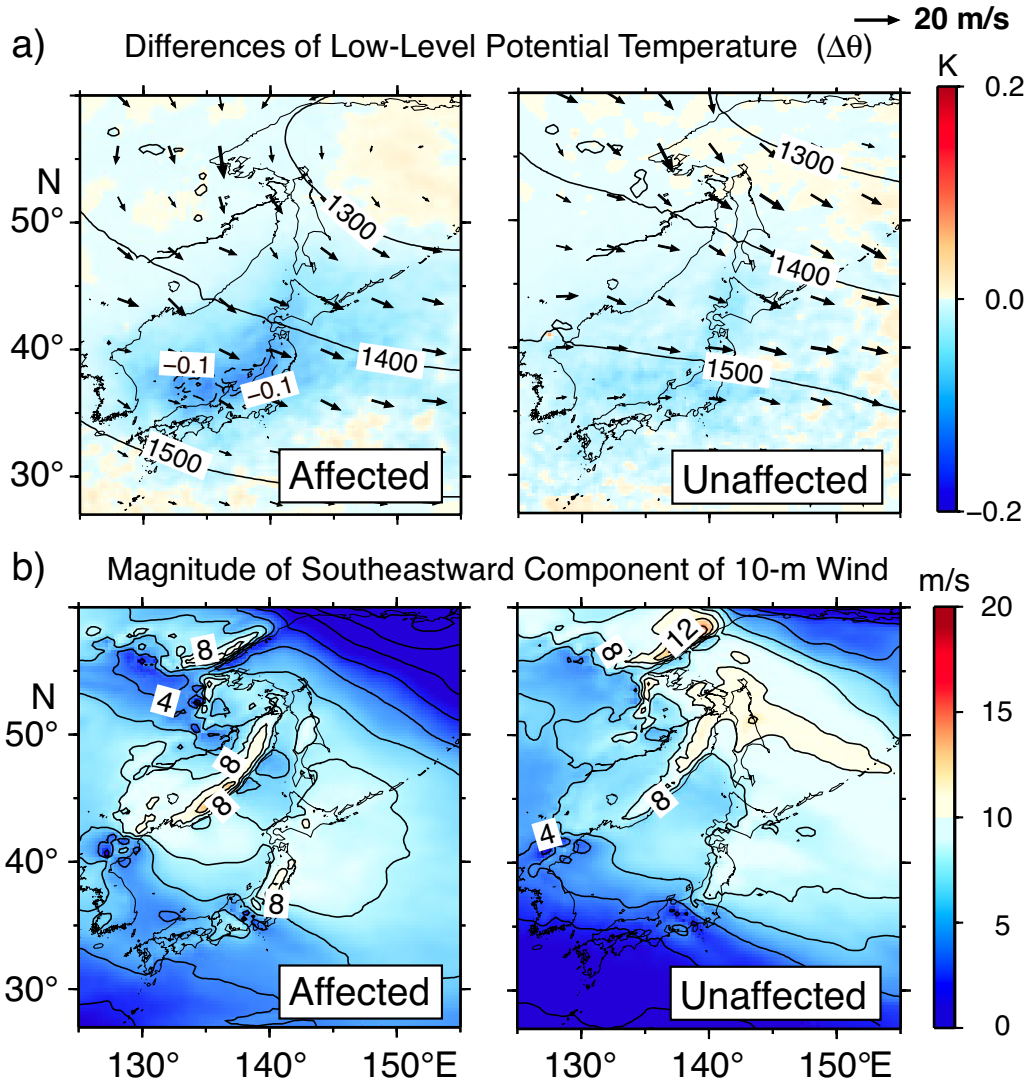

Figure 3.5: Composite maps of the potential-temperature and wind differences between two runs (AF-BF) which were averaged during the four days before the cyclone generated. The map for affected (unaffected) cyclones are placed on the left (right) panels. The panel a indicates the maps of potential temperature anomaly (color shading and dashed contours) with the geopotential height (thin black contours) and wind (vectors) at 850-hPa level in BF runs. The panel b denotes the horizontal distribution of the southeastward component of the 10-m wind. Contour intervals are 0.1 K and 100 m in panel a, and 2 m s^{-1} in panel b, respectively.

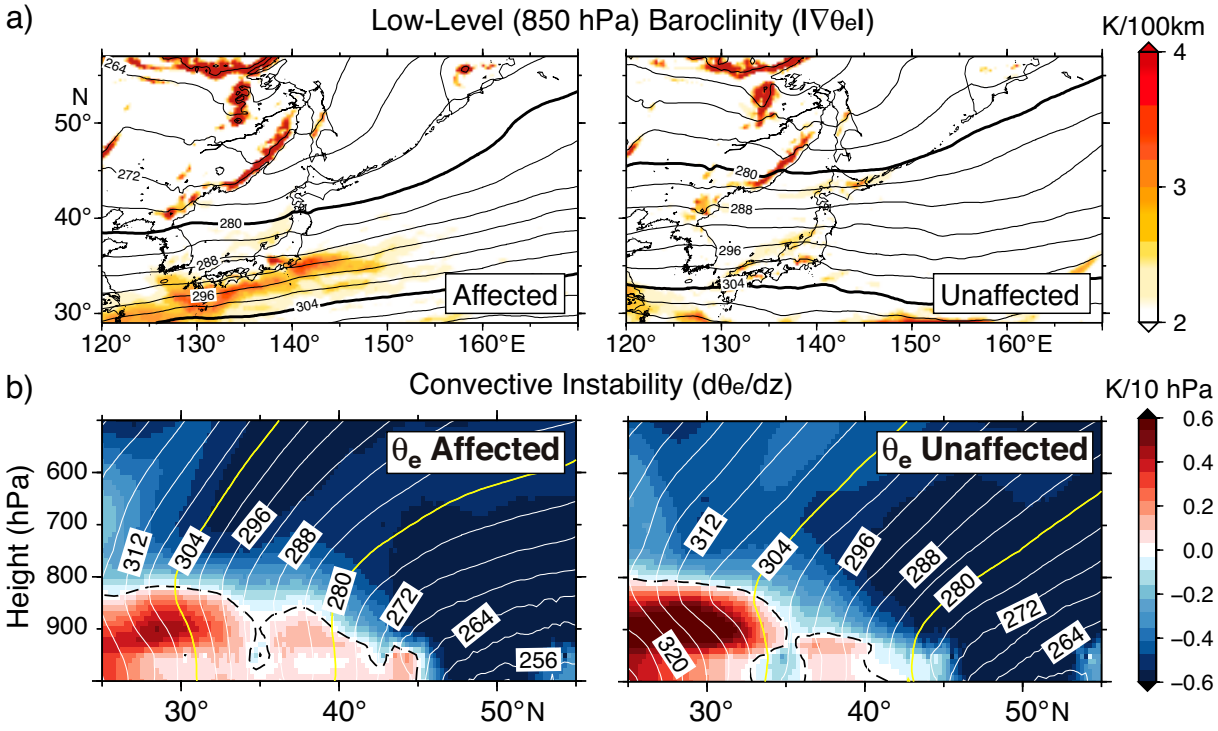

Figure 3.6: Composite maps of low-level baroclinity (a) and cross-section of the thermal structure (b, averaged over 130-140 °E) of the atmosphere above the Sea of Japan. Color shading shows the horizontal-gradient magnitude (i.e., baroclinity; a) and the vertical gradient of equivalent potential temperature (i.e., instability; b). For ease of comparison, the 280 K and 304 K isotherms are marked out by bold curves (a) and yellow curves (b), respectively. Contour intervals are 4 K in both panels.

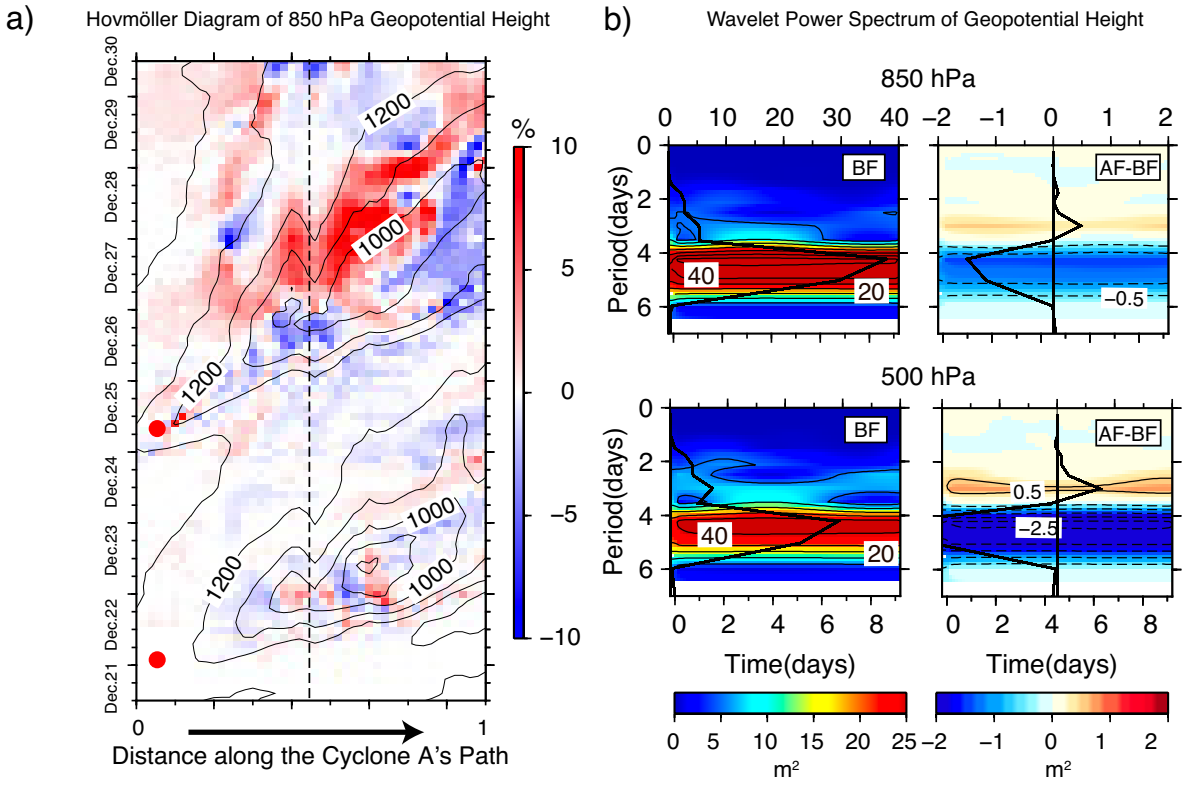

Figure 3.7: Wave-like patterns revealed in the Cyclone A. The panel a indicates a Hovmöller diagram of the geopotential height at 850-hPa level (contour) along the Cyclone A's path (see Figure 3a), of which ends are 0 and 1, respectively, on the abscissa. Also shown in the panel are the anomalies (AF-BF) normalized by SD of the geopotential height (color shading). Two red dots show the starting time of two cyclones captured in the diagram, and two dashed line shows the location for the wavelet analysis. Panel b show the normalized wavelet power spectra of the geopotential heights at 850-hPa and 500-hPa levels, respectively, where the left panels show the BF runs and right panels show the differences (AF-BF). Thick lines show the global means of the wavelet power spectra and the differences (AF-BF), respectively. Contour intervals of Figure 8a, 8b and 8c are 100 m, 5 m^2, and 0.5 m^2, respectively.

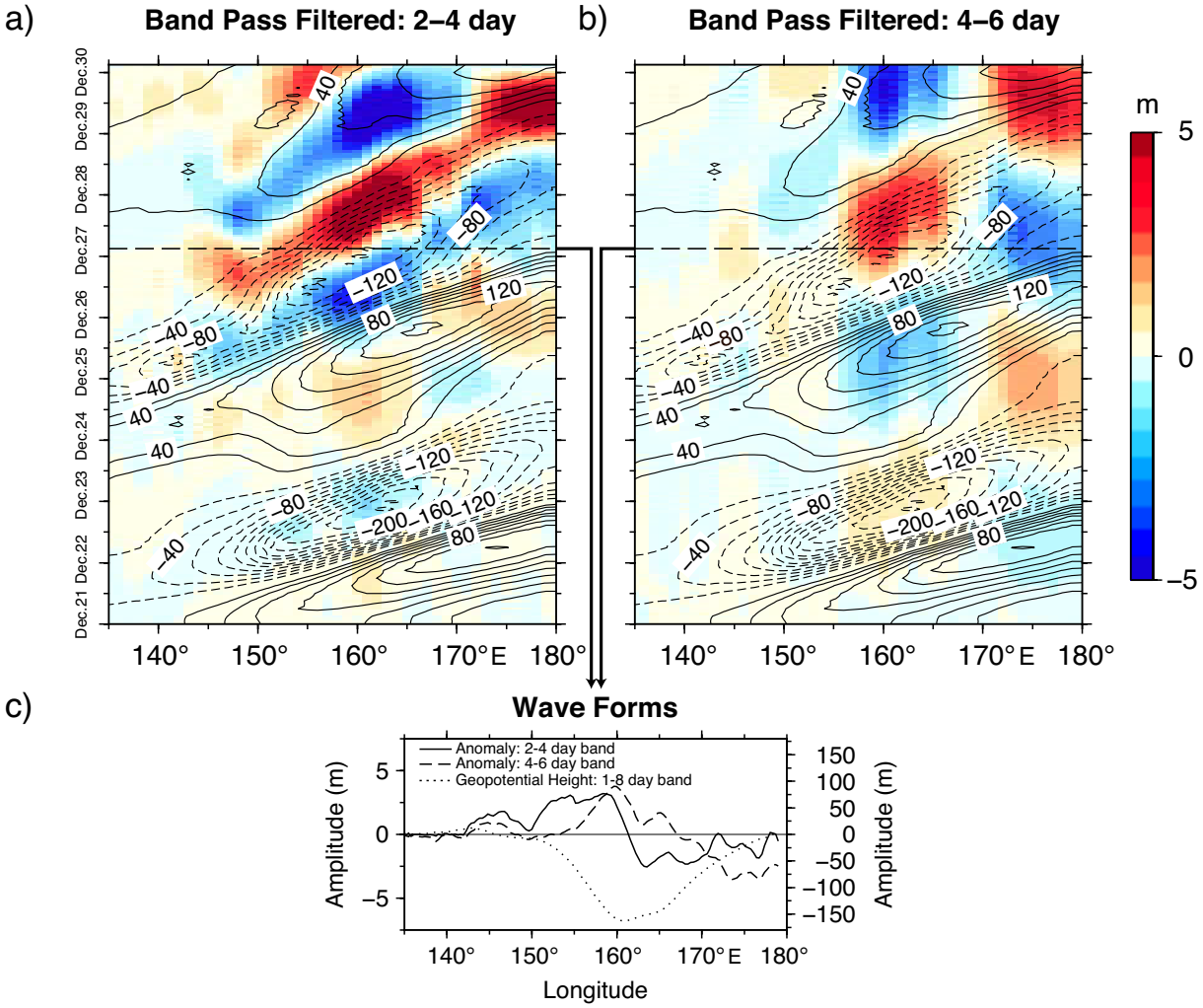

Figure 3.8: Hovmöller diagrams of the bandpass filtered geopotential height anomalies (color shading) and 1-8 day band pass filtered geopotential height in BF run (contour) at 850-hPa for showing the baroclinic waves (i.e., cyclones): (a) 2-4 day band. (b) 4-6 day band. Panel c denotes the wave forms of the short-time anomaly (black curve), long-time anomaly (dashed curve), and 1-8 band pass filtered geopotential height in BF runs (dotted curve). Contour intervals are 20 m in panel a and b.

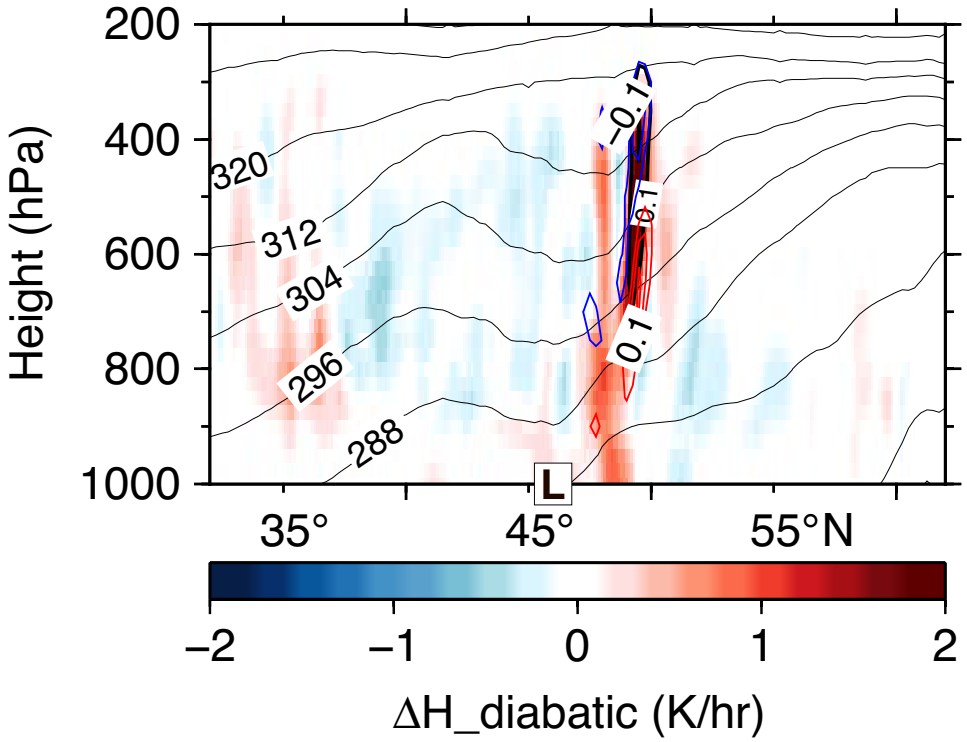

Figure 3.9: Cross-section of atmospheric properties near the cyclone B's center (showed by 'L') at which the cyclone reached the maximal CDR. The properties shown in the figure are anomalies of the diabatic heating rate (color shading), the vertical velocity (thick contours), and PV tendency due to the diabatic heating where the red (blue) contour indicates the positive (negative) values, along with the isotherms of potential temperature in BF run (thin contours). Contour intervals are 8 K ($<$ 312 K), 16K ($>$ 312 K), 0.1 m s^{-1}, and 0.05 PVU hr^{-1}, respectively.

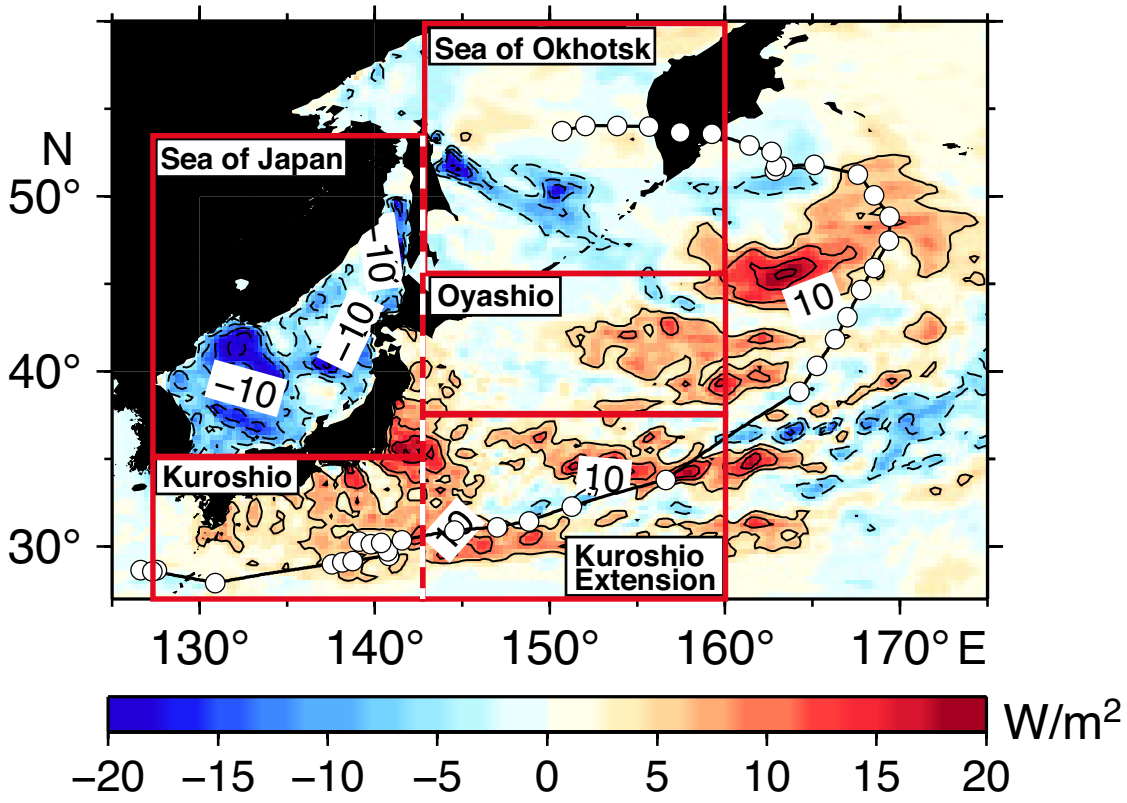

Figure 3.10: Composite map of the anomalies of the surface turbulent heat fluxes during the Cyclone B's lifetime. The path of Cyclone B is also plotted by the bold curve with white dots every 3 hours. Five regions, selected for box averaging, are indicated by the red boxes. Contour intervals are 5 W m^{-2}.

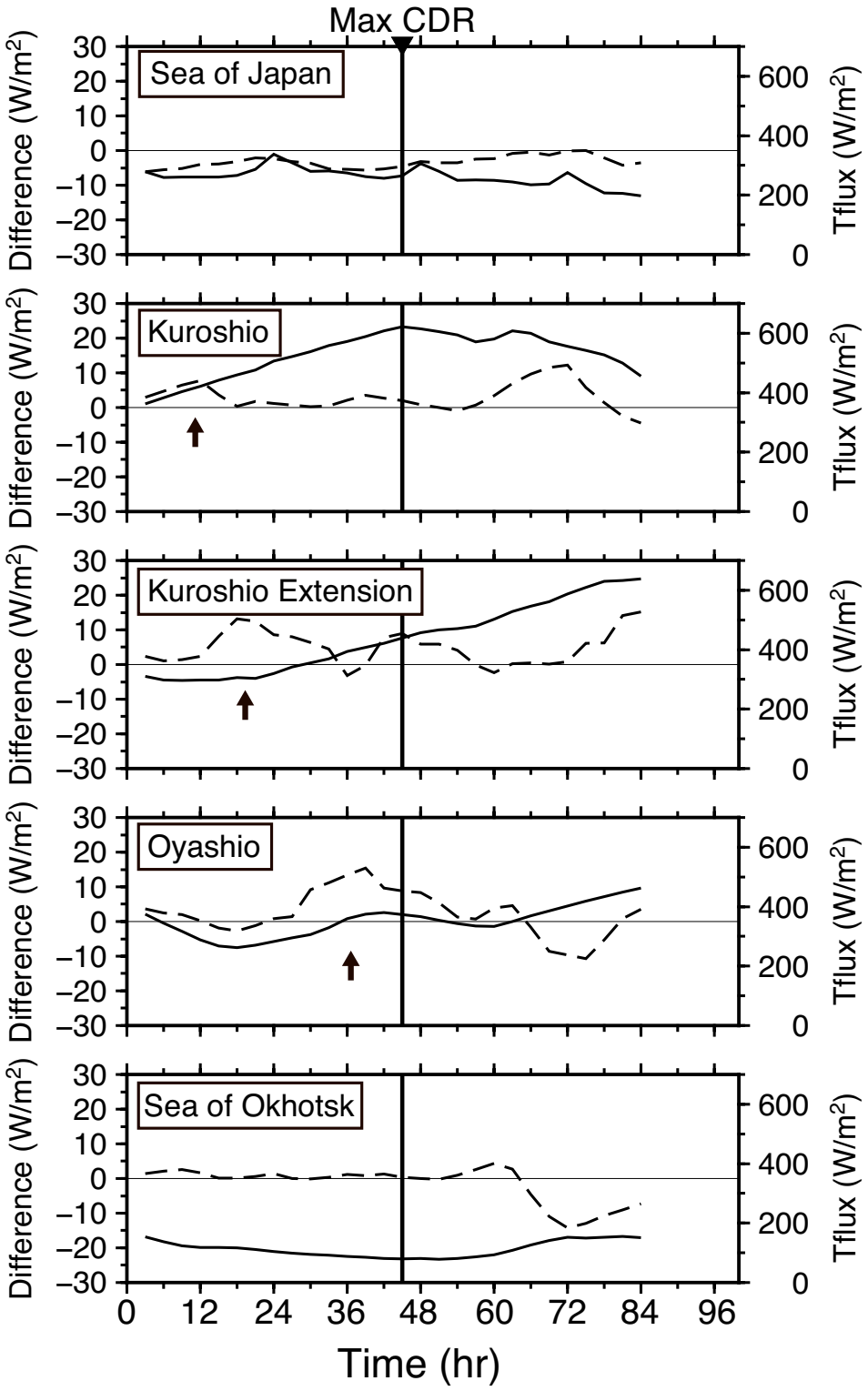

Figure 3.11: Time series of the box-averaged turbulent heat fluxes during the Cyclone B's lifetime (black curves) of five regions in our domain (see Figure 3.10) and differences between two runs (A-B, dashed curves). Arrows indicate the time when the cyclone-related positive anomalies appeared.

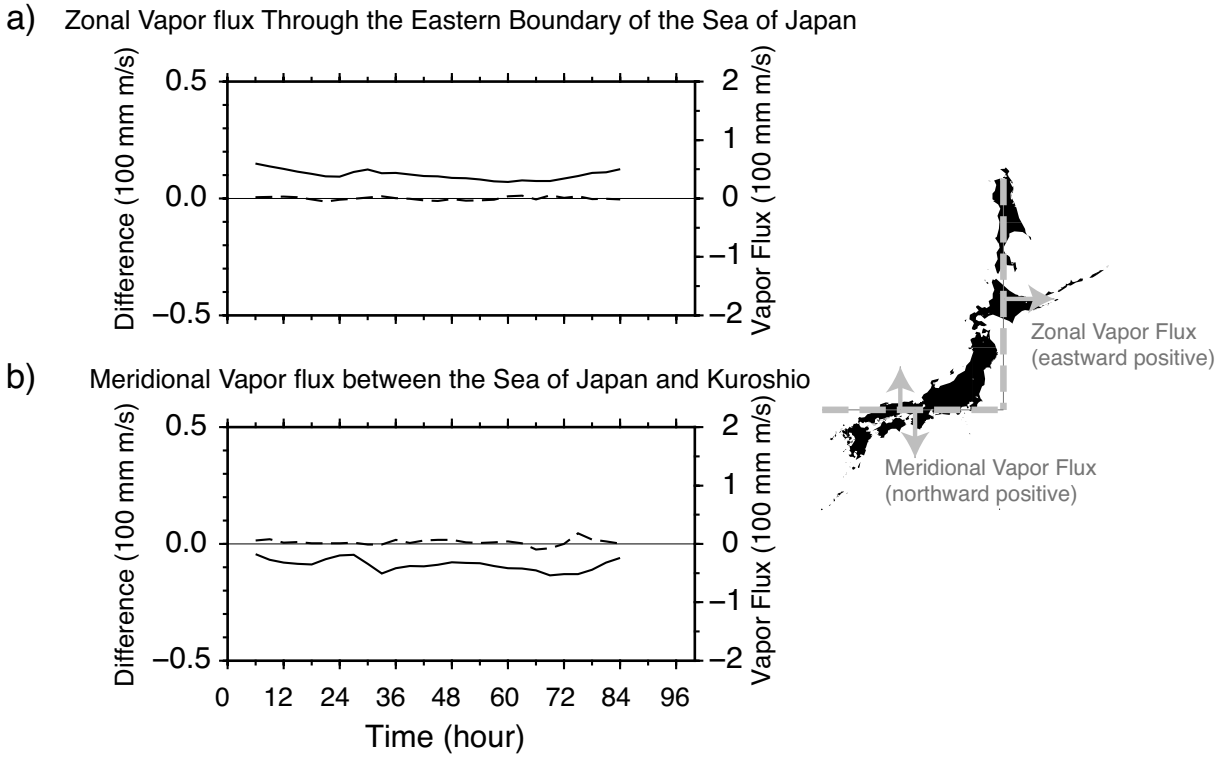

Figure 3.12: Time series of the verticalyl integrated (1000 hPa to 300 hPa) vapor fluxes across the eastern (a, 142.5 °E, 35-54 °N) and southern (b, 127-142.5 °E, 35 °N) boundaries of the Sea of Japan. Positive values show the eastward fluxes in the panel (a) and the northward fluxes in panel (b).

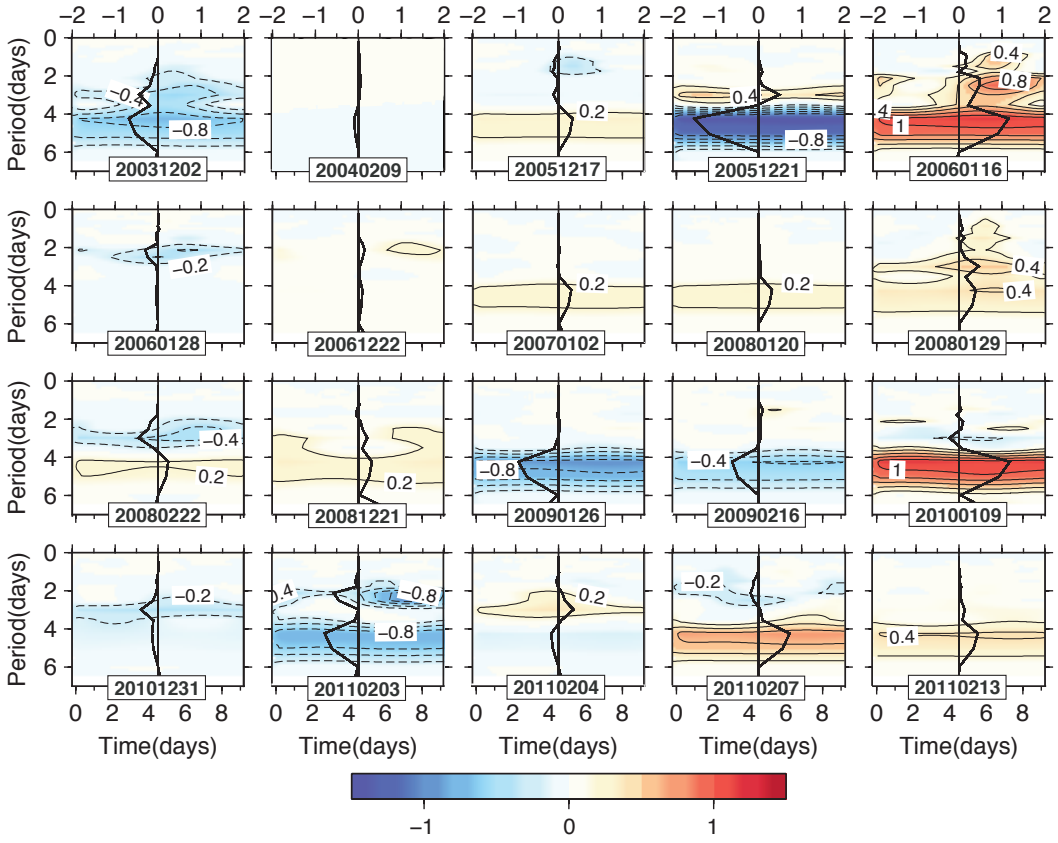

Figure 3.13: Differences in normalized wavelet power spectrum of the geopotential heights at 850-hPa level of all affected cyclones. Contour intervals are 0.2 m^2 for values $< \pm 1$ m^2 and 0.5 m^2 for larger values in all panels.

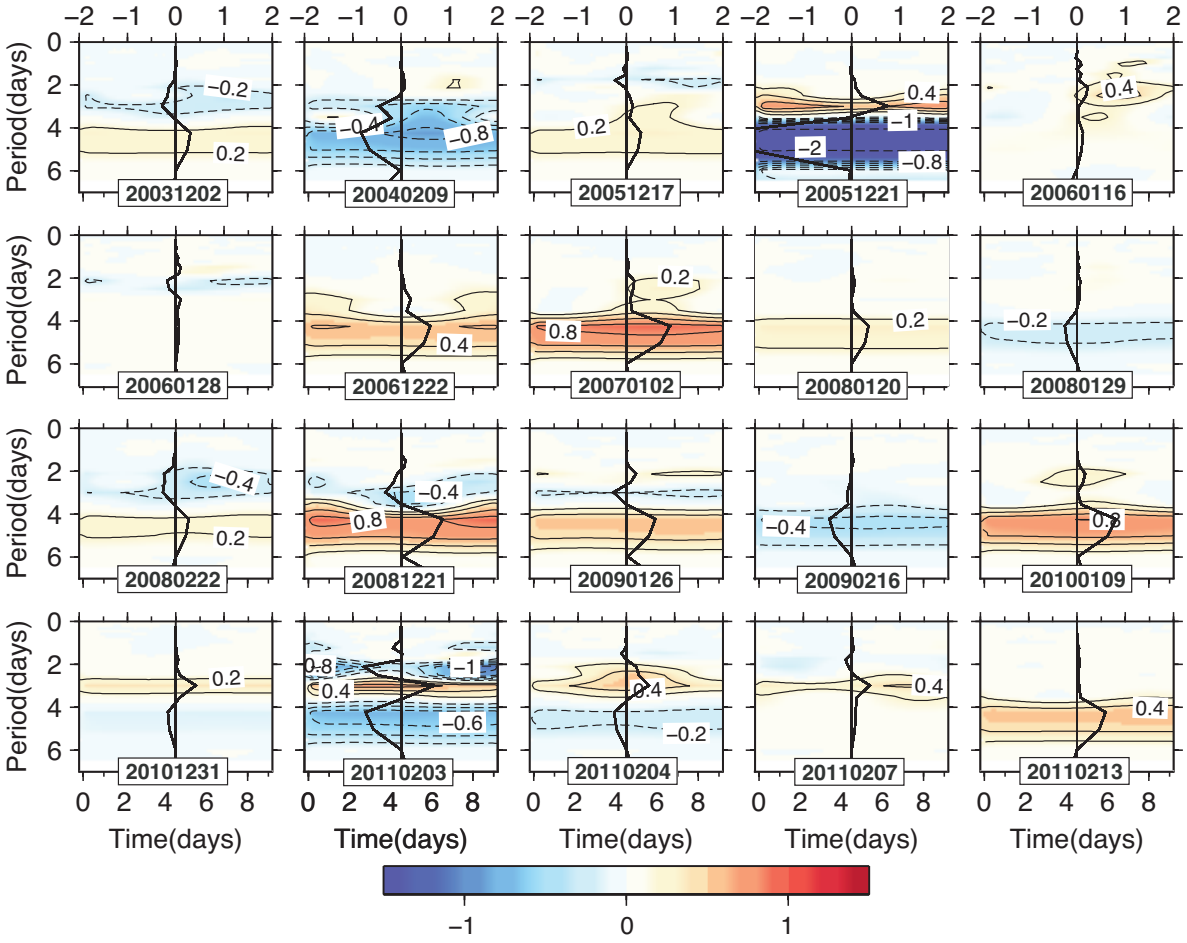

Figure 3.14: Same as Figure 3.13 but for results based on the geopotential heights at 500-hPa level.

Chapter 4

Conclusions

This study was motivated by the lack of the knowledge on the sub-weekly scale interactions between extratropical cyclones and the Sea of Japan. To reveal that, we conducted both objective analysis and the sensitivity experiments using a regional numerical model based on the observational and reanalysis datasets in this study.

In the present study, we found that the Sea of Japan experiences a strong SST reduction during the passage of winter extratropical cyclones, and it further becomes an oceanic bridge to link two consecutive cyclones. Given such facts, the sub-weekly interactions between the Sea of Japan and extratropical cyclones was constructed. The detailed findings are described as follows.

4.1 The Oceanic Response of the Sea of Japan to the Extratropical Cyclones

The mechanisms of SST reduction and frontogenesis in the winter Sea of Japan are revealed in this study (Figure 4.1). Developing extratropical cyclones induce strong cold-air outbreaks, accompanied by strong northwesterly winds transporting a cold-air mass over the entire Sea of Japan. During the cooling event, SST in the central sea is reduced remarkably because of the shallowness of the mixed layer. Upward heat flux intensifies the sharpness of the subpolar front (Figure 4.1a), in spite of a contribution much smaller than that of horizontal heat advection. Meanwhile, the strong northwesterly wind generates a strong cross-frontal Ekman flow, transporting the cold water across the isotherms. This further reduces the temperature locally along the subpolar front and intensifies the front, representing the primary contributor (Figure 4.2b). These results are apparently different from studies of wind-driven frontogenesis associated with fine-scale dynamics.

It should be noted that this cyclone-induced SST reduction may also be included in the seasonal trend, because the temperature reduction of a single cyclone is not always recovered completely after cyclone passage. It is, however, difficult to separate this contribution from the seasonal trend using the present data analyses. The timescale of SST recovery (by horizontal heat advection, eddy-induced heat transport, and subgrid-scale horizontal diffusion) must be a critical factor, and the aforementioned two-way coupling processes complicate the problem. SST recovery processes are a major scientific issue in the physical oceanography. For instance, although *Mei and Pasquero* [2013] suggested that the SST recovery time varies considerably by case, in general, recovery from SST cooling by tropical cyclones occurs on an intra-seasonal time scale (around 5–30 days; *Dare and McBride*, 2011). We may expect a similar time scale of SST recovery, even at mid-latitudes. A nu-

merical model approach incorporating a two-way coupling process is likely required to answer the above questions, so this will be the next step in the future.

4.2 The Atmospheric response of Extratropical Cyclones to the Sea of Japan

The present study investigated the effects of the cyclone-induced SST anomaly in the Sea of Japan on the following cyclones. We designed a set of sensitivity experiments of 26 cyclones with the winter climatological mean SST (BF runs; contour in Figure 3.1) and an extra negative SST anomaly (AF runs; color shading in Figure 3.1).

20 of 26 cyclones well responded to the SST anomaly, and the rest 6 cyclones were nearly unaffected. In conclusion, the low-level trough (hence, the northwesterly winds) was found to be the controlling factor of the cyclone sensitivity and therefore the connections between two consecutive cyclones (Figure 4.2a and 4.2b). A deeper (shallower) trough caused a stronger (weaker) northwesterly winds which enhanced the cold air intrusion onto the Sea of Japan. With (without) the domination of the cold air mass, a thicker (thinner) convective layer encouraged (restrained) the upward penetration of marine atmospheric boundary layer over the Sea of Japan, and therefore determine the cyclone sensitivity. In addition, this penetration further generated a band of strong baroclinity over the Kuroshio south of Japan, and potentially results in the formation of storm track there.

As for the modulations of cyclone activities, we analyzed two specific cyclones and found a wave-like pattern in the cyclone developed on December 25th, 2005 (Cyclone A) and an intensifying and path-shifting pattern in the cyclone developed on January 20th, 2006 (Cyclone B).

Analyses of the sensitivity experiments showed that the wave-like pattern superimposed on the Cyclone A was revealed owing to a linear superposition of the anomalous waves which can be separated by their periods: long-

time (4-6 days) and short-time (2-4 days) anomalies. The long-time anomaly (Figure 3.8b) had the same wavelength of the cyclone itself but with an opposite phase, indicating the anomalies caused by the cyclone weakening, while the short-time anomaly had a half-wavelength of the cyclone (and long-time anomaly). These anomalies caused by the cyclone-induced SST anomaly were weak east of Japan at the early stage, but were thereafter rapidly enhanced as they were advected by the subsequent cyclone developing over the North Pacific (see SD anomalies in the left panels of Figure 3.4). Meanwhile, the path-shifting pattern revealed in the Cyclone B was highly related to the cyclone intensification. A positive PV anomaly generated by the intensive diabatic heating was found on the northern side of cyclone center, inducing the poleward shifting. Although the SST anomaly reduced the surface heating locally over the Sea of Japan, it allowed colder air mass spreading over the surrounding areas. Such colder air mass enhanced the surface heating and moisture supplement over the Kuroshio region, and therefore intensified the cyclone passing aloft. The wavelet spectra (Figure 3.13 and 3.14) demonstrate that intensifying of the long-time waves (e.g., Cyclone B on January 20th, 2006), weakening of the long-time waves [e.g., *Yamamoto*, 2013], and energy transfer between long- and short-time waves (e.g., Cyclone A on December 25th, 2005) are found among 20 affected cyclones as well as the two cyclones described above. However, unlike the Cyclone A and B, these modulation processes are likely to be mixed in each cyclone.

What we emphasized in the present study is that a cyclone can modulate the following cyclones via cooling of seas which acts as an "oceanic bridge" connecting between the cyclones. Also, emphasized is that the role of the colder Sea of Japan is not only a local weakening source on the passing cyclones, but also a strengthening and/or wave-generating factors in the surrounding regions, and such effects can further be transported by the propagating cyclones to remote areas (Figure 4.2c). Meanwhile, our results suggest the occurrence of the energy transfer (i.e., wave-to-wave interactions) between waves with different frequencies and levels during the cyclogenesis (Figure

4.2d). However, it is still unclear how the energy transfer between baroclinic waves passing over the cooled Sea of Japan, and thus, further studies are required to uncover the dynamical processes in the future.

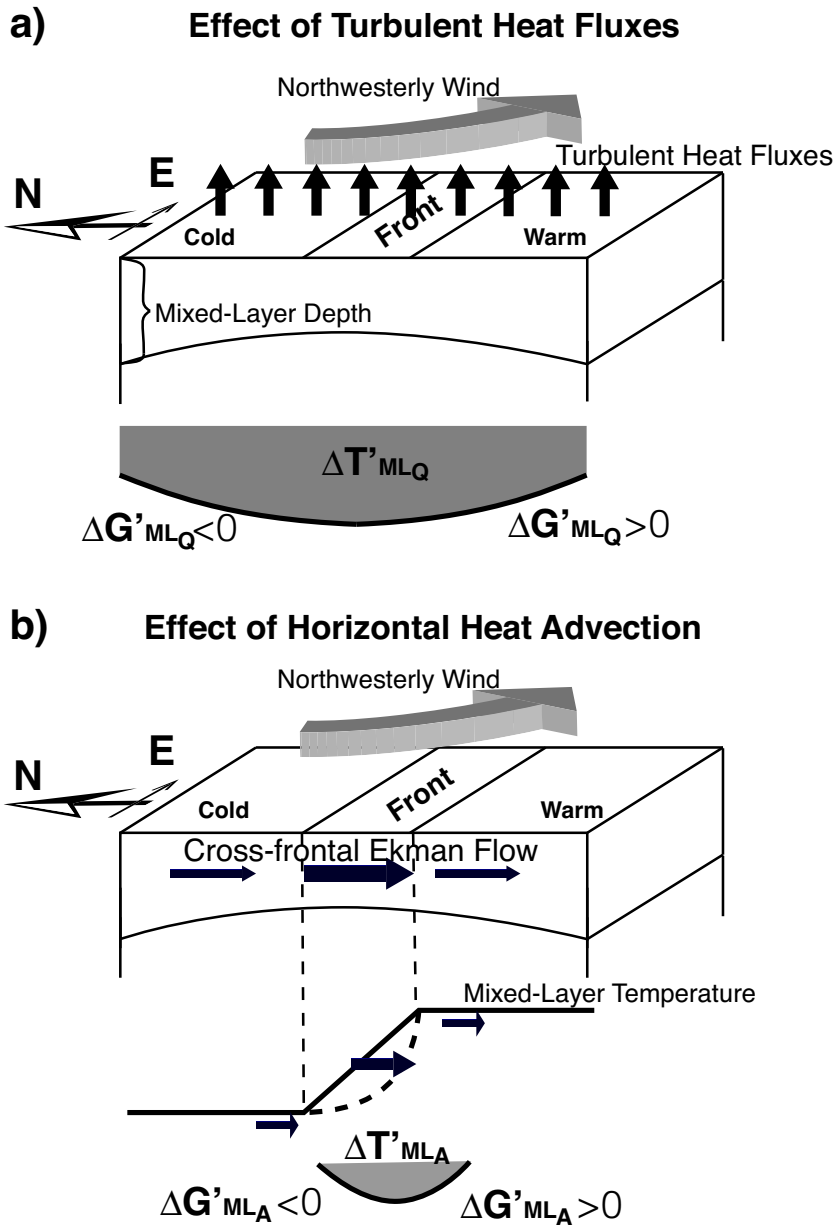

Figure 4.1: Schematic views of the oceanic responses: effects of turbulent heat fluxes (a) and horizontal heat advection (b) during passage of extratropical cyclones. Thick gray arrow represents strong northwesterly wind associated with the cyclones. In both panels, gray shading in lower portions shows temperature reduction caused by turbulent heat fluxes ($\Delta T'_{ML_Q}$) and horizontal heat advection ($\Delta T'_{ML_A}$), and slopes of solid curves represent changes of frontal sharpness ($\Delta G'_{ML_Q}$ and $\Delta G'_{ML_A}$).

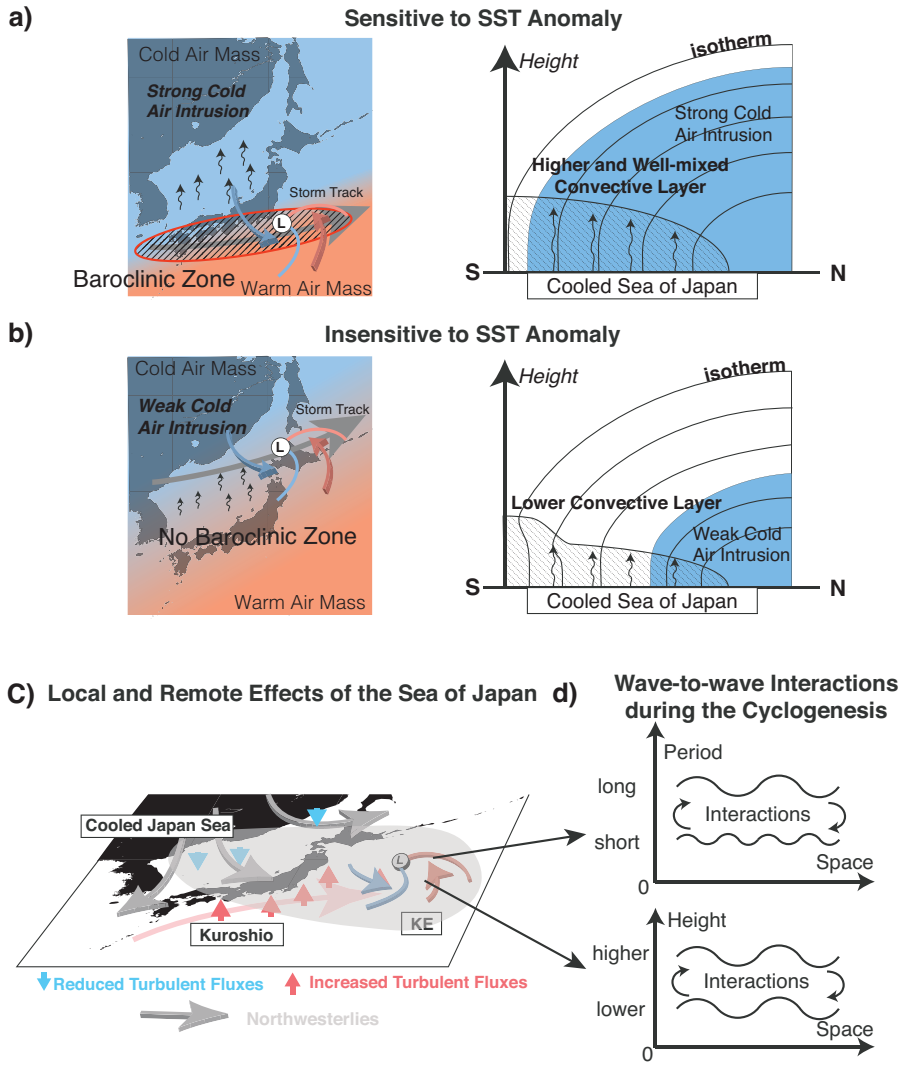

Figure 4.2: Schematic views of the atmospheric responses. Panel a and b showed the relation between large-scale backgrounds and the cyclone sensitivities. Circled **L** represents the center of a extratropical cyclone associated with the blue and red lines and arrows representing the cold and warm fronts. Black arrows in panel a and b show the effect of SST anomaly in the Sea of Japan. Panel c represents the effects of the Sea of Japan with the reduced SST. The gray arrows represent the northwesterly winds which spreading the colder air onto the surrounding regions. Blue and red arrows represent the local effects including the modulations of the cyclones and turbulent heat fluxes, while the gray shading represents the remote effects that transported by the modulated cyclones. Panel d Simplified wave-to-wave interactions between different frequencies and levels during the cyclogenesis, and the directions of energy transferring are shown by arrows.

Appendix A

Derivation of Nonlinear Anomalous Term in Equation (2.2)

For example, an anomalous temperature (T') is derived as

$$T' = T - \overline{T}, \tag{A.1}$$

where the overbar represents the seasonal trend. Substituting anomalies and seasonal trend into the nonlinear term (horizontal advection, $\mathbf{U} \cdot \nabla T$) yields

$$(\mathbf{U}' + \overline{\mathbf{U}}) \cdot \nabla(T' + \overline{T}) = \overline{\mathbf{U}} \cdot \nabla\overline{T} + \overline{\mathbf{U}} \cdot \nabla T' + \mathbf{U}' \cdot \nabla T. \tag{A.2}$$

The first term in the right-hand side is the seasonal trend of the advection term which should be removed. During our data processing, we also found that the second term is one order smaller (O(0.01 °C), Figure A.1) than the third term (O(0.1 °C)). Therefore, the non-linear anomalous advection term can be defined by $\mathbf{U}' \cdot \nabla T$ as described in Equation (2.2).

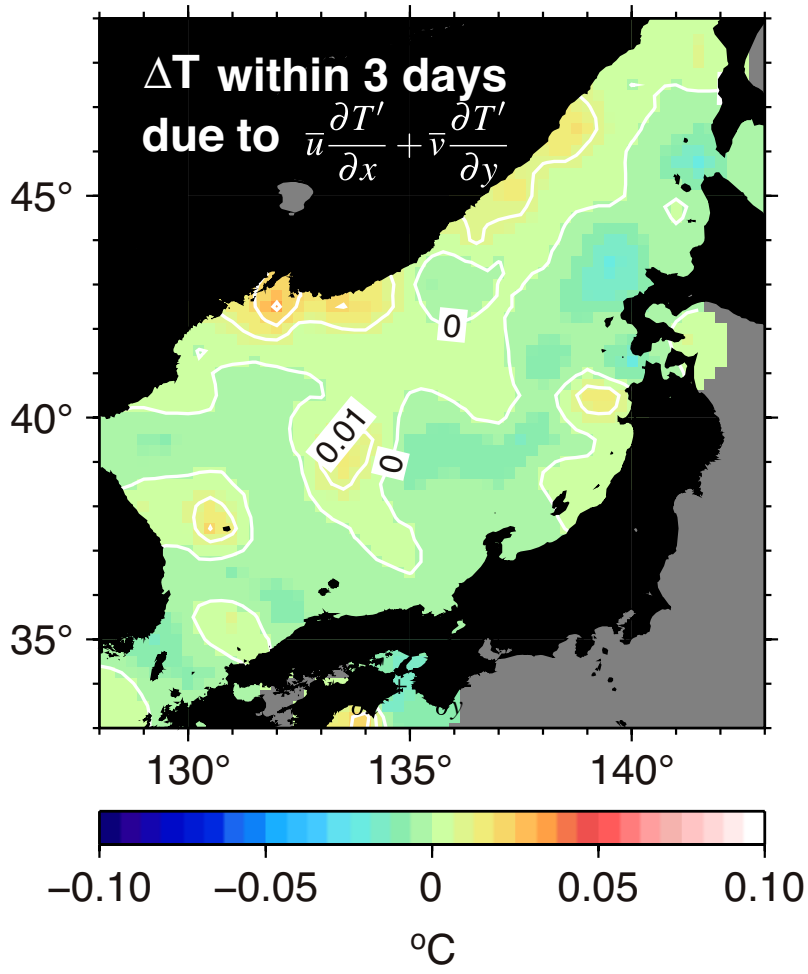

Figure A.1: The temperature reduction (ΔT) due to the second term in Equation (A.2) (mathematical expression is also showed in the figure) during the cyclones.

Appendix B

Surface Cooling Events in East Asian Marginal Seas during the Cyclones Detected in Chapter 2

In Chapter 2, we used the extreme surface heat release in the Sea of Japan as the indicator of the passage of winter cyclones. However, the same surface cooling may happen in all the marginal seas in East Asia, since the extratropical cyclones are synoptic scale eddies with a diameter over 1000 km. Thus, we extended our analysis of the surface heat fluxes to all the regions in East Asia temporally and spatially.

Figure B.1 showed the composite maps of 1-8 day band-pass filtered SLP around the peak days in the Sea of Japan same as Figure 2.3 but with an extension from two days before to three days after. These figures clearly showed the passage of the sub-weekly scale synoptic cyclone in the East Asian regions. The low-pressure system was firstly generated over the East Asian continent, however, it remained weak until moved over the relatively

warm marginal seas (Figure B.1I). It developed rapidly near the Sea of Japan (Figure B.1II and III), and then moved northeastward with a center south of Sea of Okhotsk on one day after (Figure B.1IV). The cyclone passed the entire East Asian region within five days (Figure B.1I to V).

Similarly, the strong surface cooling can be seen in the map of turbulent heat flux anomalies (difference from the climatological winter mean, Figure B.2). At first, a small anomaly appeared in Bo Hai Sea on Day I (Figure B.2I) when the cyclone generated (Figure B.1I). This anomaly extended to the Yellow Sea, the East China Sea, and the western part of Sea of Japan on the next day (Figure B.2II). Then, the strongest heat release was found in the East China Sea, the Sea of Japan, and the Kuroshio region on Day III (Figure B.2III), followed by the strong cooling in Kuroshio Extension on Day IV.

To find the detailed affecting time on each region, we plotted the time series of the turbulent heat flux anomalies based on the area averaged results (Figure B.3b). The heat release was firstly appeared in the Yellow Sea and East China Sea on Day II. However, the largest cooling was found on the next day. The Sea of Japan showed the largest heat release among all the regions (over 160 W m^{-2}, upward positive), followed by the Yellow Sea and the East China Sea and the Kuroshio region (about 150 W m^{-2}). Relatively lesser heat release in the Oyashio region and Kuroshio Extension can be seen on Day IV. The daily differences (i.e., temporal deviation) clearly showed the affecting time which is summarized in Table B.1 along with the area averaged SST reduction (seasonal trend was also removed as in Chapter 2).

Although most of East Asian regions experienced the same cooling time, the Sea of Japan had the greatest SST reduction. Figure B4 showed a horizontal map of the SST reductions in East Asia which was calculated by the difference between two days after and the two days before. Besides the Sea of Japan that we have discussed in Chapter 2, the Yellow Sea and the East

China Sea were also greatly cooled by the cyclone, especially the coastal areas. It is possibly because of the relatively shallow depth of those regions [*Xie et al.*, 2002]. Interestingly, although the Kuroshio region release a great amount of heat (maximum over 200 W m^{-2}) during the cyclone, it showed very small temperature reduction when seeing the temperature changes in a longer time than the cyclone affecting time. This fact suggested the heat advection of the strong warm current may fasten the temperature recovery in the ocean. However, in those regions which had few heat supplement from the warm current, the temperature recovery needs more time.

There was no great heat loss and temperature reduction found in the Oyashio region and the Sea of Okhotsk. This is because these regions had much colder SST than other regions, and they also located away from the cyclone's center where the strongest heat releasing happened [e.g., *Hirata et al.*, 2015].

Results of this Appendix suggested that, although the surface cooling was not limited in the Sea of Japan, it still experienced the largest SST reduction if the cyclone passed over the Sea of Japan. One may consider that this cold Sea of Japan would affect the next passing cyclone and therefore become the link between two consecutive passing cyclones which will be discussed in Chapter 3.

Finally, it should be noted that our results are based on the extreme cooling events in the Sea of Japan, which leads to the exclusion of the cyclones that passing too far away from the Sea of Japan. To confirm whether the Sea of Japan experiences the greatest SST reduction during all the cyclones generated in East Asia, further analyses and comparisons based on the cooling events in other regions are needed which should be the future work of this topic.

Table B.1: Cyclone affecting time on the regions in East Asia and the area averaged SST reduction

	Yellow Sea & East China Sea	**Sea of Japan**	**Kuroshio Region**	**Kuroshio Extension**	**Oyashio Region**	**Sea of Okhotsk**
Cooling Period* **(based on the Figure B.3b)**	Day II to Day IV	Day II to Day IV	Day II to Day IV	Day III to Day V	Day III to Day V	Day III to Day V
ΔSST (° C)	−0.179	−0.259	−0.143	−0.097	−0.022	−0.003

* The Day I-VI correspond the panels in Figure B.1 and B.2.

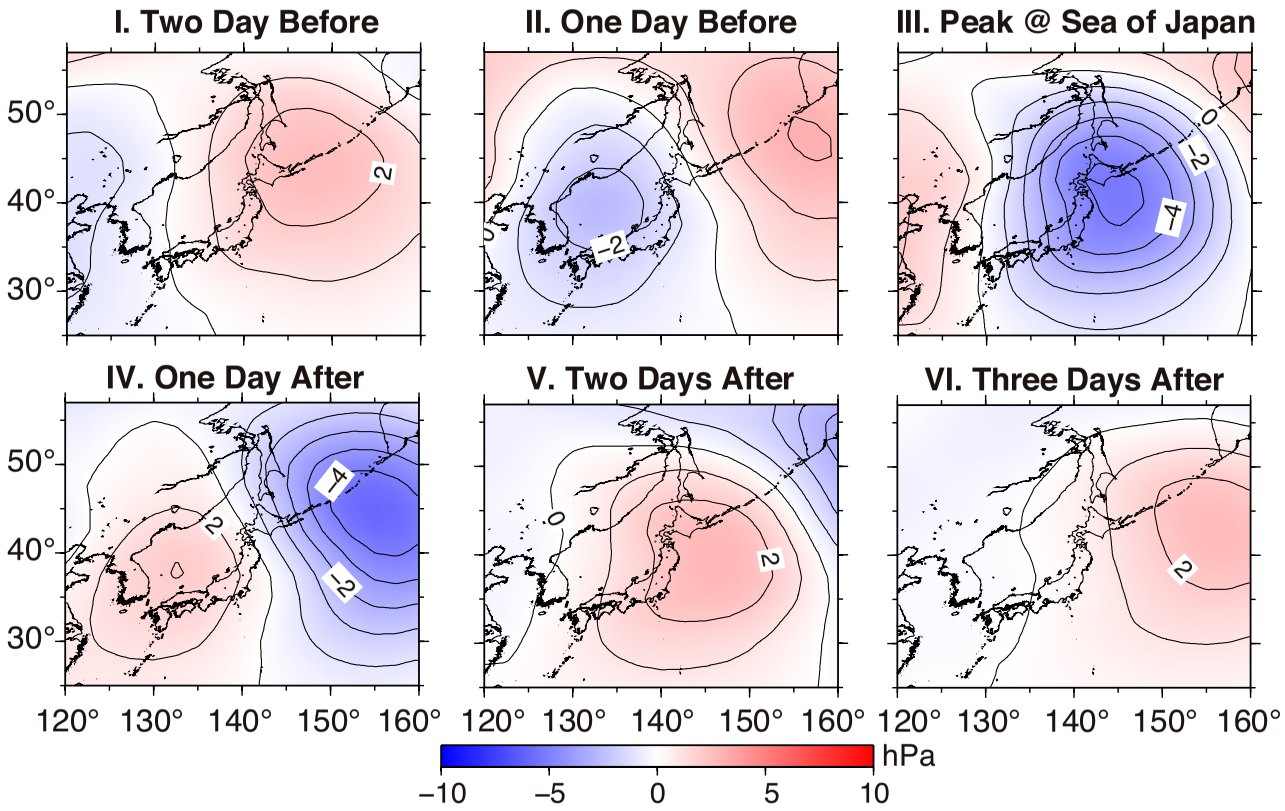

Figure B.1: Composite maps of 1-8 day band-pass filtered SLP. Same as Figure 2.3 but for an extended period.

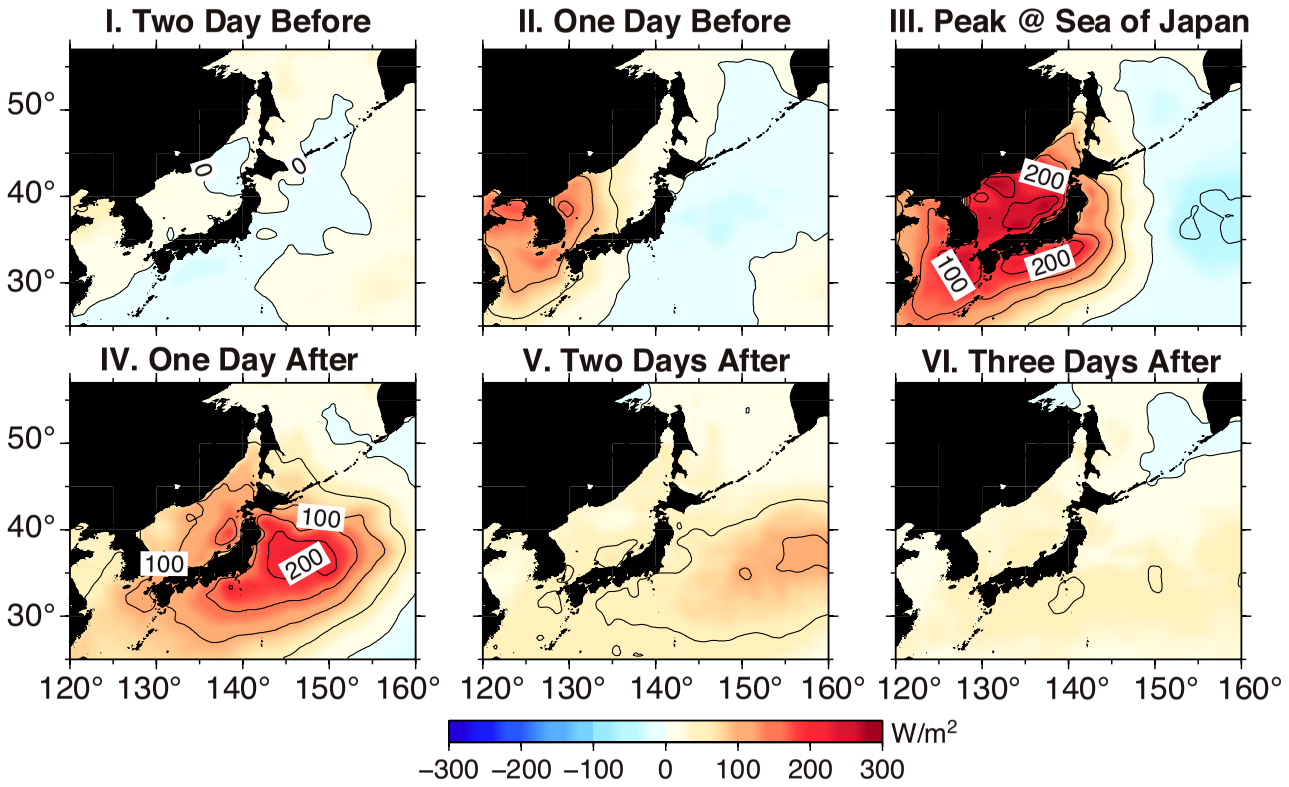

Figure B.2: Composite maps of anomalies of surface turbulent heat fluxes during the same period in Figure B.1. Contour interval is 50 W m^{-2}.

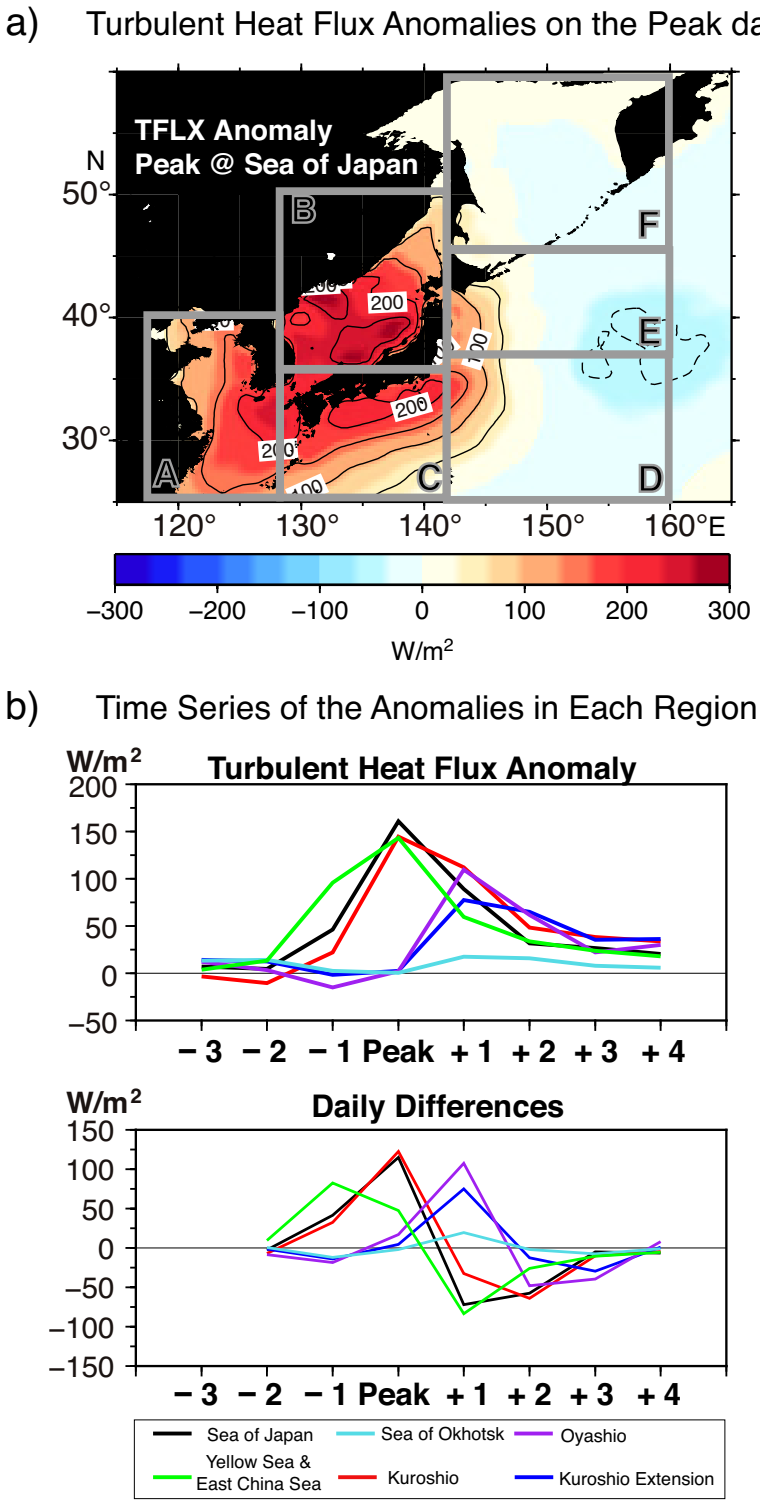

Figure B.3: (a) Anomaly of the surface turbulent heat fluxes on Peak days which is same as the Figure B2III. Gray boxes showed the five major regions in East Asian for the box averaging. (b) Time series of the box averaged flux anomalies (upper panel) in five regions (color lines) and their daily differences (i.e., time deviations, lower panel).

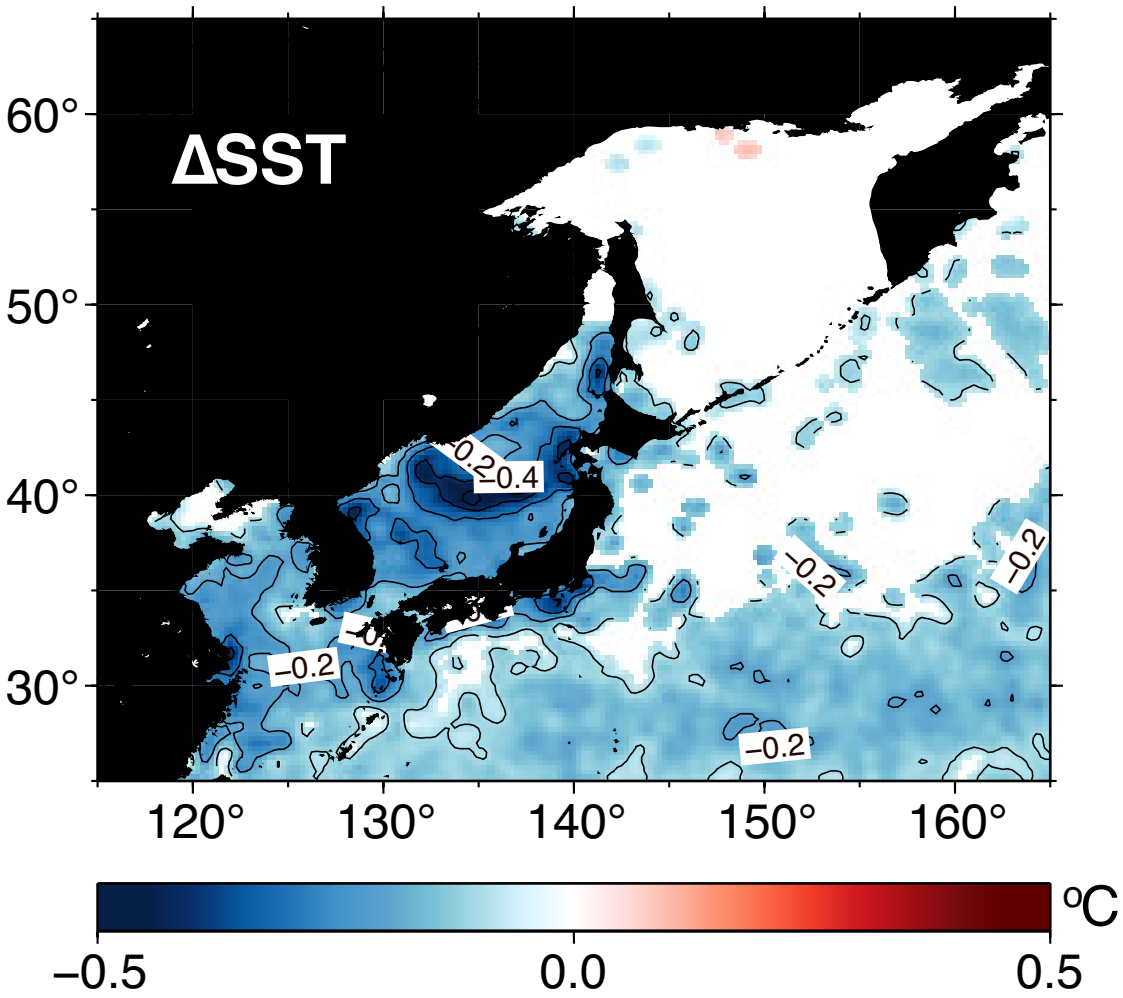

Figure B.4: Composite map of the SST reduction in East Asia during the passage of cyclones. Only significant results are plotted (95 % confidence level suggested by a student-t test).

Appendix C

Ensemble Simulations for Results Validation in Chapter 3

In this study, the SST anomalies given to the Sea of Japan was, on average, very small (-0.25 °C) compared to the zonal SST difference ($\sim$ 16 K; see Figure 3.1), and thus, our results might appear vulnerable to small fluctuations in SST anomaly which possibly grow to other situations as time goes on. We therefore need to examine whether or not our results are robust to SST fluctuations, especially when the SST anomaly used in AF runs is much smaller than other similar studies [e.g., *Yamamoto and Hirose*, 2007; *Yamamoto*, 2013].

For validating our modelled results mentioned in the present study, we carried out a set of 10-member ensemble simulations for AF runs, forced by different SST anomalies. The 'new' SST anomalies used in each member were the combination of 'old' anomaly (color shading in Figure 3.1) and normally distributed random noise with the same standard deviation of the 'old' anomaly.

In spite of small fluctuations given to the SST anomaly as a lower boundary condition, all experiments show the poleward shifting and cyclone deepening (Figure C.1). As shown in Figure C.2, a clear S-shape trough-ridge structure can be seen, which were similar as the Figure 3 of *Yamamoto* [2013] but with opposite sign, indicating a strengthened cyclone due to the colder Sea of Japan. In Figure C.3, the ensemble means of the anomalies of diabatic heating rate, the PV tendency due to the diabatic heating, and vertical velocity (only the results over 95% confidence level were plotted), which were similar as the results of one single sensitivity experiment in Figure 3.9, where the enhanced diabatic heating and anomalies of positive PV tendency and upward velocity were all revealed on the northern side of the cyclone center ('L' in Figure C.3).

Therefore, our results could be validated and our conclusions are confirmed to be robust. Moreover, these results also suggested that, in a small marginal sea at least, the negative SST anomaly itself is important for the synoptic scale cyclones, as well as the horizontal SST distribution such the oceanic frontal structure [e.g., *Yamamoto and Hirose*, 2007].

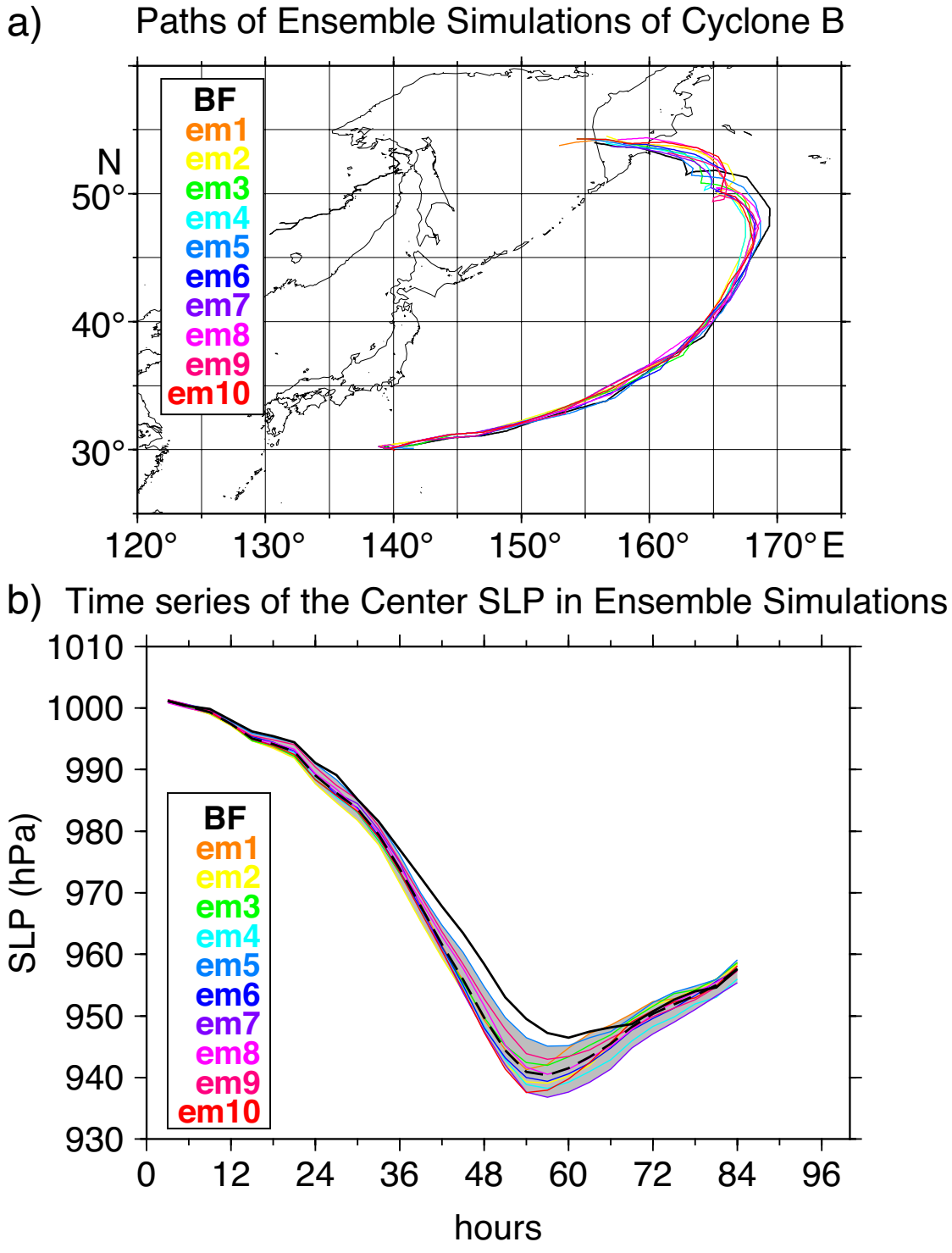

Figure C.1: Results of ensemble experiments for the Cyclone B in Chapter 3. The results of BF run are shown by black curves and other colored curves are for the ensemble members: a) the cyclone paths; (b) the time evolutions of the central SLPs with the ensemble mean values showed by dashed line.

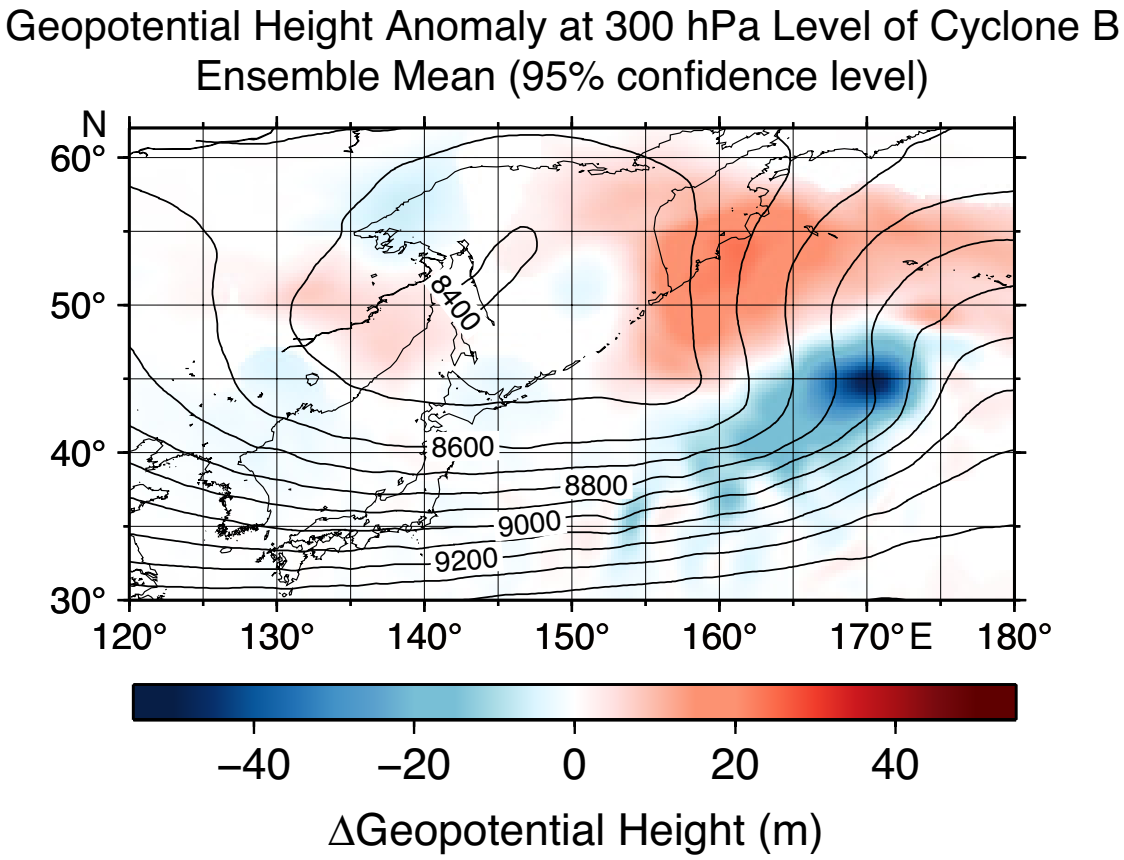

Figure C.2: A S-shape trough-ridge anomalies geopotential height at 300-hPa level when the Cyclone B reached its maximum deepening rate. Only significant results are plotted (95 % confidence level suggested by a student-t test). Contour interval is 100 m.

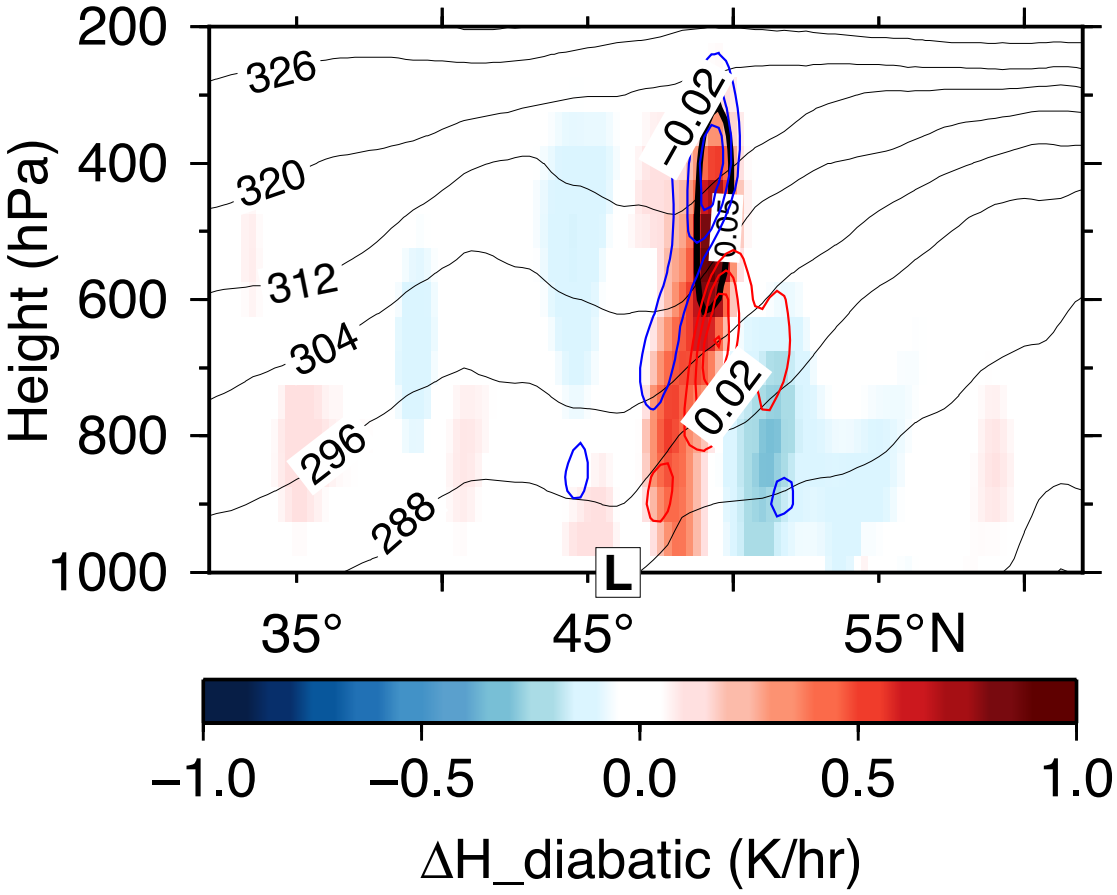

Figure C.3: Same as the Figure 3.9 but for the values of ensemble mean. Only significant results are plotted (95 % confidence level suggested by a student-t test). Contour intervals are 8 K ($<$ 312 K), 16K ($>$ 312 K), 0.05 m s^{-1}, and 0.01 PVU hr^{-1}, respectively.

List of References

Banzon, V., T. M. Smith, T. M. Chin, C. Liu, and W. Hankins (2016), A long-term record of blended satellite and in situ sea-surface temperature for climate monitoring, modeling and environmental studies, *Earth System Science Data*, *8*(2), 165–176, doi:10.5194/essd-8-165-2016.

Bao, J., J. Wilczak, J. Choi, and L. Kantha (2000), Numerical simulations of air–sea interaction under high wind conditions using a coupled model: A study of hurricane development, *Monthly Weather Review*, *128*(7), 2190–2210, doi:10.1175/1520-0493(2000)128<2190:NSOASI>2.0.CO;2.

Belkin, I., and P. Cornillon (2003), Sst fronts of the pacific coastal and marginal seas, *Pacific Oceanography*, *1*(2), 90–113.

Bjerknes, J., and H. Solberg (1922), Life cycle of cyclones and the polar front theory of atmospheric circulation.

Blackmon, M. L., J. M. Wallace, N.-C. Lau, and S. L. Mullen (1977), An observational study of the northern hemisphere wintertime circulation, *Journal of the Atmospheric Sciences*, *34*(7), 1040–1053, doi:10.1175/1520-0469(1977)034<1040:AOSOTN>2.0.CO;2.

Blender, R., K. Fraedrich, and F. Lunkeit (1997), Identification of cyclone-track regimes in the north atlantic, *Quarterly Journal of the Royal Meteorological Society*, *123*(539), 727–741, doi:10.1002/qj.49712353910.

Brayshaw, D. J., B. Hoskins, and M. Blackburn (2008), The storm-track re-

sponse to idealized sst perturbations in an aquaplanet gcm, *Journal of the Atmospheric Sciences*, *65*(9), 2842–2860, doi:10.1175/2008JAS2657.1.

Catto, J., C. Jakob, G. Berry, and N. Nicholls (2012), Relating global precipitation to atmospheric fronts, *Geophysical Research Letters*, *39*(10), doi:10.1029/2012GL051736.

Catto, J. L., and S. Pfahl (2013), The importance of fronts for extreme precipitation, *Journal of Geophysical Research: Atmospheres*, *118*(19), doi:10.1002/jgrd.50852.

Chang, E. K., S. Lee, and K. L. Swanson (2002), Storm track dynamics, *Journal of Climate*, *15*(16), 2163–2183.

Chelton, D. B., and S.-P. Xie (2010), Coupled ocean-atmosphere interaction at oceanic mesoscales, *Oceanography*, *23*, 52–69, doi:10.5670/oceanog.2010.05.

Chen, S. S., W. Zhao, J. E. Tenerelli, R. H. Evans, and V. Halliwell (2001), Impact of the avhrr sea surface temperature on atmospheric forcing in the japan/east sea, *Geophysical research letters*, *28*(24), 4539–4542.

Choi, H., and Y. Zhang (2005), Monthly variation of sea-air temperature differences in the korean coast, *Journal of Oceanography*, *61*(2), 359–367, doi:10.1007/s10872-005-0046-y.

Choi, Y. (1996), Open-ocean convection in the japan (east) sea, *La mer*, *34*, 259–272.

Choi, Y. J., and J.-H. Yoon (2010), Structure and seasonal variability of the deep mean circulation of the east sea (sea of japan), *Journal of oceanography*, *66*(3), 349, doi:10.1007/s10872-005-0046-y.

Chu, P. C., J. Lan, and C. Fan (2001), Japan sea thermohaline structure and circulation. part i: Climatology, *Journal of Physical Oceanography*, *31*(1), 244–271, doi:\text{10.1175/1520-0485(2001)031<0244:JSTSAC>2.0.CO;2}.

Dare, R. A., and J. L. McBride (2011), Sea surface temperature response

to tropical cyclones, *Monthly Weather Review*, *139*(12), 3798–3808, doi:10.1175/MWR-D-10-05019.1.

Ding, J. C., Yihuiand Chan (2005), The east asian summer monsoon: an overview, *Meteorology and Atmospheric Physics*, *89*(1), 117–142, doi:10.1007/s00703-005-0125-z.

Ding, Y., and T. N. Krishnamurti (1987), Heat budget of the siberian high and the winter monsoon, *Monthly Weather Review*, *115*(10), 2428–2449, doi:10.1175/1520-0493(1987)115<2428:HBOTSH>2.0.CO;2.

Dorman, C., R. Beardsley, R. Limeburner, S. Varlamov, M. Caruso, and N. Dashko (2005), Summer atmospheric conditions over the japan/east sea, *Deep Sea Research Part II: Topical Studies in Oceanography*, *52*(11), 1393–1420, doi:10.3402/tellusa.v66.23210.

Dorman, C. E., R. C. Beardsley, N. Dashko, C. Friehe, D. Kheilf, K. Cho, R. Limeburner, and S. Varlamov (2004), Winter marine atmospheric conditions over the japan sea, *Journal of Geophysical Research: Oceans (1978–2012)*, *109*(C12), doi:10.1029/2001JC001197.

Flaounas, E., V. Kotroni, K. Lagouvardos, and I. Flaounas (2014), Cyclotrack (v1. 0)–tracking winter extratropical cyclones based on relative vorticity: sensitivity to data filtering and other relevant parameters, *Geoscientific Model Development*, *7*(4), 1841–1853, doi:10.5194/gmd-7-1841-2014.

Fu, S., J. Sun, and J. Sun (2014), Accelerating two-stage explosive development of an extratropical cyclone over the northwestern pacific ocean: a piecewise potential vorticity diagnosis, *Tellus A*, *66*, doi:10.3402/tellusa.v66.23210.

Graff, L. S., and J. LaCasce (2012), Changes in the extratropical storm tracks in response to changes in sst in an agcm, *Journal of Climate*, *25*(6), 1854–1870, doi:10.1175/JCLI-D-11-00174.1.

Hirata, H., R. Kawamura, M. Kato, and T. Shinoda (2015), Influential role of moisture supply from the kuroshio/kuroshio extension in the rapid de-

velopment of an extratropical cyclone, *Monthly Weather Review*, *143*(10), 4126–4144, doi:10.1175/MWR-D-15-0016.1.

Hirose, N., K. Nishimura, and M. Yamamoto (2009), Observational evidence of a warm ocean current preceding a winter teleconnection pattern in the northwestern pacific, *Geophysical Research Letters*, *36*(9), doi:10.1029/2009GL037448.

Hirose, N., K. Takayama, J.-H. Moon, W. Tatsuro, and N. Yoshinori (2013), Regional data assimilation system extended to the east asian marginal seas, *Sea and Sky*, *89*(2), 1–9.

Hodges, K. (1999), Adaptive constraints for feature tracking, *Monthly Weather Review*, *127*(6), 1362–1373, doi:10.1175/1520-0493(1999)127<1362:ACFFT>2.0.CO;2.

Hoskins, B. J., and P. J. Valdes (1990), On the existence of storm-tracks, *Journal of the atmospheric sciences*, *47*(15), 1854–1864, doi:0.1175/1520-0469(1990)047<1854:OTEOST>2.0.CO;2.

Hoskins, B. J., and N. V. West (1979), Baroclinic waves and frontogenesis. part ii: Uniform potential vorticity jet flows-cold and warm fronts, *Journal of the Atmospheric Sciences*, *36*(9), 1663–1680, doi:10.1175/1520-0469(1979)036<1663:BWAFPI>2.0.CO;2.

Inatsu, M. (2009), The neighbor enclosed area tracking algorithm for extratropical wintertime cyclones, *Atmospheric Science Letters*, *10*(4), 267–272, doi:10.1002/asl.238.

Inatsu, M., H. Mukougawa, and S.-P. Xie (2003), Atmospheric response to zonal variations in midlatitude sst: Transient and stationary eddies and their feedback, *Journal of Climate*, *16*(20), 3314–3329.

Isobe, A. (1999), The taiwan-tsushima warm current system: Its path and the transformation of the water mass in the east china sea, *Journal of oceanography*, *55*(2), 185–195.

Isobe, A., and R. C. Beardsley (2007), Atmosphere and marginal-sea interaction leading to an interannual variation in cold-air outbreak activity over the japan sea, *Journal of Climate*, *20*(23), 5707–5714, doi:10.1175/2007JCLI1779.1.

Isobe, A., and S. Kako (2012), A role of the yellow and east china seas in the development of extratropical cyclones in winter, *Journal of Climate*, *25*(23), 8328–8340, doi:10.1175/JCLI-D-11-00391.1.

Isoda, Y. (1994a), Interannual sst variations to the north and south of the polar front in the japan sea (proceedings of the seventh japan and east china seas study workshop), *La mer*, *32*(4), p285–293.

Isoda, Y. (1994b), Interannual sst variations to the north and south of the polar front in the japan sea, *La mer*, *32*, 285–293.

Iwasaki, S., A. Isobe, and S. Kako (2014), Atmosphere–ocean coupled process along coastal areas of the yellow and east china seas in winter, *Journal of Climate*, *27*(1), 155–167, doi:10.1175/JCLI-D-13-00117.1.

Kanamitsu, M., W. Ebisuzaki, J. Woollen, S.-K. Yang, J. Hnilo, M. Fiorino, and G. Potter (2002), NcepâĂŞdoe amip-ii reanalysis (r-2), *Bulletin of the American Meteorological Society*, *83*(11), 1631–1643, doi:10.1175/BAMS-83-11-1631.

Kang, S. K., Y. H. Seung, J. J. Park, J.-H. Park, J. H. Lee, E. J. Kim, Y. H. Kim, and M.-S. Suk (2016), Seasonal variability in middepth gyral circulation patterns in the central east/japan sea as revealed by long-term argo data, *Journal of Physical Oceanography*, *46*(3), 937–946, doi:10.1175/JPO-D-15-0157.1.

Kawabe, M. (1982), Branching of the tsushima current in the japan sea, *Journal of the Oceanographical Society of Japan*, *38*(2), 95–107.

Kawai, H. (2004), Innovation and intellectual property rights, in *Tsushima Warm Current-Ocean Structure and Fishery*, pp. 7–26, Fishery Society of Japan, Tokyo.

Kawamura, H., and P. Wu (1998), Formation mechanism of japan sea proper water in the flux center off vladivostok, *Journal of Geophysical Research: Oceans (1978–2012)*, *103*(C10), 21,611–21,622, doi:10.1029/98JC01948.

Kazmin, A. S., and M. M. Rienecker (1996), Variability and frontogenesis in the large-scale oceanic frontal zones, *Journal of Geophysical Research: Oceans*, *101*(C1), 907–921, doi:10.1029/95JC02992.

Kelly, K. A., R. J. Small, R. Samelson, B. Qiu, T. M. Joyce, Y.-O. Kwon, and M. F. Cronin (2010), Western boundary currents and frontal air–sea interaction: Gulf stream and kuroshio extension, *Journal of Climate*, *23*(21), 5644–5667, doi:10.1175/2010JCLI3346.1.

Keyser, D., B. D. Schmidt, and D. G. Duffy (1989), A technique for representing three-dimensional vertical circulations in baroclinic disturbances, *Monthly Weather Review*, *117*(11), 2463–2494, doi:10.1175/1520-0493(1989)117<2463:ATFRTD>2.0.CO;2.

Kim, C.-H., and J.-H. Yoon (1996), Modeling of the wind-driven circulation in the japan sea using a reduced gravity model, *Journal of Oceanography*, *52*(3), 359–373, doi:10.1007/BF02235930.

König, W., R. Sausen, and F. Sielmann (1993), Objective identification of cyclones in gcm simulations, *Journal of Climate*, *6*(12), 2217–2231.

Kwon, Y.-O., M. A. Alexander, N. A. Bond, C. Frankignoul, H. Nakamura, B. Qiu, and L. A. Thompson (2010), Role of the gulf stream and kuroshioâĂŞoyashio systems in large-scale atmosphereâĂŞocean interaction: A review, *Journal of Climate*, *23*(12), 3249–3281, doi:10.1175/2010JCLI3343.1.

Large, W., and S. Pond (1981), Open ocean momentum flux measurements in moderate to strong winds, *Journal of Physical Oceanography*, *11*(3), 324–336.

Lee, C. M., L. N. Thomas, and Y. Yoshikawa (2006), Intermediate water formation at the japan/east sea subpolar front, *Oceanography*, *19*(3), 110–121, doi:10.5670/oceanog.2006.48.

Lee, D.-K., and P. Niiler (2005), The energetic surface circulation patterns of the japan/east sea, *Deep Sea Research Part II: Topical Studies in Oceanography*, *52*(11), 1547 – 1563, doi:10.1016/j.dsr2.2003.08.008.

Lim, S., C. J. Jang, J. Park, et al. (2012), Climatology of the mixed layer depth in the east/japan sea, *Journal of Marine Systems*, *96*, 1–14, doi:10.1016/j.jmarsys.2012.01.003.

Ma, X., P. Chang, R. Saravanan, D. Wu, X. Lin, L. Wu, and X. Wan (2015), Winter extreme flux events in the kuroshio and gulf stream extension regions and relationship with modes of north pacific and atlantic variability, *Journal of Climate*, *28*(12), 4950–4970, doi:10.1175/JCLI-D-14-00642.1.

Ma, X., P. Chang, R. Saravanan, R. Montuoro, H. Nakamura, D. Wu, X. Lin, and L. Wu (2017), Importance of resolving kuroshio front and eddy influence in simulating the north pacific storm track, *Journal of Climate*, *30*(5), 1861–1880, doi:10.1175/JCLI-D-16-0154.1.

Masunaga, R., H. Nakamura, T. Miyasaka, K. Nishii, and B. Qiu (2016), Interannual modulations of oceanic imprints on the wintertime atmospheric boundary layer under the changing dynamical regimes of the kuroshio extension, *Journal of Climate*, *29*(9), 3273–3296, doi:10.1175/JCLI-D-15-0545.1.

Mei, W., and C. Pasquero (2013), Spatial and temporal characterization of sea surface temperature response to tropical cyclones, *Journal of Climate*, *26*(11), 3745–3765, doi:10.1175/JCLI-D-12-00125.1.

Minobe, S., A. Kuwano-Yoshida, N. Komori, S.-P. Xie, and R. J. Small (2008), Influence of the gulf stream on the troposphere, *Nature*, *452*(7184), 206–209.

Morimoto, A., and T. Yanagi (2001), Variability of sea surface circulation in the japan sea, *Journal of Oceanography*, *57*(1), 1–13, doi:10.1023/A:1011149401735.

Nakamura, H. (1992), Midwinter suppression of baroclinic wave activity in the pacific, *Journal of the Atmospheric Sciences*, *49*(17), 1629–1642.

Nakamura, H., T. Izumi, and T. Sampe (2002), Interannual and decadal modulations recently observed in the pacific storm track activity and east asian winter monsoon, *Journal of Climate*, *15*(14), 1855–1874, doi:10.1175/1520-0442(2002)015<1855:IADMRO>2.0.CO;2.

Nakamura, H., T. Sampe, Y. Tanimoto, and A. Shimpo (2004), Observed associations among storm tracks, jet streams and midlatitude oceanic fronts, *EarthâĂŹs Climate: The Ocean–Atmosphere Interaction, Geophys. Monogr*, *147*, 329–345, doi:10.1029/147GM18.

NCEP (2000), Operational model global tropospheric analyses continuing from July 1999, *Research Data Archive at the National Center for Atmospheric Research, Computational and Information Systems Laboratory, Boulder, CO. Available: http://rda. ucar. edu/datasets/ds083*, doi:10.5065/D6M043C6.

Neiman, P. J., and M. Shapiro (1993), The life cycle of an extratropical marine cyclone. part i: Frontal-cyclone evolution and thermodynamic air-sea interaction, *Monthly Weather Review*, *121*(8), 2153–2176, doi:10.1175/1520-0493(1993)121<2153:TLCOAE>2.0.CO;2.

Nonaka, M., H. Nakamura, B. Taguchi, N. Komori, A. Kuwano-Yoshida, and K. Takaya (2009), Air-sea heat exchanges characteristic of a prominent midlatitude oceanic front in the south indian ocean as simulated in a high-resolution coupled gcm, *Journal of Climate*, *22*(24), 6515–6535, doi:10.1175/2009JCLI2960.1.

Ogawa, F., H. Nakamura, K. Nishii, T. Miyasaka, and A. Kuwano-Yoshida (2012), Dependence of the climatological axial latitudes of the tropospheric westerlies and storm tracks on the latitude of an extratropical oceanic front, *Geophysical Research Letters*, *39*(5), doi:10.1029/2011GL049922.

Overland, J. E., J. M. Adams, and N. A. Bond (1999), Decadal variability of the aleutian low and its relation to high-latitude circulation, *Journal of Climate*, *12*(5), 1542–1548, doi:0.1175/1520-0442(1999)012<1542:DVOTAL>2.0.CO;2.

Papritz, L., S. Pfahl, H. Sodemann, and H. Wernli (2015), A climatology of cold air outbreaks and their impact on air–sea heat fluxes in the high-latitude south pacific, *Journal of Climate*, *28*(1), 342–364, doi:10.1175/JCLI-D-14-00482.1.

Parfitt, R., A. Czaja, S. Minobe, and A. Kuwano-Yoshida (2016), The atmospheric frontal response to sst perturbations in the gulf stream region, *Geophysical Research Letters*, *43*(5), 2299–2306, doi:10.1002/2016GL067723.

Park, J.-H., and D. R. Watts (2005), Response of the southwestern japan/east sea to atmospheric pressure, *Deep Sea Research Part II: Topical Studies in Oceanography*, *52*(11), 1671–1683, doi:10.1016/j.dsr2.2003.08.007.

Park, J. J., and K. Kim (2013), Deep currents obtained from argo float trajectories in the japan/east sea, *Deep Sea Research Part II: Topical Studies in Oceanography*, *85*, 169–181, doi:10.1016/j.dsr2.2012.07.032.

Park, K.-A., D. S. Ullman, K. Kim, J. Y. Chung, and K.-R. Kim (2007), Spatial and temporal variability of satellite-observed subpolar front in the east/japan sea, *Deep Sea Research Part I: Oceanographic Research Papers*, *54*(4), 453–470, doi:10.1016/j.dsr.2006.12.010.

Paulson, C. A., and J. J. Simpson (1977), Irradiance measurements in the upper ocean, *Journal of Physical Oceanography*, *7*(6), 952–956.

Pinto, J. G., U. Ulbrich, G. Leckebusch, T. Spangehl, M. Reyers, and S. Zacharias (2007), Changes in storm track and cyclone activity in three sres ensemble experiments with the echam5/mpi-om1 gcm, *Climate Dynamics*, *29*(2-3), 195–210, doi:10.1007/s00382-007-0230-4.

Prants, S. V., M. V. Budyansky, and M. Y. Uleysky (2017), Statistical analysis of lagrangian transport of subtropical waters in the japan sea based on aviso altimetry data, *Nonlinear Processes in Geophysics*, *24*(1), 89, doi:10.5194/npg-24-89-2017.

Putrasahan, D. A., A. J. Miller, and H. Seo (2013), Isolating mesoscale coupled ocean–atmosphere interactions in the kuroshio extension region, *Dy-*

namics of Atmospheres and Oceans, *63*, 60–78, doi:10.1016/j.dynatmoce.2013.04.001.

Ren, X., W. Perrie, Z. Long, and J. Gyakum (2004), Atmosphere–ocean coupled dynamics of cyclones in the midlatitudes, *Monthly weather review*, *132*(10), 2432–2451, doi:10.1175/1520-0493(2004)132<2432:ACDOCI>2.0.CO;2.

Ren, X., X. Yang, and C. Chu (2010), Seasonal variations of the synoptic-scale transient eddy activity and polar front jet over east asia, *Journal of Climate*, *23*(12), 3222–3233, doi:10.1175/2009JCLI3225.1.

Reynolds, R. W., T. M. Smith, C. Liu, D. B. Chelton, K. S. Casey, and M. G. Schlax (2007), Daily high-resolution-blended analyses for sea surface temperature, *Journal of Climate*, *20*(22), 5473–5496, doi:10.1175/2007JCLI1824.1.

Roebber, P. J. (1984), Statistical analysis and updated climatology of explosive cyclones, *Monthly Weather Review*, *112*(8), 1577–1589, doi:10.1175/1520-0493(1984)112<1577:SAAUCO>2.0.CO;2.

Sampe, T., H. Nakamura, A. Goto, and W. Ohfuchi (2010), Significance of a midlatitude sst frontal zone in the formation of a storm track and an eddy-driven westerly jet, *Journal of Climate*, *23*(7), 1793–1814, doi:10.1175/2009JCLI3163.1.

Schultz, D. M., and G. Vaughan (2011), Occluded fronts and the occlusion process: A fresh look at conventional wisdom, *Bulletin of the American Meteorological Society*, *92*(4), 443–466, doi:10.1175/1520-0493(1998)126<1767:TEOLSF>2.0.CO;2.

Schultz, D. M., D. Keyser, and L. F. Bosart (1998), The effect of large-scale flow on low-level frontal structure and evolution in midlatitude cyclones, *Monthly weather review*, *126*(7), 1767–1791, doi:10.1175/1520-0493(1998)126<1767:TEOLSF>2.0.CO;2.

Senjyu, T., and H. Sudo (1994), The upper portion of the japan sea proper water; its source and circulation as deduced from isopycnal analysis, *Journal of Oceanography*, *50*(6), 663–690, doi:10.1007/BF02270499.

Senjyu, T., H.-R. Shin, J.-H. Yoon, Z. Nagano, H.-S. An, S.-K. Byun, and C.-K. Lee (2005), Deep flow field in the japan/east sea as deduced from direct current measurements, *Deep Sea Research Part II: Topical Studies in Oceanography*, *52*(11), 1726–1741, doi:10.1016/j.dsr2.2003.10.013.

Seo, H., Y.-O. Kwon, and J.-J. Park (2014), On the effect of the east/japan sea sst variability on the north pacific atmospheric circulation in a regional climate model, *Journal of Geophysical Research: Atmospheres*, *119*(2), 418–444, doi:10.1002/2013JD020523.

Shaman, J., R. M. Samelson, and E. Skyllingstad (2010), AirâĂŞsea fluxes over the gulf stream region: Atmospheric controls and trends, *Journal of Climate*, *23*(10), 2651–2670, doi:10.1175/2010JCLI3269.1.

Shapiro, M. A., and D. A. Keyser (1990), *Fronts, jet streams, and the tropopause*, US Department of Commerce, National Oceanic and Atmospheric Administration, Environmental Research Laboratories, Wave Propagation Laboratory.

Shaw, T., M. Baldwin, E. Barnes, R. Caballero, C. Garfinkel, Y.-T. Hwang, C. Li, P. O'Gorman, G. Rivière, I. Simpson, et al. (2016), Storm track processes and the opposing influences of climate change, *Nature Geoscience*, doi:10.1038/ngeo2783.

Skamarock, W. C., J. B. Klemp, J. Dudhia, D. O. Gill, D. M. Barker, W. Wang, and J. G. Powers (2008), A description of the advanced research wrf version 2, *Tech. rep.*, NCAR Technical Note NCAR/TN-475+STR, doi:doi:10.5065/D68S4MVH.

Small, R., S. Xie, L. OâĂŹNeill, H. Seo, Q. Song, P. Cornillon, M. Spall, S. Minobe, et al. (2008), Air-sea interaction over ocean fronts and eddies, *Dy-*

namics of Atmospheres and Oceans, *45*(3), 274–319, doi:10.1016/j.dynatmoce.2008.01.001.

Song, L., L. Wang, W. Chen, and Y. Zhang (2016), Intraseasonal variation of the strength of the east asian trough and its climatic impacts in boreal winter, *Journal of Climate*, *29*(7), 2557–2577, doi:10.1175/JCLI-D-14-00834.1.

Takikawa, T., and J.-H. Yoon (2005), Volume transport through the tsushima straits estimated from sea level difference, *Journal of oceanography*, *61*(4), 699–708, doi:10.1007/s10872-005-0077-4.

Talley, L. D., D.-H. Min, V. B. Lobanov, V. A. Luchin, V. I. Ponomarev, A. N. Salyuk, A. Y. Shcherbina, P. Y. Tishchenko, and I. Zhabin (2006), Japan/east sea water masses and their relation to the sea's circulation, *Oceanography*, *19*, doi:10.5670/oceanog.2006.42.

Tamarin, T., and Y. Kaspi (2016), The poleward motion of extratropical cyclones from a potential vorticity tendency analysis, *Journal of the Atmospheric Sciences*, *73*(4), 1687–1707, doi:10.1175/JAS-D-15-0168.1.

Teague, W., K. Tracey, D. Watts, J. Book, K.-I. Chang, P. Hogan, D. Mitchell, M.-S. Suk, M. Wimbush, and J.-H. Yoon (2005), Observed deep circulation in the ulleung basin, *Deep Sea Research Part II: Topical Studies in Oceanography*, *52*(11), 1802–1826, doi:10.1016/j.dsr2.2003.10.014.

Thomas, L. N., and C. M. Lee (2005), Intensification of ocean fronts by down-front winds, *Journal of Physical Oceanography*, *35*(6), 1086–1102, doi:10.1175/JPO2737.1.

Toba, Y., K. T OMIZAWA, Y. Kurasawa, and K. HANAWA (1982), Seasonal and year-to-year variability of the tsushima, *La mer*, *20*, 41–51.

Torrence, C., and G. P. Compo (1998), A practical guide to wavelet analysis, *Bulletin of the American Meteorological society*, *79*(1), 61–78, doi:10.1175/1520-0477(1998)079<0061:APGTWA>2.0.CO;2.

Trenberth, K. E., and D. P. Stepaniak (2003), Covariability of components of poleward atmospheric energy transports on seasonal and interannual timescales, *Journal of climate*, *16*(22), 3691–3705, doi:10.1175/1520-0442(2003)016<3691:COCOPA>2.0.CO;2.

Trenberth, K. E., W. G. Large, and J. G. Olson (1990), The mean annual cycle in global ocean wind stress, *Journal of Physical Oceanography*, *20*(11), 1742–1760.

Uccellini, L. W., P. J. Kocin, and J. M. Sienkiewicz (1999), Advances in forecasting extratropical cyclogenesis at the national meteorological center, in *The life cycles of extratropical cyclones*, pp. 317–336, Springer.

Uda, M. (1934), The results of simultaneous oceanographic investigations in the japan sea and its adjacent waters in may and june, 1932, *J. Imp. Fish. Exp. St.*, *5*, 57–190.

Uda, M. (1936), Results of simultaneous oceanographic investigations in the japan sea and its adjacent waters during october and november, 1933, *J. Imp. Fish. Exp. St.*, *7*, 91–151.

Willison, J., W. A. Robinson, and G. M. Lackmann (2013), The importance of resolving mesoscale latent heating in the north atlantic storm track, *Journal of the Atmospheric Sciences*, *70*(7), 2234–2250, doi:10.1175/JAS-D-12-0226.1.

Xie, S.-P., J. Hafner, Y. Tanimoto, W. T. Liu, H. Tokinaga, and H. Xu (2002), Bathymetric effect on the winter sea surface temperature and climate of the yellow and east china seas, *Geophysical Research Letters*, *29*(24), 81–1, doi:10.1029/2002GL015884.

Yamamoto, M. (2013), Effects of a semi-enclosed ocean on extratropical cyclogenesis: The dynamical processes around the japan sea on 23–25 january 2008, *Journal of Geophysical Research: Atmospheres*, *118*(18), 10–391, doi:10.1002/jgrd.50802.

Yamamoto, M., and N. Hirose (2007), Impact of sst reanalyzed using OGCM

on weather simulation: A case of a developing cyclone in the japan sea area, *Geophysical Research Letters*, *34*(5), doi:10.1029/2006GL028386.

Yamamoto, M., and N. Hirose (2011), Possible modification of atmospheric circulation over the northwestern pacific induced by a small semi-enclosed ocean, *Geophysical Research Letters*, *38*(3), doi:10.1029/2010GL046214.

Yoon, J.-H., and H. Kawamura (2002), The formation and circulation of the intermediate water in the japan sea, *Journal of Oceanography*, *58*(1), 197–211, doi:10.1023/A:1015893104998.

Yoshida, A., and Y. Asuma (2004), Structures and environment of explosively developing extratropical cyclones in the northwestern pacific region, *Monthly Weather Review*, *132*(5), 1121–1142, doi:10.1175/1520-0493(2004)132<1121:SAEOED>2.0.CO;2.

Yoshida, A., and Y. Asuma (2008), Numerical study of explosively developing extratropical cyclones in the northwestern pacific region, *Monthly Weather Review*, *136*(2), 712–740, doi:10.1175/2007MWR2111.1.

Yoshiike, S., and R. Kawamura (2009), Influence of wintertime large-scale circulation on the explosively developing cyclones over the western north pacific and their downstream effects, *Journal of Geophysical Research: Atmospheres*, *114*(D13), doi:10.1029/2009JD011820.

Yoshikane, T., F. Kimura, and S. Emori (2001), Numerical study on the baiu front genesis by heating contrast between land and ocean, *Journal of the Meteorological Society of Japan. Ser. II*, *79*(2), 671–686, doi:10.2151/jmsj.79.671.

Yoshikawa, Y., C. M. Lee, and L. N. Thomas (2012), The subpolar front of the japan/east sea. part iii: Competing roles of frontal dynamics and atmospheric forcing in driving ageostrophic vertical circulation and subduction, *Journal of Physical Oceanography*, *42*(6), 991–1011, doi:10.1175/JPO-D-11-0154.1.

You, Y., K.-I. Chang, J.-Y. Yun, and K.-R. Kim (2010), Thermocline circulation and ventilation of the east/japan sea, part i: Water-mass characteristics and transports, *Deep Sea Research Part II: Topical Studies in Oceanography*, *57*(13), 1221–1246, doi:10.1016/j.dsr2.2009.12.011.

Zhang, Y., K. R. Sperber, and J. S. Boyle (1997), Climatology and interannual variation of the east asian winter monsoon: Results from the 1979–95 ncep/ncar reanalysis, *Monthly Weather Review*, *125*(10), 2605–2619, doi:10.1175/1520-0493(1997)125,2605:CAIVOT.2.0.CO;2.

Zhang, Y., Y. Ding, and Q. Li (2012), A climatology of extratropical cyclones over east asia during 1958–2001, *Acta Meteorologica Sinica*, *26*(3), 261–277, doi:10.1007/s13351-012-0301-2.

Zhao, N., A. Manda, and Z. Han (2014), Frontogenesis and frontolysis of the subpolar front in the surface mixed layer of the japan sea, *Journal of Geophysical Research: Oceans*, *119*(2), 1498–1509, doi:10.1002/2013JC009419.

Zhao, N., S. Iwasaki, A. Isobe, R.-C. Lien, and B. Wang (2016), Intensification of the subpolar front in the sea of japan during winter cyclones, *Journal of Geophysical Research: Oceans*, *121*(4), 2253–2267, doi:10.1002/2015JC011565.

Zolina, O., and S. K. Gulev (2003), Synoptic variability of ocean-atmosphere turbulent fluxes associated with atmospheric cyclones, *Journal of Climate*, *16*(16), 2717–2734.